IMPROVING COMPRESSIVE STRENGTH OF HIGH MODULUS CARBON-FIBER REINFORCED POLYMERIC COMPOSITE WITH VARYING MODULUS FIBERS

by

Sarvenaz Ghaffari

DISSERTATION

Submitted in partial fulfillment of the requirements
for the degree of Doctor of Philosophy at
The University of Texas at Arlington
December, 2019

Arlington, Texas

Supervising Committee:

Andrew Makeev, Supervising Professor
Erian A. Armanios
Wendy Shen
Daniel P. Cole
Ashfaq Adnan

ABSTRACT

IMPROVING COMPRESSIVE STRENGTH OF HIGH MODULUS CARBON-FIBER REINFORCED POLYMERIC COMPOSITE WITH VARYING MODULUS FIBERS

Sarvenaz Ghaffari, Ph.D.

The University of Texas at Arlington, 2019

Supervising Professor: Andrew Makeev

There has been a strong demand in using high-modulus (HM) carbon-fiber composites potentially enabling lightweight aircraft structures with significant weight savings. However, extremely low fiber-direction compressive strength has been a well-recognized weakness of the HM composites, preventing their implementation in aircraft platforms. Fiber-direction compressive strength of HM and intermediate-modulus (IM) carbon fiber-reinforced polymers (CFRP's) is presumably governed by microstructural stability. However, strong decrease in fiber-direction compressive strength of HM carbon-fiber composites, compared to their intermediate modulus (IM) counterparts, contradicts predictions from available microstructural buckling theories. A recent work demonstrated that significant improvement in the fiber-direction compressive strength of HM carbon-fiber composites can be achieved by hybridizing IM and HM carbon fibers in HM CFRP toughened with nano-silica. In particular, a new HM material solution

achieving fiber-direction compressive strength of IM legacy composites but with more than 30% higher axial modulus has been developed.

On the other hand, enabling effective design of the new high-performing composite material requires accurate physics-based models to capture fiber-direction compressive strength behavior of HM CFRPs. Such models would provide the most effective way to explore diverse material design options with optimum microstructural configurations. The absence of accurate models has been attributed to complexity and potential multiplicity of the governing failure modes and their interaction. Therefore, observing the fiber-direction compressive failure presumably governed by microstructural stability has been a major prerequisite for developing a rigorous modeling strategy. Kink-band formation in HM CFRPs was observed for the first time. This observation confirms that fiber-direction compressive strength is indeed governed by microstructural stability, which can be used as a basis for accurate model development.

Furthermore, some of the major challenges in developing models capturing the microstructural stability include meeting their input data requirements. In order to generate such data and observe the physics phenomenon at a scale small enough for the important features to be captured, in-situ scanning electron microscopy (SEM) based experiments are introduced to measure the essential microstructural material properties, e.g. fiber-to-matrix interface shear strength behavior within the actual composite ply.

This work looks into weak fiber-matrix interface as a potential mechanism driving the fiber-direction compressive strength decrease of the HM CFRP's. The experiments show approximately 30% decrease in the average values of the fiber-matrix interface shear strength for the HM carbon fibers compared to the IM carbon fibers in the new material system. And such a strong reduction corresponds to a 22% lower fiber-direction compressive strength of the HM

CFRP. In addition, the fiber-matrix interface shear strength reduction correlates with decreasing fiber-direction compression strength predicted by a microstructural buckling model which properly accounts for the fiber-matrix interface shear strength behavior. The results support the idea of integrating off-the-shelf IM carbon fibers with stronger fiber-matrix interface and higher shear modulus into a HM carbon-fiber composite to improve fiber-direction compressive strength of the HM composite material system.

ACKNOWLEDGEMENTS

I owe my deepest gratitude to my supervisors Dr. Andrew Makeev for his guidance, flexibility, and seemingly infinite patience during the completion of my degree. There are no proper words to convey my sincere appreciation and respect for him. He has inspired me and convincingly encouraged me to believe in myself as an independent researcher and gave me endless support and guidance throughout my graduate studies. He has taught me more than I could ever give him credit for here. His expertise was invaluable in the formulation of this research topic and methodology. He has been a true mentor and friend, and I am so fortunate to have had such an amazing advisor.

My sincere thanks must also go to the members of my thesis advisory and exam committee: Dr. Erian Armanios, Dr. Dan Cole, Dr. Ashfaq Adnan and Dr. Wendy Shen for their insightful comments and suggestions and review my dissertation.

I would also like to thank Dr. Robert Haynes, Dr. Dan Cole and Dr. Todd Henry for offering me the summer internship opportunities in their group at Army Research Lab (ARL) and leading me working on such an exciting project.

Thank you to Dr. Dan Magagnosc at ARL for manufacturing the test specimens.

Additionally, I would like to express my extreme gratitude to Sanjit Bhowmick at Bruker, for his invaluable contribution to the experimental work used in this research.

I must thank my colleagues at AMSL: Brian Shonkwiler who patiently taught me all I know as an experimentalist and Dr. Guillaume Seon and Dr. Dmytro Kuksenko for the work in FEM modeling. Their help has been invaluable for my research. And to my friends, Julia, Katya, Bastiaan, Johnny, Louis and Md for their support and encouragement over the years.

Last but not least, I would like to thank my parents, Soheila and Parviz who have

unconditionally supported me throughout my academic career. I am forever indebted to them for giving me the opportunities that have made me who I am. It was their love that raised me up again when I got weary. I am grateful to my brother, Soroush, for always being there for me as a friend. Specially listening to his everyday life stories as a PhD student make me realize how fortunate I am to be a part of AMSL and work with such amazing people.

This research was partially funded by the U.S. Government under Agreement No. W911W6-17-2-0002. Such support is gratefully acknowledged.

LIST OF FIGURES

LIST OF TABLES

Table of Contents

CHAPTER 1

Introduction

1.1 Motivation

Carbon fiber-reinforced polymer matrix composite (CFRP) materials are increasingly used in rotorcraft primary structures due to the high industrial demand for lightweight material with better performance. Their high strength-to-weight ratio and their fatigue and corrosion resistance characteristic make them superior to conventional materials. Carbon fibers that are used in high-performance composites can be classified into three categories of the intermediate modulus (IM), high modulus (HM) and high strength (HS) fibers. High stiffness and modulus of HM carbon fibers make them an ideal choice for implementation into primary structures in order to achieve optimum performace with significant weight saving. However, extremely low fiber-direction compressive strength has been a well-recognized weakness of the HM carbon-fiber composites that prevent their implementation in aircraft platforms. From the structural application point of view, microstructural stability is one of the main drivers of fiber-direction compressive strength behavior of HM and IM CFRP's. While, strong decrease in fiber-direction compressive strength of HM composites, compared to their IM counterparts, contradicts predictions from available microstructural buckling theories. According to these theories, increasing the modulus of the fiber should improve the overall compressive strength behavior of the composite material. Although, the result of the experimental work that has been performed across different fiber and resin combinations [1] illustrate an opposite behavior. For instance, IM7/F3G composite material with 40 Msi (275GPa) fiber modulus and 24.8 Msi (171 GPa) average composite axial modulus generate fiber-direction compressive strength of 240 Ksi (1.65 GPa).While advanced carbon/epoxy tape composite HM63/F3G with higher young’s modulus of 64 Msi (441 Gpa) and average axial modulus of 34.5 Msi (238 GPa), with the same matrix system can only exhibit 157 Ksi (1.08 GPa) fiber-direction compressive strength. In addition, HM carbon fibers with the highest fiber-direction young’s modulus produce composites with the lowest compressive strength, e.g. Toray M55J/2500 carbon/epoxy tape composite with a 40 Msi (276 GPa) average Young’s modulus has a 129 ksi (0.889 GPa) fiber-direction compressive strength [2].

Consequently, this work targets the development of microstructural methods for developing high-performance composite materials. The main motivation of this work comes from substantial need from industry for developing a continuous HM CFRPs approaching fiber-direction compressive strength of IM carbon legacy composites at 30% (or greater) higher Young’s modulus.

On the other hand, increasing demand for composite material has caused a major increase in the need for predictive analysis tools for better understanding their behavior under various loading scenarios or different structural configurations. For that reason, determining accurate and reliable failure criteria for composite material has been an active field of research for several decades [3].The use of computational models for predicting deformation, strength, and fatigue performance of composites can significantly reduce development costs by replacing some of the physical tests while providing valuable insight to achieve optimized designs.

In general, design or optimization of the new high performing composite materials rely on traditional and time consuming trial and error technique which requires a large number of experimental iterations and limits the possibility of exploring diverse material design and process options. This stems from the fact that there are no accurate physics-base models available to precisely capture fiber direction compressive strength performance of the composite material.

Having access to such model would enable the effective design of the new high performing composite material and achieve the desired performance with optimum configuration with much less experimental iteration. The absence of such models has been attributed to multiplicity and complexity of the governing failure modes and their interaction. In fact, composite materials represent very complex systems, including many components, e.g., carbon fiber, polymer matrix, fiber sizing, matrix toughening nanoparticles, etc. In order to prepare an accurate model for these multicomponent materials, micromechanical performance of each constituent and the complex interaction between them should be included in the model. Although, one of the main challenges in developing models to capture the microstructural stability phenomena which will eventually affect fiber-direction compression strength performance of the composite, is providing an accurate input for the microstructural modelling. Nanoindentation is one of the common testing techniques to determine the properties of the material in micro or nanoscale. In this effort, nanoindentation was used to characterize the properties of the micro-constituents and provide an accurate input parameters for micromechanical modeling of a composite.

1.2 Objective:

In the absence of accurate models to predict fiber-direction compressive strength of HM carbon-fiber polymeric composites, this effort will take an experimental approach to reinforce material surrounding HM fibers to improve microstructural stability phenomena with the goal to overcome the well-recognized weakness of HM CFRP composites and achieve the desired improvement of compressive strength. The result of the experimental effort will be presented in chapter 2.

Furthermore, as it was mentioned before, the ultimate aim is to enable effective design of the novel high-performing composite systems. To achieve this goal, we need to generate an accurate physics-base model that can precisely capture behavior and performance of the composite material under different loading scenarios in various directions. All the features and events leading to failure of the composite structure need to be recognized, characterized and implemented into the model. Therefore, an analytical model cannot be developed without observing the phenomenon at a scale small enough for the important features to be captured. Consequently, nanoindentation was selected to characterize the properties of the micro-constituents and quantify input properties for strength model and eventually provide an accurate input parameters for micromechanical modeling of a composite with the focus on fiber-matrix interface properties.

In chapter 3, an innovative micromechanical characterization technique with in-situ scanning electron microscopy (SEM) based experiments will be introduced to measure the properties of the laminate constituents within the actual composite ply. The developed technique will eventually be employed to obtain the properties of matrix and fiber-matrix interface properties. Standing challenges in the available specimen fabrication and configuration will be addressed and novel methods to improve the consistency of the test results will be provided.

In chapter 4, we will look into fiber-matrix interface as a potential mechanism driving the compression strength improvement of the new material system. It focuses on the study of fiber-matrix interface at the micromechanical length scale for the determination of interfacial strength for higher length scale models. In-situ SEM based experiments will be used to measure fiber-matrix interface shear strength. Furthermore, the proposed micromechanical characterization technique will be used to study the failure phenomena by observing and measuring their attributes. Microstructural buckling model will be generated and the prediction from the model will be compared to the experimental results.

In addition, observing the fiber-direction compressive failure presumably governed by microstructural stability has been a major prerequisite for developing a rigorous modeling strategy. As we currently assume fiber microbuckling (fiber kinking) is the dominant failure mode, we must observe the kink-band formation for the practical material range including HM, IM, and hybrid carbon fiber-reinforced composites. Then we can focus on developing fiber-direction compressive strength models that reflect the physics phenomenon. It is worth noting that fiber-direction failure in HM CFRPs is not well-documented in literature, which raises the question whether the fiber-direction compressive strength of PAN-based continuous HM CFRPs and HM/IM hybrids is indeed governed by microstructural stability (fiber kinking), as it is most commonly accepted and observed in IM CFRPs. Chapter 5 presents our initial results assuring the pertinence of microbuckling in HM CFRPs.

Finally, the conclusions and perspectives are stated in the final chapter

CHAPTER 2

Improving compressive strength of high modulus carbon-fiber reinforced polymeric composites through fiber hybridization

The chapter presents experimental effort on designing a new HM CFRP composite to achieve the desired improvement of compressive strength behavior. Observations of the compressive strength behavior across different fiber and resin combinations inspired the idea of hybridizing carbon fibers with varying moduli.

2.1 Background:

As a matter of fact, it is well-known that composites do not perform as well in compression as in tension [4, 5, 6]. The difference between their responses under various types of loading is a limiting factor in design of the composite structures. Therefore, development of analytical and numerical models for the prediction of fiber-direction compressive failure of composites has been an active field of research. Development of compression failure theories has been difficult due to the complexity and multiplicity of failure modes that can occur with variations in constituent properties and laminate construction. When fiber reinforced composite structures are subjected to compressive load along their fiber direction, they usually fail due to material failure at the constituents level [7], followed by damage propagation through the entire structure. Generally, composite structures are faced with four different failure modes under application of compressive load:

1. **Microbuckling:** This theory is based on a micromechanical approach that fibers are supported by an elastic foundation provided by the matrix and the failure is caused by fiber instability. It is mostly common in composites with strong matrix and fibers.
2. **Fiber kinking**: large number of the literatures on longitudinal compressive failure of composites are dedicated to kink-band formation since it is the most recognized failure mode in this loading configuration. Many models and formulations to predict the compressive strength associated with kink band formation can be found in the literature [7, 8, 9, 5, 10, 11]. This theory is based on the assumption that there is an area of misaligned fibers in the composite. Under a compressive load, fibers rotate until the failure stress of the matrix is reached. Therefor failure is caused by matrix failure. Moreover, there are experimental evidences which suggest that this mode of failure in carbon fiber epoxy composites are controlled by shear yield strength of the matrix [12, 5, 13, 14, 15].
3. **Fiber failure:** Simple failure of the fibers due to pure compression. It depends on fiber's properties and it is mostly common in composites with weak fibers.
4. **Longitudinal cracking or splitting:** Debonding between matrix and fibers or separation within the matrix. It is common in composites with weak interface.

Among these failure modes, fiber microbuckling and kinking failures have been the most accepted modes of failure of advanced carbon/epoxy composites under fiber-direction compression, with sometimes conflicting views in the literature whereas kinking should be considered as an independent failure mechanism or a final consequence of fiber microbuckling [16, 17]. In the pioneering work of Dow and Gruntfest [18] , and in a more systematic way by

Rosen [19] , fiber microbuckling was suggested for the first time as the principal mechanism responsible for the low compressive strength of advanced composites. In the analytical microbuckling model proposed by Rosen (Fig.1), fibers were represented as two-dimensional layers supported by an elastic matrix with two possible modes of buckling failure, whether adjacent fibers deform out-of-phase (extensional mode) or in-phase (shear mode) [1].The derived expressions for the compression strength of both modes can be described by the following equations:

- For the extension mode:

$$\sigma_c = 2V_f\left(\frac{V_f E_m E_f}{3(1-V_f)}\right)^{1/2} \tag{2-1}$$

- For the shear mode:

$$\sigma_c = \frac{G_m}{(1-V_f)} \tag{2-2}$$

Where σ_c is the unidirectional compressive strength of the composite, E_f is the fiber axial modulus and G_m is the elastic shear modulus of matrix.

Typically, shear buckling mode is giving lower strength for most of the cases, and the composite in-plane shear modulus is identified as the primary driver for compressive strength [20]. Indeed, an increase of compressive strength due to the increase of fiber modulus E_f is predicted for the extensional mode and the compressive strength should remain constant according to the expression of σ_c in the shear mode. Thus, the decrease in fiber-compressive strength introduced by HM fibers in the same matrix system and at the same fiber volume fraction cannot be captured using Rosen's model.

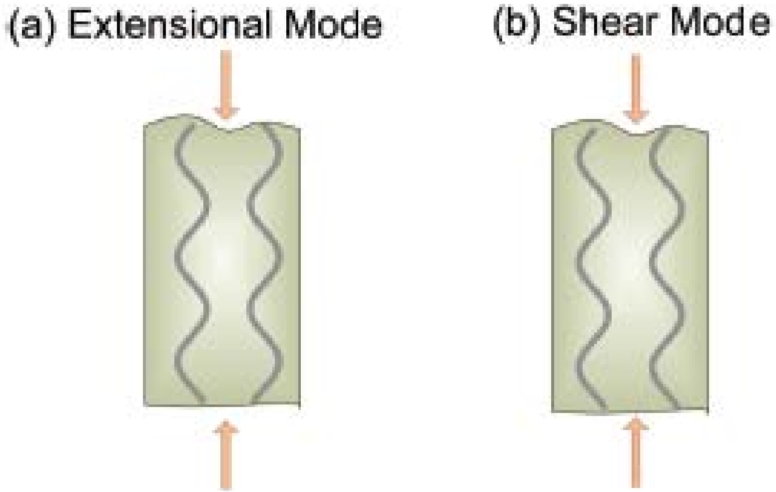

Figure 1. Microbuckling Theory: (a) Extensional mode, (b) Shear mode *[21]*.

Independent of Rosen, similar analytical microbuckling formulation were obtained by Hayashi [22] , Schuerch [23] and Chung et al. [24]. However, composite compression strength values achieved with these theoretical methods were significantly higher than the measured strengths from experiments [25]. Typical overestimation of the compressive strength by up to two orders of magnitude using the Rosen's model compared to experimental data for common advanced carbon/epoxy composites has been well recognized in the literature [26, 14, 16] and encouraged further improvements of the fiber microbuckling models. Researchers have proposed many extensions and improvements to the Rosen's model to explain this over-prediction. They introduced new parameters to the model to include the effect of small imperfections such as fiber misalignment, fiber volume fraction, plastic behavior of the matrix and etc. to explain this variation. For instance, Lager and June [25] modified equation (2-1) and (2-2) by including a coefficient that accounts for softening of the matrix with increasing applied load. Their experimental strengths agreed better with predicted strength from modified equations, but they were still significantly higher than experimental results.

Argon [14] developed the first kinking model by recognizing the importance of the initial fiber misalignment angle on the reduction of the compressive strength. He identifies composite shear strength and the initial fiber misalignment angle as the main parameters controlling the compressive strength, but his model was independent of fiber volume fractions. He predicts that the area of the composite with misaligned fibers with respect to the axis of compressive load, will undergo kinking failure. This phenomena will occur at a stress lower than the ideal buckling strength derived by Rosen. The composite compressive strength based on his method is given by:

$$\sigma_c = \frac{\tau^c}{\phi} \tag{2-3}$$

Where τ^c is composite shear strength and ϕ is fiber misalignment angle.

Then, Budiansky [13, 5] extended Argon's formula to a more general expression. According to his theory, if yield strain is much smaller that misalignment angle his equation will be similar to Argon's expression while for the case of $\phi = 0$ the formula will be similar to Rosen's model:

$$\sigma_c = \frac{\tau^c}{\gamma^c + \phi} = \frac{G}{1 + \frac{\phi}{\gamma^c}} \tag{2-4}$$

Where $\gamma^c = \frac{\tau^c}{G}$= yield strain

Daniel et al [27] suggested to integrate initial fiber misalignment with measured composite in-plane shear modulus. This method accounted for matrix nonlinearity and misalignment.

The results of all these efforts indicate that initial fiber misalignment can plays a leading role in compressive strength performance of the composites. Explicit modeling of the initial fiber misalignment and incorporation of shear non-linear constitutive models for the matrix is also included in FE-based micromechanical models of fiber kinking [28, 29, 30].

Soon after, Madhukar and Drzal [31] presented an important effect of fiber-matrix interface on the performance of the composite material by experimentally quantifying the relationship between fiber-matrix adhesion with the compressive properties and failure modes of unidirectional CFRP composites. They used three identical sets of composites with different fiber-to-matrix interface shear strength properties. The interfacial shear strength was modified by changing the fiber surface treatment. The results demonstrate an increase in compressive strength performance with increasing the interface shear strength. In addition, regarding the failure modes, it was observed that poor fiber-matrix bonding can cause a delamination failure. While increase of the interface strength leads to shear failure driven by in-phase microbuckling of the fibers. The same results were observed by Ha and Nairn [32].

On the other hand, Lo and Chim [26] derived a new model to describe compressive behavior of unidirectional composites by included the effects of resin stiffness, fiber anisotropy, fiber misalignment and waviness, fiber-to-matrix interface, and void content. Although some interesting results have been obtained by this model, but due to the existence of empirical factors in their equation, it was hard to verify the accuracy of the predicted strength value when the experimental results were not available.

$$\sigma_c = \frac{G_{12}}{1.5+12\left(\frac{6}{\pi}\right)^2\left(\frac{G_{12}}{E_{11}}\right)} \tag{2-5}$$

$$G_{12} = G_m \frac{(1+v_f)G_{f12}+(1-v_f)G_m}{(1-v_f)G_{f12}+(1+v_f)G_m} \tag{2-6}$$

$$E_{11} = V_f E_{f11} + (1 - V_f)E_m + \frac{4v_f(1-V_f)G_m(v_{f12}-v_m)^2}{\frac{(1-V_f)G_m}{K_{f23}}+\frac{V_f G_m}{K_m}+1} \tag{2-7}$$

Where G_m shows matrix shear modulus, $E_{f11}$is fiber longitudinal modulus and V_f defines the fiber volume fraction.

Later on, Dharan et al. [33], approached the microbuckling phenomena by proposing a low modulus interphase layer between the fiber and the matrix and make a three-phase model to explain the observed compression strength. By using their equation for calculation of the critical compression stress, the predicted value of compressive strength was successfully reduced but this model incorrectly further lowers in-plane shear modulus of the composite.

$$\sigma_c = \frac{1}{\left(\frac{1-V_f}{G_m V_f}\right)+2\left(\frac{h_i}{G_i h_f}\right)V_f} = \frac{1}{\left(\frac{1-V_f}{G_m}\right)+2\left(\frac{h_i}{h_f}\right)\left(\frac{1}{G_i}\right)V_f} = \frac{G_m}{1-V_f+2\left(\frac{h_i}{h_f}\right)\left(\frac{G_m}{G_i}\right)V_f} \tag{2-8}$$

Where G represents shear modulus, h represents thickness and V_f stands for fiber volume fraction. Consequently, over the past decades, the development of advanced kinking theory models has significantly improved the understanding of fiber-direction compressive failure in advanced composites. Yet, basic kinking models do not provide with a satisfactory rational for the reduction in compressive strength in HM carbon/epoxy composites. As evidenced, in most of the proposed analytical models, there is a direct relation between fiber modulus and the compressive strength of the composite. Therefore, by increasing the fiber elastic modulus, the compressive strength of the composite is expected to increase. While this is exactly opposite of the results that we have achieve experimentally. Indeed, under similar manufacturing/curing conditions, significant changes in the non-linear shear behavior of polymer matrix supporting the fibers are not to be expected. Similarly, it seems reasonable to assume that initial fiber misalignment is reduced with the introduction of stiffer fibers, which would lead to an increase in compressive strength according to kinking theories. Figure 6 present's results of 2D FE micromechanical analysis run for illustration purposes using Abaqus Riks Analysis to predict fiber kinking instability, similar to the work by Kyriakides *et al* in [30]. In this model, an initial fiber misalignment is introduced as shown in Figure 1a) and a Drucker-Prager model is used to account for the matrix non-linearity similarly to the model used in [28]. Linear elastic behavior of the fibers and a perfect bond of the matrix-fiber interface throughout the simulation are assumed. As shown in Figure 1c, the maximum compressive stress obtained in 2D FE kinking analysis is slightly increased when the fiber Young's modulus is increased between 20 Msi (140 GPa) and 60 Msi (410 GPa), which contradicts the compressive strength reduction measured experimentally.

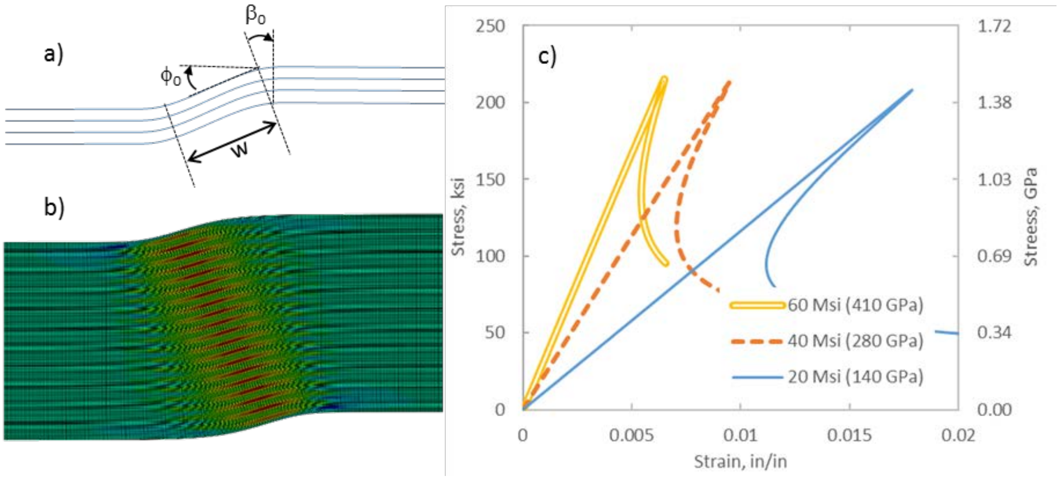

Figure 2. Example of 2D Riks Analysis using Abaqus FE solver showing a) approximation of the initial misalignment angle used in the FE model, b) development of localized shear stress into a kink-band and c) effect of different fiber Young's modulus on the kinking stress-strain response.

Inconsistency in predicting fiber-direction compressive strength using available analytical and numerical models indicates the potential complexity of the failure mechanisms. As mentioned before , fiber breakage and longitudinal splitting are other possible failure modes that could occur during fiber-direction compression of composites, in addition to the microbuckling and kinking failure modes. It is worth noting that pitch-based fibers introduced at the early stages of the HM carbon fiber development exhibited very low compressive strength attributed to premature fiber failure due to splitting [26, 16]. However, the compressive strain-to-failure capacity of modern PAN-based HM carbon fibers has significantly improved since to overcome such early limitations [34]. Nevertheless, localized fiber breakages could still occur and they may be precursors to kinking failure. Similarly, a weak matrix-to-fiber interface may lead to early microbuckling or kinking failure.

Absence of accurate models to predict fiber-direction compressive strength of HM carbon-fiber polymeric composites, and substantial need from industry for developing a continuous HM CFRP approaching fiber-direction compressive strength of IM carbon legacy composites at 30%

(or greater) higher Young’s modulus, inspired the idea to experimentally improve microstructural stability of the HM CFRP composite by reinforcing material surrounding HM fibers in order to develop fiber-direction compressive strength behavior of HM composites.

2.2 Nano-Sized Reinforcement of the Matrix:

Nano-sized structural reinforcement techniques is one of the common methods to increase matrix and composite shear modulus throughout the material to better support the fibers and improve matrix-to-fiber interface properties. If we consider shear microbuckling as a dominate failure mode in HM CFRP composite material and identify in-plane shear modulus as the primary driver for compressive failure phenomena, improvement of the shear modulus of the material can lead to an increase of fiber-direction compressive strength performance. Among many candidates for improving compressive and interlaminar properties of fiber-reinforced polymer composite materials are nanosilica-loaded matrices [35]. Nanosilica is silica particles with the size of 100-nm in diameter. They enables high loading with minimum impact on viscosity in addition to the fact that they can be uniformly dispersed through surface chemistry technology [36, 37] . In 2009, 3M launched matrix Resin 3831, a 36% nanosilica weight content 250° F curing epoxy resin system designed for use in composite manufacturing processes [37]. Initial implementation of this resin in the sporting goods market increased compression-dominated bending failure loads by 60-90% [37]. It is known that incorporation of hard particles into polymers increases their modulus and fracture resistance characteristics [38, 36, 37, 35]. In the past, micron-scale inorganic fillers have been used to modify cured resin properties, but when processed into fiber-reinforced composite structures, these large particles were filtered out by the reinforcing fibers.

Another undesirable effect of conventional micron-size fillers is increased resin viscosity before curing, which can compromise composite processing qualities [35, 36, 37]. For that reason, 3M attempted to achieve the desirable resin modulus and laminate compression strength improvements through the incorporation of smaller, nano-sized silica particles into thermoset-matrix resins [36, 37]. Patz Materials and Technologies (PMT) began working with 3M to address specific applications where 3M's nanosilica technology could yield significant benefit for composite structures [35]. PMT would formulate the applicable thermosetting polymer technology for the specific application and 3M would apply the nanosilica to that polymer. The key to the performance of the nanosilica in each polymer system is 3M's ability to tailor the surface chemistry for the nanosilica particles. For each formulated product that PMT supplied, 3M would develop the appropriate surface chemistry for the nanoparticles. This allows the nanosilica particles to become an integral part of the polymer system and the desired particle attributes could be realized in the composite structure. This also allows the particles to flow freely with the polymer system thus only minimally increasing the viscosity of the formulated product. While dispersion of nanosilica particles in 350° F curing resins has not always been uniform, results for 250° F curing PMT resins are consistent. Figure 3 shows a representative 250° F cured carbon/epoxy composite laminate with 36% weight content of silica particles evenly dispersed between 7-μm diameter TR50S carbon fibers [35, 36, 37]. It is worth noting that HM and IM carbon fibers studied in this work had 5 micron diameter.

For recent effort by Rotorcraft Industry and Academia, PMT made 12 inches (30.48 cm) wide unidirectional prepreg tapes using IM7, HM63, and HS40 carbon fibers [39, 40, 41]. HS and HM fibers are representative of high modulus carbon fibers. The areal weight of carbon fibers are 145 g/m^2. The fiber volume fraction was approximately 60%. Prepreg tapes were made in two different batches. One batch was made without any nanoadditives which was called as control group. While the rest were produced with up to 40% resin weight content of nanosilica. The 250° F curing epoxy matrices generated by PMT were as follow:

- Control epoxy resin without any nanoadditives -F4A
- 40% nanosilica weight content- F3G

Some of the best-performing legacy toughened epoxies including 250° F curing Cytec Solvay 381 [35, 42] , Hexcel 913 [43] and a 350° F curing Hexcel 8552 [44] common in aircraft applications are also included in material characterization. In particular, as IM7/8552 has become a benchmark 350° F curing prepreg for aircraft structures, it is used in this work to normalize the compressive strength material performance improvement.

Indeed, the results of the recent material characterization effort demonstrated that reinforcement of epoxy matrix with 40% nanosilica weight content for IM carbon fiber and glass fiber composites can cause as high as 45% increase in compressive strength performance [35]. Because of the successful outcomes of the reinforced matrix in IM CFRP composites, the same process was applied to HM composite material system. However, replacement of the IM fibers with HM fibers with the same toughened epoxy matrix did not make as noticeable improvement as IM CFRP composite.

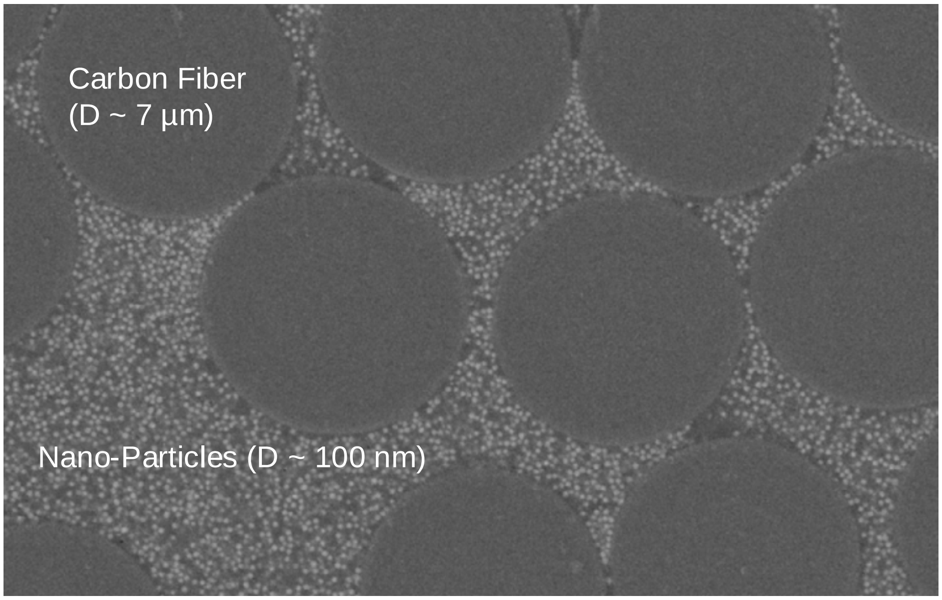

Figure 3. SEM image of a carbon/epoxy laminate cross section demonstrating even dispersion and lack of conglomeration for the nanosilica particles [35, 36, 37].

For instance, distributing 40% Nanosilica in a low-viscosity epoxy control resin had the following effect on the fiber-direction compressive strength:

- Intermediate modulus carbon fiber:
  - IM7/F4A (Control) =184 ksi ; IM7/F3G (40% Nanosilica) = 240.5 ksi
- High modulus carbon fiber:
  - HM63/F4A (Control) =137 ksi; HM63/F3G (40% Nanosilica) = 157 ksi

As a result, it was concluded that nanosilica alone cannot provide enough support to HM fibers.

Figure 4 illustrates fiber-direction compressive strength vs average axial modulus for several HM and IM carbon/epoxy unidirectional tape composites. All the results presented in that figure are normalized to IM7/8552 legacy composite material system with 215 ksi (1.48 GPa) compressive strength and a 22.8 Msi (157 GPa) axial modulus values. The compressive strength values are all measured according to SACMA SRM 1R-94 [45] testing of tabbed unidirectional laminates.

As can be seen in Fig.4, even with nanosilica reinforcement of the matrix material the compressive strength of the HM composite material is still lower than IM composite. Alternatively, thorough investigation of the experimental results presented in Fig.5 and Table 1 indicates a notable trend between fiber-direction compressive strength and the ratio of shear modulus to axial modulus of composites across different fiber and resin combinations. This implies that increasing the ratio of shear modulus to axial modulus of the composite, will improve the compressive strength of the material.

Moreover, as demonstrated in Table.1, the shear modulus of IM carbon fiber composites is higher than HM carbon fiber composites with the same epoxy resin. Hence, the same matrix can provide better support to IM fibers compare to HM fibers.

Therefore, it inspired the idea of integrating IM fibers into HM fiber prepreg to overcome the challenge of inadequate support to HM fibers for the new composite material system and overcome the challenge of inadequate support to HM fibers. Besides, the matrix Nano-sized structural reinforcement was still supposed to be added to the matrix with the goal to enhance microstructural stability governing compression strength.

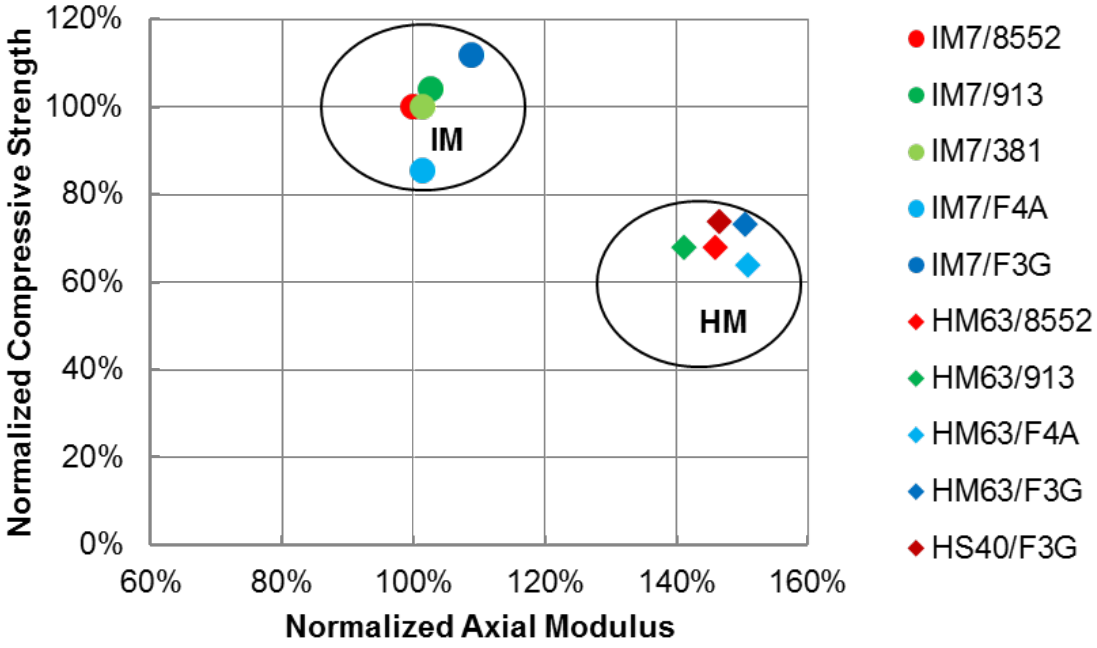

Figure 4. Axial modulus and fiber-direction compressive strength of HM and IM carbon fiber-reinforced epoxy-matrix tape composites. Notes: 8552 – 350° F curing toughened legacy epoxy; 913, 381 – 250° F curing toughened legacy epoxies; F4A – 250° F curing untoughened low viscosity epoxy (Control); F3G – 250° F curing Nanosilica toughened epoxy (40% Nanosilica by resin weight).

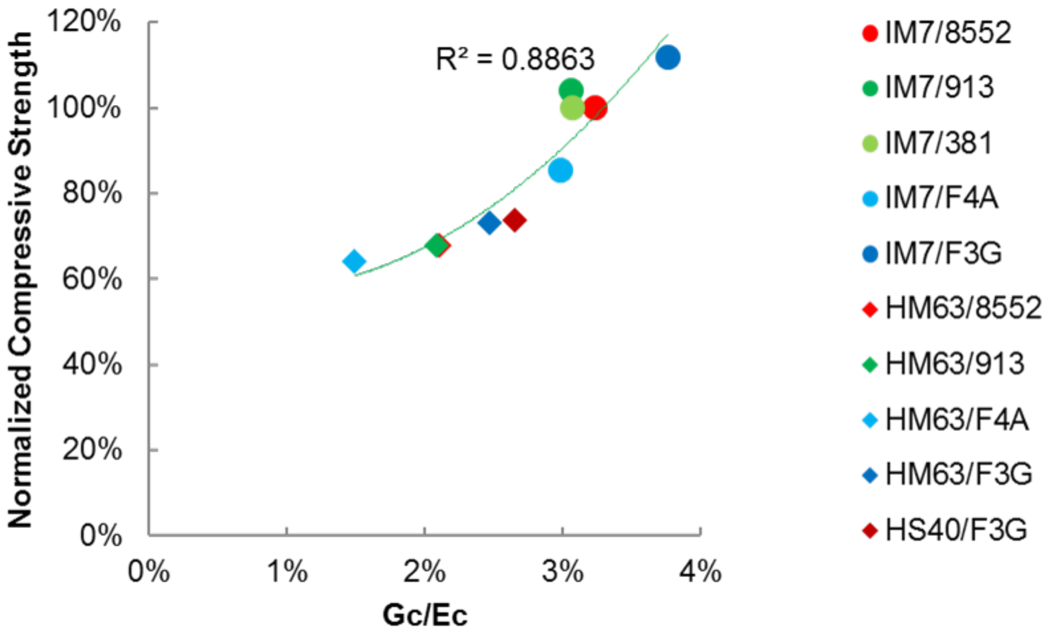

Figure 5. Strong correlation of compressive strength and ratio of the shear modulus to axial modulus for the tape composite material systems across different fiber and resin combinations.

Table 1 Modulus and strength data for HM and IM carbon/epoxy 250° F curing tape composites. Notes: Ec – average axial modulus of composite material, Gc – shear modulus of composite material, Sc – fiber-direction compressive strength. Conversion factor: 1 psi = 6.895 kPa

Material	Fiber Modulus (Msi)	Resin Modulus (Msi)	Average axial modulus(E_c) (Msi)	Shear Modulus(G_c) (Msi)	Gc/E_c, %	S_c (ksi)
IM7/913	40	0.492	23.4	0.717	3.06	223.9
HM63/913	64	0.492	32.2	0.674	2.09	145.9
IM7/F4A	40	N/A	23.1	0.69	2.99	183.9
HM63/F4A	64	N/A	34.4	0.514	1.49	137.3
IM7/F3G	40	0.893	24.8	0.932	3.76	240.5
HM63/F3G	64	0.893	34.3	0.847	2.47	157.2

2.3 Fiber Hybridization:

For the fabrication process, the first attempt to hybridize the IM and HM carbon fibers was to use PMT prepreg production facility with the goal to make the 50/50 mix of the Hexcel HM63 and IM8 12K carbon fiber tows. IM8 fiber has a slightly higher modulus (45 Msi /310 GPa), compared to IM7 fiber (40 Msi /276 GPa) [39, 46]. A 12 inch (30.48 cm) wide unidirectional prepreg tape was produced at PMT using F3G epoxy with 35% by weight resin content (60% fiber volume fraction). The IM8 fibers were run first, and HM63 fibers were quizzed into IM8 fibers afterward at 40 psi pressure. The resulting hybrid prepreg had a 171.3 ksi fiber-direction compressive strength with the coefficient of variation of 1.91%. The compressive strength of the new hybrid panel was considerably lower that what it was expected to be. As a result, it was assumed that poor hybridization of the HM and IM carbon fibers might be responsible for this low compressive strength performance. To investigate this hypothesis, we looked at cross-section of a cured hybrid panel with optical microscope. As illustrated in Figure 7, a distinct HM63 and IM8, 3 mil (76 µm) thick half-ply layer structure can be observed, which proves the poor comingling of HM and IM fibers.

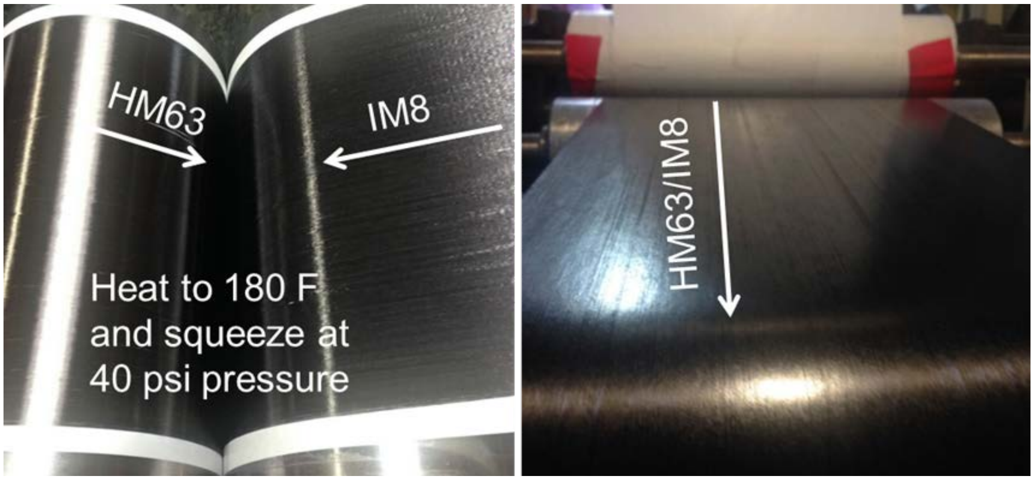

Figure 6. Hybridization process at PMT facility.

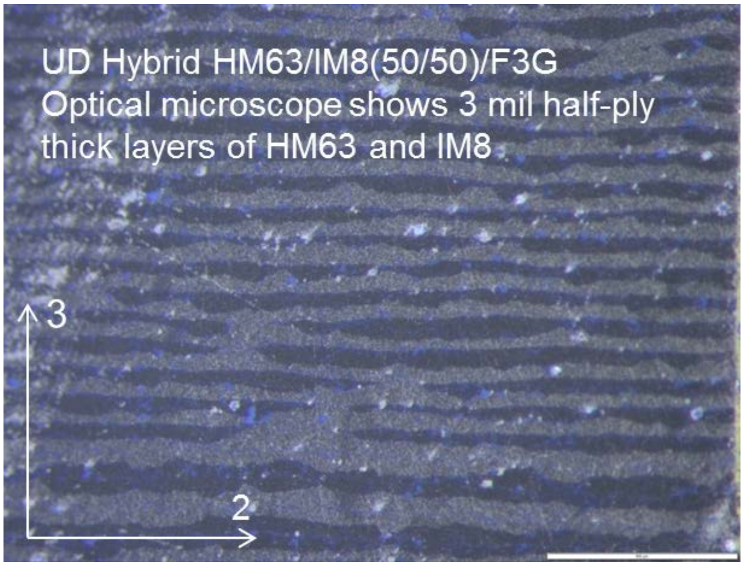

Figure 7. Hybrid composite with poor comingling of HM and IM fibers.

The second prepreg manufacturing iteration focused on increasing the squeeze pressure to 60 psi (414 KPa) to improve hybridization. Accordingly, fiber-direction compressive strength increased from 171 ksi or 1.18 GPa (COV 1.91%) to 177 ksi or 1.22 GPa (COV 3.76%). But then again, it was still lower than 200 ksi or 1.38 GPa threshold of IM carbon/epoxy tape composites.

Figure.8 indicates that, despite 50% pressure increase, half-ply layers of HM and IM fibers were still present. Hence, an increase of squeeze pressure cannot significantly affect the hybridization process. While, adequate reinforcement of the material surrounding HM fibers requires comingling at the filament level which has yet to be demonstrated.

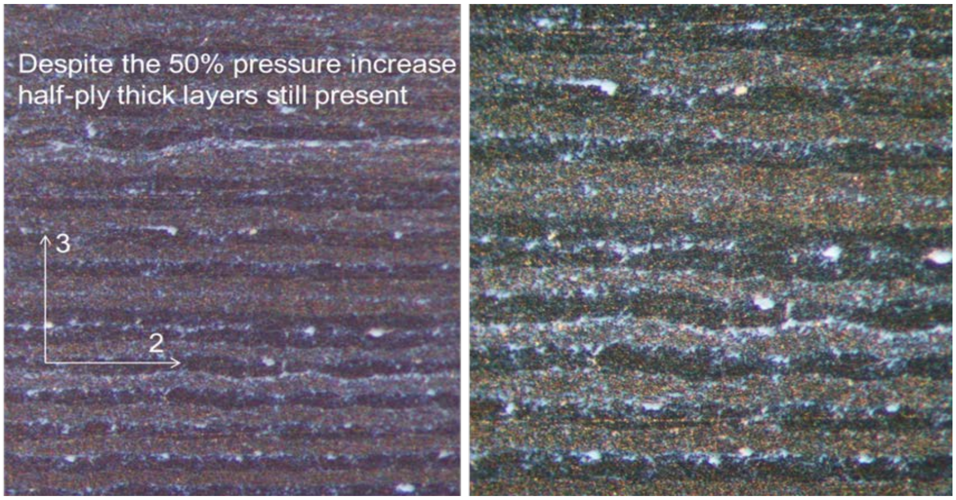

Figure 8. Hybridization associated with 50% increase in squeeze pressure.

Accordingly, a textile company Sakai Ovex demonstrated their comingling technology by preparing a trial composite prepreg with mixing two types of fibers with different diameters. Micrograph in Figure 9 shows the initial results of their prepreg composite. As can be seen, both fibers are distributed through the whole panel which proves the validity of their technology.

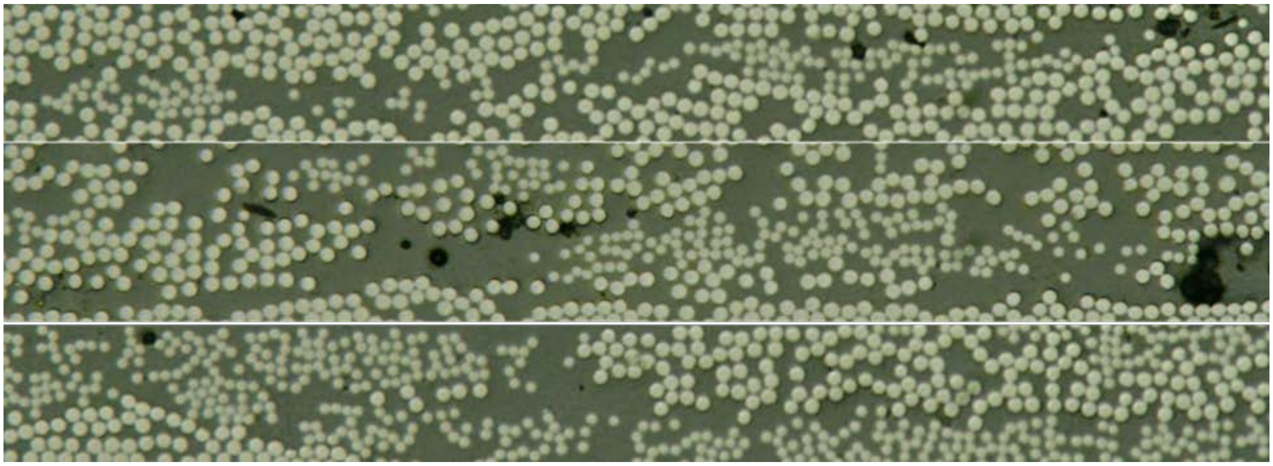

Figure 9. Micrograph demonstrating the comingling of HM Mitsubishi HS40 with 5 µm diameter carbon fibers and standard-modulus Teijin HTS40 with 7 µm diameter at Sakai Ovex

For this project, the same process has been done to comingle the Mitsubishi HS40 12K HM carbon fibers and MR70 12K IM fibers into a 30 mm wide unidirectional dry fiber tape. Both HM and IM fibers have the same 5µm diameter. The unidirectional prepreg has been fabricated at PMT using the Sakai dry fiber tape and 3831 off-the-shelf 250˚F curing resin from 3M; similar to F3G. A 35% resin areal weight corresponding to approximately 60% fiber volume fraction has been targeted and achieved. Figure 10 shows the prepreg fabrication process at PMT facility.

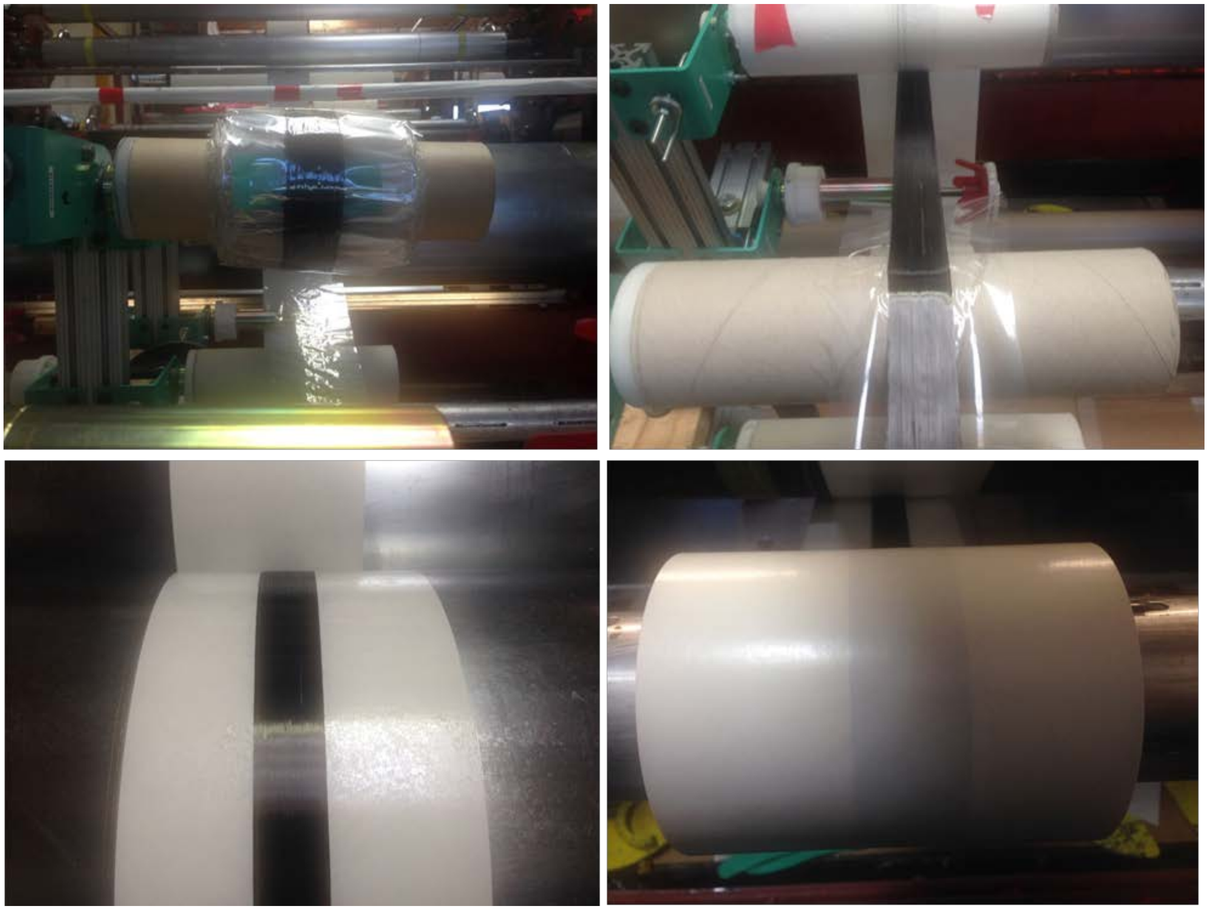

Figure 10. HS40/MR70/3831 prepreg fabrication at PMT.

Finally, the amount of prepreg that we got was just enough to make two 1 foot long, 1.2 in. wide, and 0.16 in. thick unidirectional panels.

For the first panel, the general hand layup process was used to make the laminate. But, since unidirectional prepreg tape had a lot of fiber waviness, the quality of the first panel was tremendously affected, and laminate had an excessive amount of fiber misalignment (Figure.11).

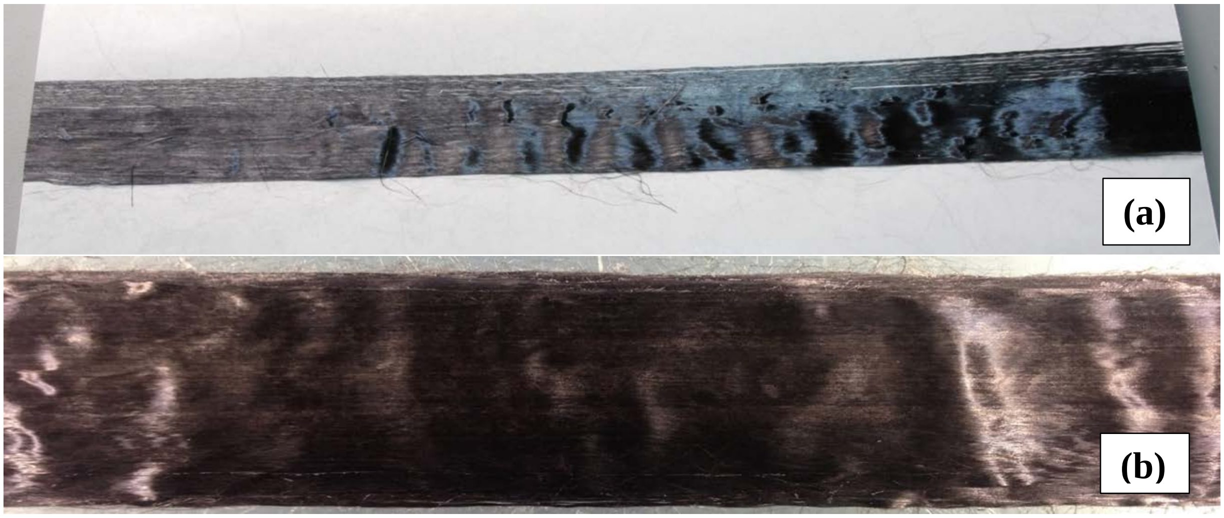

Figure 11. (a)Unidirectional prepreg tape (b) 1st laminate: fiber misalignment in the first panel affecting the layup quality

To reduce the amount of waviness in the second panel, the tooling was heated to reduce the resin viscosity and allow the plies to stretch. Then, the roller was used to roll away from the center of each ply to reduce the wrinkles in the layup process. Therefore, the layup quality of second composite panel was improved considerably (Fig.12).

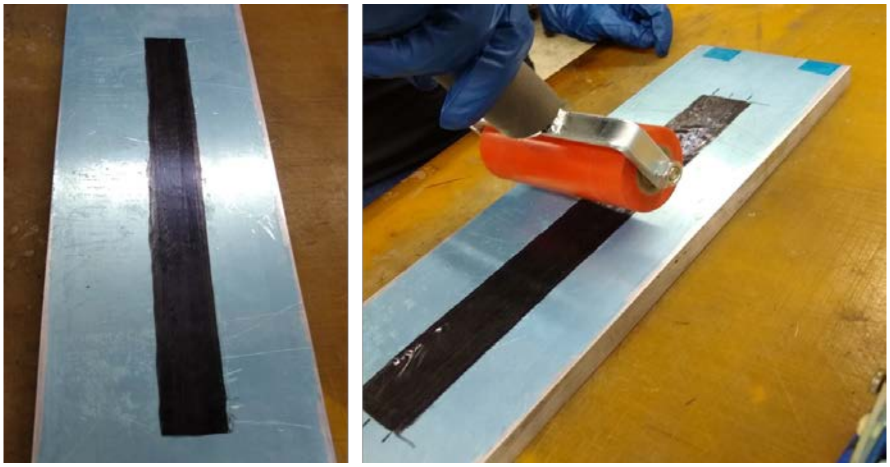

Figure 12. Layup process in the second unidirectional panel

Figure 13 shows the cured panel.

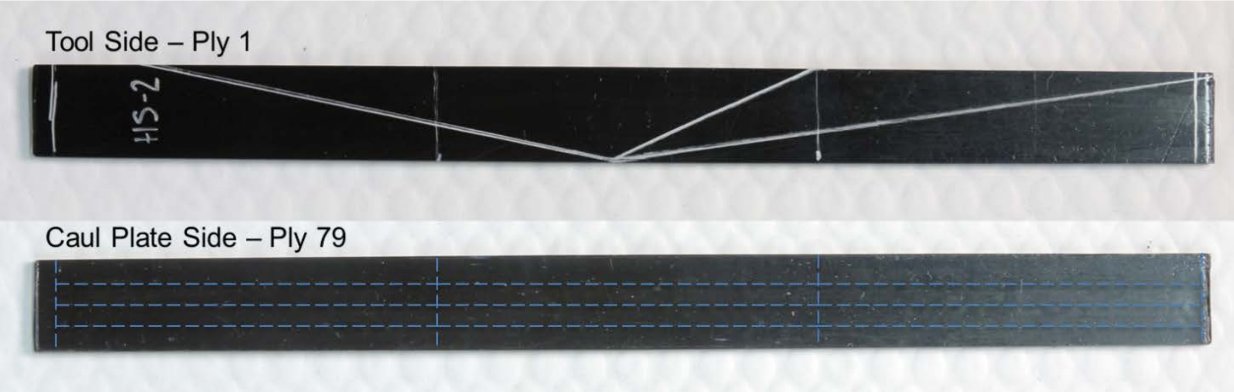

Figure 13.the cured HS40/MR70/3831 panel used in material characterization testing

Furthermore, as a result of the limited material availability, standard testing could not be performed to measure the material properties including axial modulus, shear modulus, and fiber-direction compressive strength. Therefore, our three-point bend test method based on Digital Image Correlation (DIC) was implemented to simultaneously measure these properties. Our DIC data-driven methodology to simultaneously assess axial and shear material properties has been well documented in literatures [47, 48, 49, 50]. Also, we have previously conducted a study on IM7/F7 carbon epoxy tape material system to determine a three-point bend test configuration that produces similar values of the fiber-direction compressive strength as SACMA SRM 1R-94 [45]. F7 epoxy resin is a 350° F curing equivalent of the F4A control resin developed by PMT as a basis for nanosilica reinforcement of the epoxy matrix.

In three-point bend test assessment, The support length to coupon thickness aspect ratio L/T and loading nose diameter was varied in order to minimize the shear stress near the loading nose and increase the fiber-direction compressive stress in order to produce compression failure which matches the SACMA SRM 1R-94 compressive strength. Figure 14 shows that L/T between 16 and 25 including:

(A) A 4 in. support length and 0.25 in. coupon thickness and width (L/T 16) with 2 in. loading nose diameter

(B) A 4 in. support length and 0.16 in. coupon thickness and width (L/T 25) with 0.5 in. loading nose diameter

Are the acceptable test configurations.

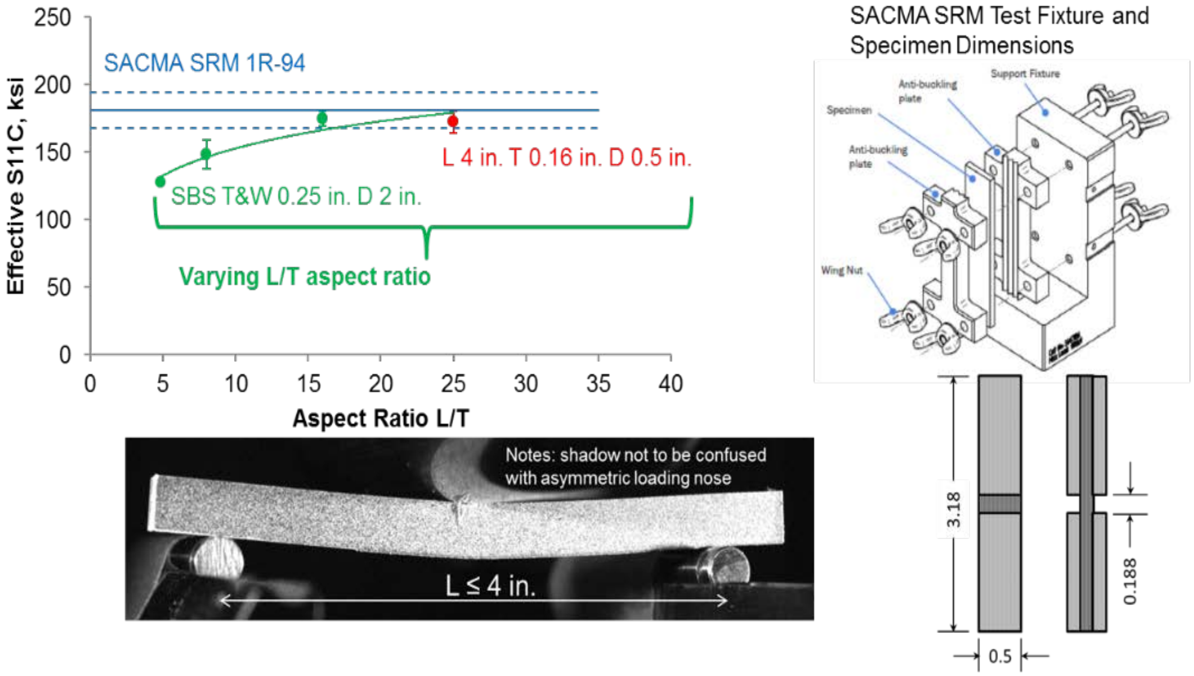

Figure 14. Test method for fiber direction compressive strength assessment

2.4 Mechanical testing:

For mechanical testing, six beams with a rectangular cross-section of 3.88 x 0.16 x 0.16 in. were extracted from the unidirectional cured HS40/MR70/3831 panel with the fibers parallel to the beam axis. 3.6 in support length with 0.5 in loading nose diameter were utilized. Specimens were placed in the ASTM D2344 test fixture, and the tests were carried out in an Instron E3000 electric load frame under stroke control at a constant cross-head speed of 0.05 in/min till failure. The applied load was continuously recorded during the test with the load cell of 2100 N, and the displacement was measured by means of DIC. All coupons failed in the middle of the specimen, and the average axial modulus value for the composite was 30.1Msi (COV 2%); the average shear modulus value is 1.02 Msi (COV 4%), and the average fiber-direction compressive strength value is 204 ksi (COV 5%). Therefore, the fiber direction compressive strength of the new hybrid HM composite move toward the strength of the IM carbon/epoxy legacy composites, while the axial modulus increased by 30% (Figure.10). Also, Figure 11 shows that fiber-direction compressive strength increases with increasing shear modulus to axial modulus ratio of composites.

Figure 15. Unidirectional coupons for mechanical testing. The coupon dimensions are 3.88 x 0.16 x 0.16 in. (99 x 4 x 4 mm).

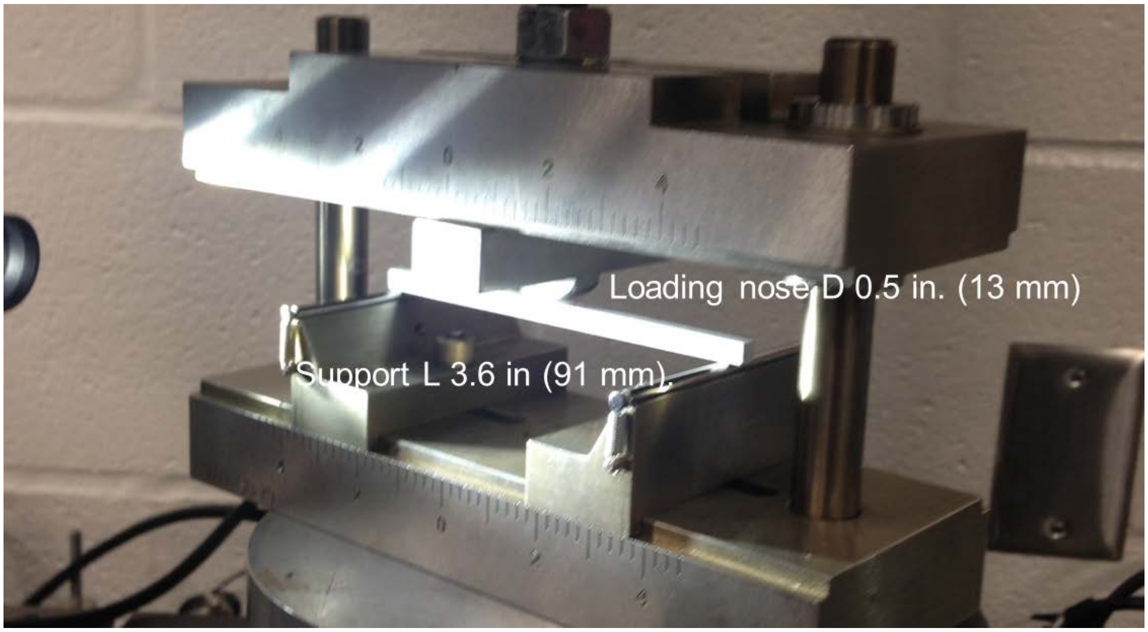

Figure 16. Three-point bend test setup.

It is worth noting that these results were achieved from the specimens with a significant amount of manufacturing defects and in-plane fiber misalignment. So, by improving the quality of the manufacturing and reducing the number of defects, superior properties can be obtained.Table.2 summarizes the material properties of the unidirectional carbon/epoxy tape composite material systems used in this effort including the new hybrid composite.

Table 2 Table 3. Material data for the unidirectional carbon/epoxy tape composite systems

Material	Ef, Msi	Er, Msi	Ec, Msi	Gc, Msi	Gc/Ec, %	Sc, ksi
IM7/913	40	0.492	23.4	0.717	3.06	223.9
HM63/913	64	0.492	32.2	0.674	2.09	145.9
IM7/F4A	40	N/A	23.1	0.69	2.99	183.9
HM63/F4A	64	N/A	34.4	0.514	1.49	137.3
IM7/F3G	40	0.893	24.8	0.932	3.76	240.5
HM63/F3G	64	0.893	34.3	0.847	2.47	157.2
HM/IM/3831	56.5 Avg	0.893	30.1	1.02	3.39	204

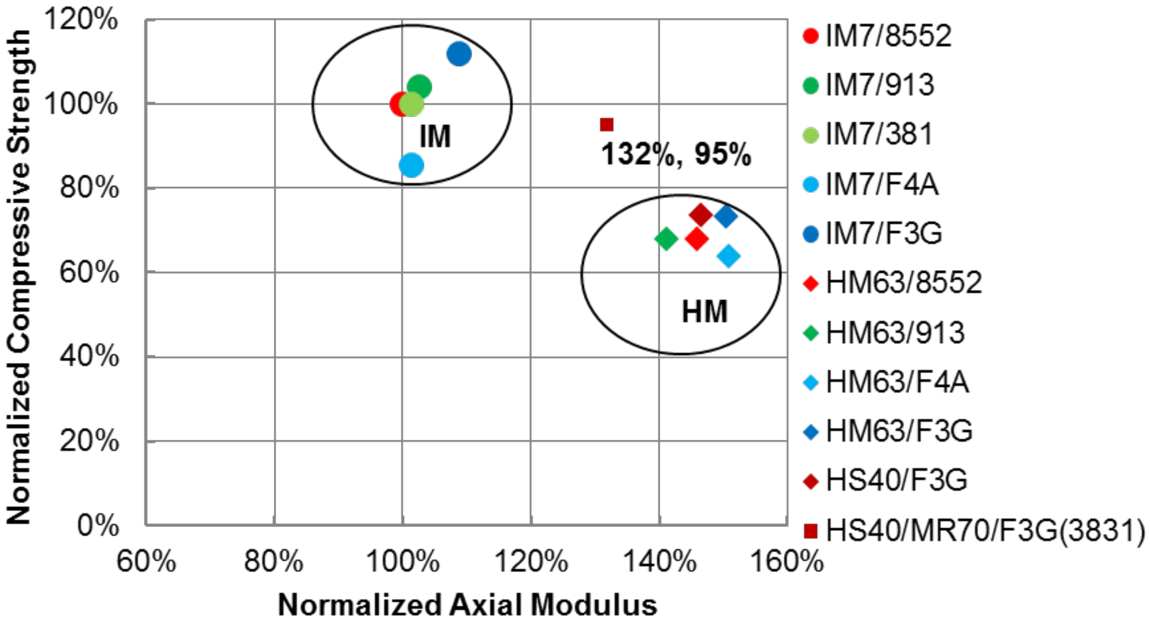

Figure 17. Compressive performance of tape composites. New hybrid HM carbon/epoxy material is approaching fiber-direction compressive strength of IM carbon legacy composites at more than 30% higher modulus.

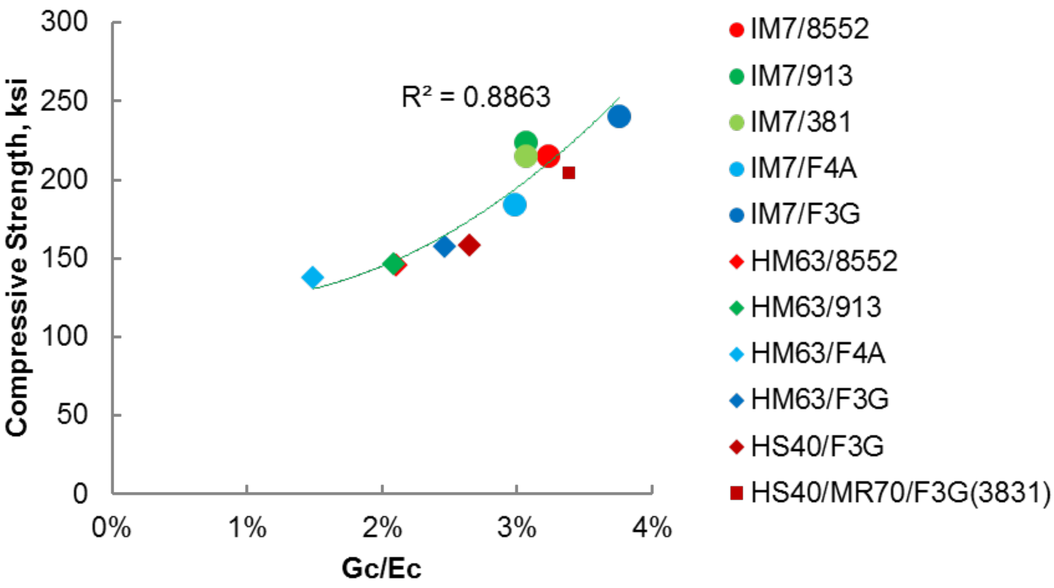

Figure 18. A relation between the shear modulus to axial modulus ratio and the fiber-direction compressive strength for the new composite material is consistent with the general trend. The compressive strength of the new material could be increased with reducing fiber waviness.

2.5 Concluding remarks:

The effort started from experiments with various IM and HM carbon-fiber / epoxy-matrix composites including those toughened with nanosilica. Observation of the compressive strength behavior across different fiber and resin combinations showed a remarkable trend that fiber-direction compressive strength increases with increasing the shear modulus to axial modulus ratio of composite material systems. This observation inspired attempts of hybridizing carbon fibers with varying moduli for the desired improvement of compressive strength. The results, shown in Figure 17, demonstrate that the new hybrid material approaching fiber-direction compressive strength of IM carbon legacy composites at more than 30% higher modulus [1]. So, comingling IM and HM fibers at filament level in addition to the matrix nano-sized structural reinforcement throughout the composite provides additional support to HM fibers, increasing shear modulus to axial modulus ratio of the composite material and therefore improve microstructural stability which leads to fiber-direction compressive strength behavior.

CHAPTER 3

Micromechanical characterization of composite constituents

Nanoindentation is one of the common testing techniques to determine the properties of the material in micro or nanoscale. We will use this method to provide accurate input parameters for micromechanical modeling of a composite. In this chapter, an innovative micromechanical characterization technique is developed to measure the properties of the laminate constituents within the actual composite ply. The developed technique will eventually be employed to obtain the matrix and interface properties of the new composite material.

3.1 Background:

Nanoindentation is a testing technique for characterization of the mechanical properties of a vast range of materials in micro or nanoscale. During the nanoindentation, a very small diamond tip is pressed into the flat, polished, defect free sample surface. The load in the tip is increased as it penetrates and the applied load and the displacement into the surface are continuously recorded to generate the load-displacement curve. Mechanical properties can be directly extracted from the load–displacement curves; data of one complete cycle of loading and unloading; without additional characterization of the residual imprints [51, 52]. Originally, indentation experiments were used to measure hardness of a material, until Ternovskii et al. [53] introduced the stiffness equation to measure the reduced modulus by using the measured load-displacement data. The stiffness equation is

$$S = \frac{dP}{dh} = \frac{2E_r\sqrt{A}}{\sqrt{\pi}} \tag{3-1}$$

Where S is the stiffness in the contact between the indenter and the specimen, which is equal to the slope of the upper portion of the unloading data, E_r is the reduced modulus for the material, and A is the projected contact area of the indent measured from the indentation hardness impression.

It is worth noting that equation (3-1) is derived based on the elastic contact theory [54]. Nanoindentation experiment evaluate the reduced modulus of the material instead of the elastic modulus. Reduced modulus is combination of indenter modulus and sample modulus (equation.3-2). As a result, elastic modulus of the sample being tested can be calculated from the reduced modulus. Definition of the reduced elastic modulus of the indentation test (E_r), which includes the effects of non-rigid indenters on the load-displacement behavior is

$$\frac{1}{E_r} = \frac{1-\nu_s^2}{E_s} + \frac{1-\nu_i^2}{E_i} \qquad (3\text{-}2)$$

Where E_i and ν_i are elastic modulus and Poisson's ratio of the indenter tip respectively and E_s and ν_s represent the corresponding quantities of the specimen.

In 1992, Oliver and Pharr [52] demonstrated that nanoindentation can also be used as a technique to extract elastic material properties of materials. According to their research, stiffness equation can be applied to all axisymmetric indenters with any infinitely smooth profile. Their proposed procedure to extract material properties from load-displacement curves became the most common and well-known technique being used to extract the reduced modulus information for most commercial nanoindenters. Accurate calibration of the tip area function and frame compliance of the instrument are the main requirements of Oliver and Pharr method toward achieving precise results from nanoindentation test. The tip area function is calculated by indenting into a known material such as quartz or fused-silica at different loads. Then these data will be fitted so that the area matches the correct value for the reduced modulus of the material.

Furthermore, since slope of the unloading curve is how the reduced modulus is being calculated, small change in the frame compliance of the instrument can significantly affect the measurement of reduced modulus. Therefore, accurate calibration of the frame compliance can help with more precise measurements. The frame compliance calibration is performed by conducting several high load indents into quartz or steel sample to measure how much the nanoindentation instrument compress during an indent.

The nanoindentation system applies load to the indenter tip to force the tip into the surface while simultaneously superimposing an oscillating force with a force amplitude which is normally several order of magnitude smaller than the nominal load. This technique allow us to accurately measure contact stiffness at all depth. Moreover, stiffness values enable us to calculate the contact radius at any depth with more precision.

Furthermore, this technique assumes that the depth of the material in contact with the indenter tip is less than the maximum indentation depth through this equation:

$$h_c = h_{max} - \varepsilon \frac{P_{max}}{S} \tag{3-3}$$

Where ε is a geometric constant that depends on indenter geometry. It is equal to 0.75 for a Berkovich tip, 0.72 for a conical indenter and 1 for a flat punch.

On the other hand, hardness of the materials can be determined as follow:

$$H = \frac{P_{max}}{A} \tag{3-4}$$

Where P_{max} is the maximum load on the indenter tip and A is a projected contact area which is a function of contact depth.

The indenter area function, A, is calculated using the unloading curve. It is based on the proposed assumption of Oliver.et al [52] that the elastic modulus is independent of the indentation depth. Then, by modelling the load frame and specimen as two spring attached in series and rewriting equation (3-1) with respect to the total measured compliance, the contact area can be described as:

$$A = \frac{\pi}{4}\frac{1}{{E_r}^2}\frac{1}{(c-c_f)^2} \tag{3-5}$$

$$c = c_s + c_f \tag{3-6}$$

Where C is total measured compliance, c_s is the compliance of the specimen and c_f represents machine compliance.

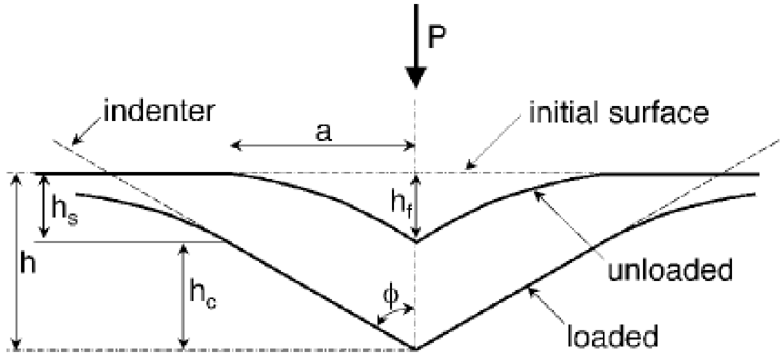

Figure 19. schematic illustration of the unloading process showing parameters characterizing the contact geometry [55]

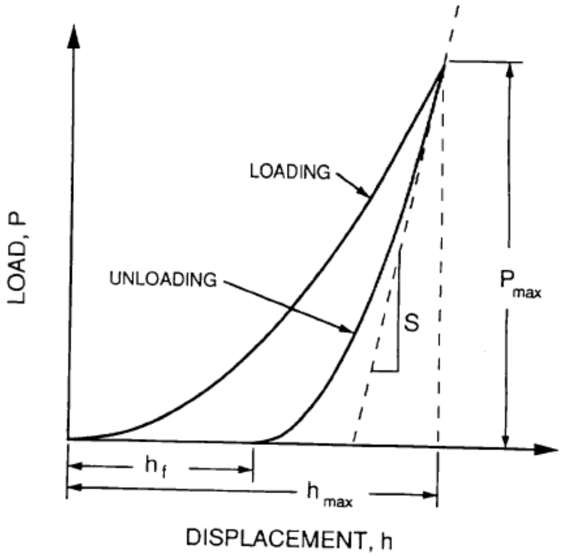

Figure 20. A schematic representation of load versus indenter displacement data for an indentation experiment. The quantities shown are Pmax : the peak indentation load; hm.dX: the indenter displacement at peak load; hf. the final depth of the contact impression after unloading; and S: the initial unloading stiffness [52]

3.2 Matrix characterization:

Mechanical characterization of the matrix can be determined with performing nanoindentation test into the resin pockets on a polished cross-section of the composite materials. It is important for the resin rich area to be sufficiently far from the fibers to avoid the constraining stiffening effect of the fibers on matrix properties.

To characterize matrix properties, Hysitron Ti 950 triboindenter was chosen to conduct the tests and a Berkovich diamond tip was used to perform indentations (Fig.21). The following epoxy matrices were studied in this effort : (1) 350 °F curing Hexcel 8552 [44] which is common in aircraft applications and (2) 250 °F curing PMT epoxy resin with 40% nanosilica weight content.

In the first attempt, four nanoindentation with different indentation depths of 220, 370, 540 and 700 nm were conducted on 8552 epoxy matrix. The load was held at maximum displacement for 10 s to reduce the creep deformation upon unloading; which can induce inaccurate prediction of the material properties [56]. The applied load and the displacement into the surface were continuously recorded during the test to obtain the load-displacement curves (Figure.23b).

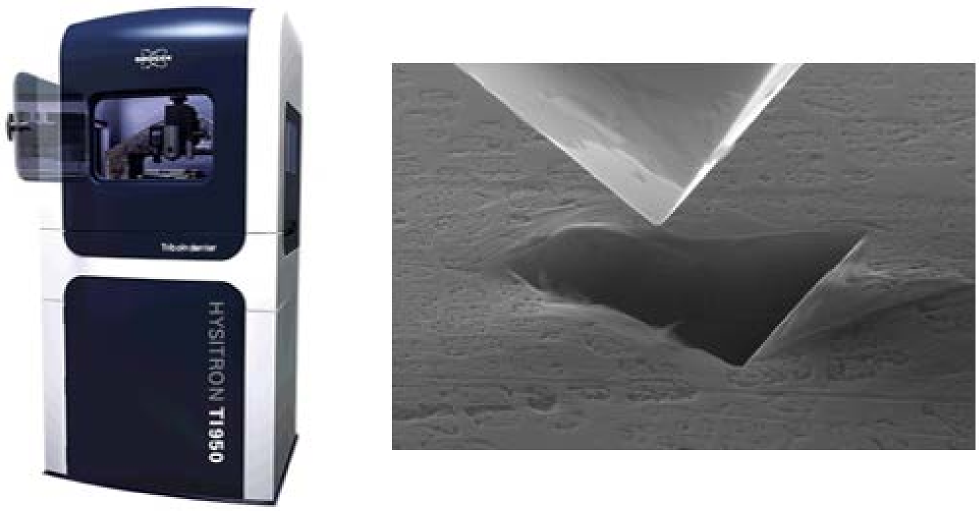

(a) (b)

Figure 21. a) Hysitron TI950 Nanoindentation test machine [57] , b) SEM micrograph of the Berkovich tip [58]

The reduced elastic modulus extracted from the machine was equal to 6.7 GPa (0.97 Msi) with COV of 8% (Figure.23b). Then the elastic modulus was determined by following the procedure indicated above (equation (3-2)). The averaged measured elastic modulus of the 8552 matrix was 5.71 GPa (0.82 Msi).This value of matrix modulus is higher than experimental value provided by the supplier (0.677 Msi). The difference obtained can attributed to the complex stress state surrounding the indentation area or the constraint effects of the fibers around the resin pocket. One approach to improve such effect is to identify and indent on the bigger resin pockets.

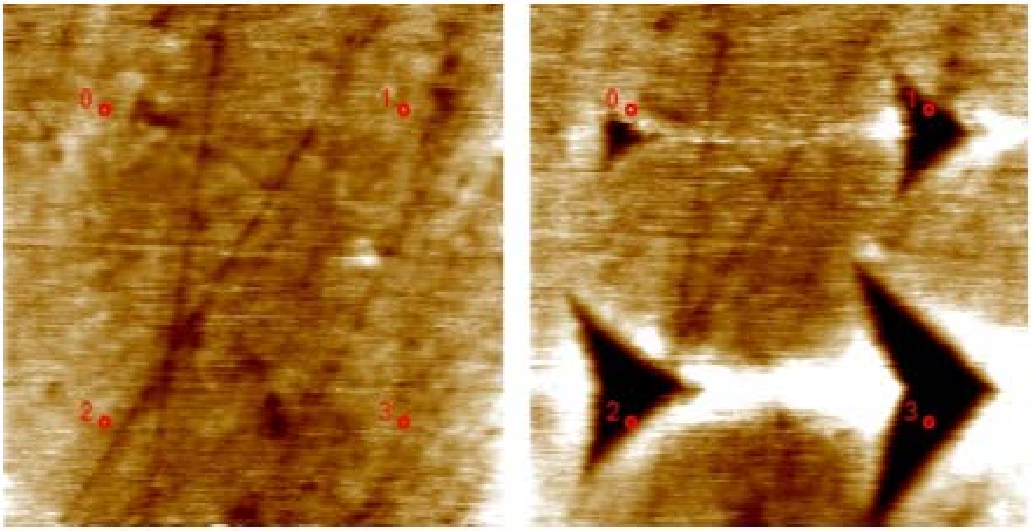

(a) (b)

Figure 22. Optical microscopy image of the nanoindentations in a resin pocket
a) Before indentation, b) After indentation

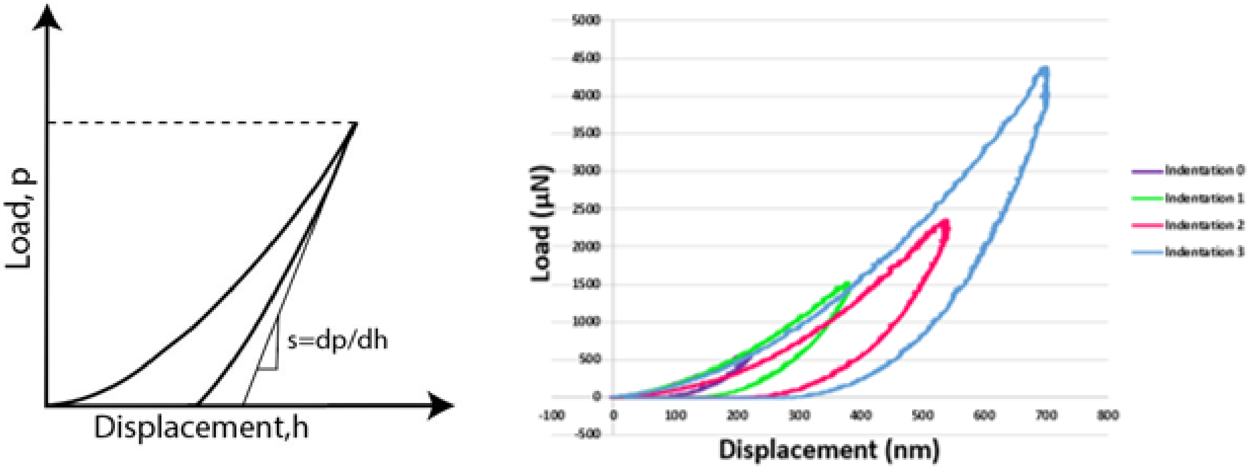

(a) (b)

Figure 23. a) Schematic of a typical indentation load-displacement data, b) Load vs. displacement curves for indentations test with various depth in the 8552 epoxy resin.

On the other hand, according to some literature [3], increasing the applied load by the indenter to create a deep imprint can lead to an inaccurate measurement of the matrix properties. Because, as the indentation depth increases, the matrix thermal residual stresses generated during the manufacturing process will start to interfere with accurate measurement of the properties. Therefore, In order to investigate this assumption, new experiments under displacement control mode was performed on the same epoxy matrix. While the maximum indentation depth was increased to 2000 nm.

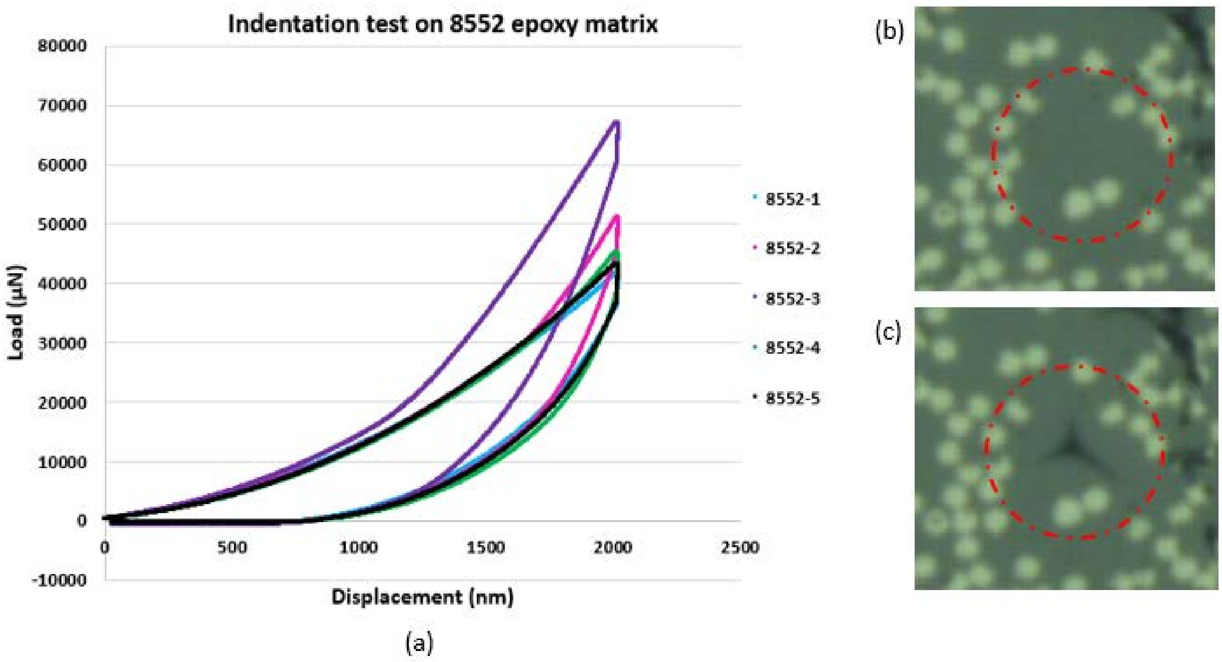

Figure 24. a) Load vs. displacement curves for indentations test in the 8552 epoxy resin, b) optical micrograph of the resin pocket before indentation, c) optical micrograph of the resin pocket after indentation

Figure 24, summarized the load-displacement (indentation depth) curves for the tests on 8552 epoxy matrix. Average reduced modulus of the 8552 epoxy matrix from these tests was 6.85 Gpa (0.99 Msi) with COV of 11%. This value provides the elastic modulus of 5.84 Gpa (0.84 Msi). The measured value of the modulus is in a good agreement with the results presented before with small indentation depth experiments. Therefore, it can be concluded that the extracted matrix properties would not be affected by the depth of indentation.

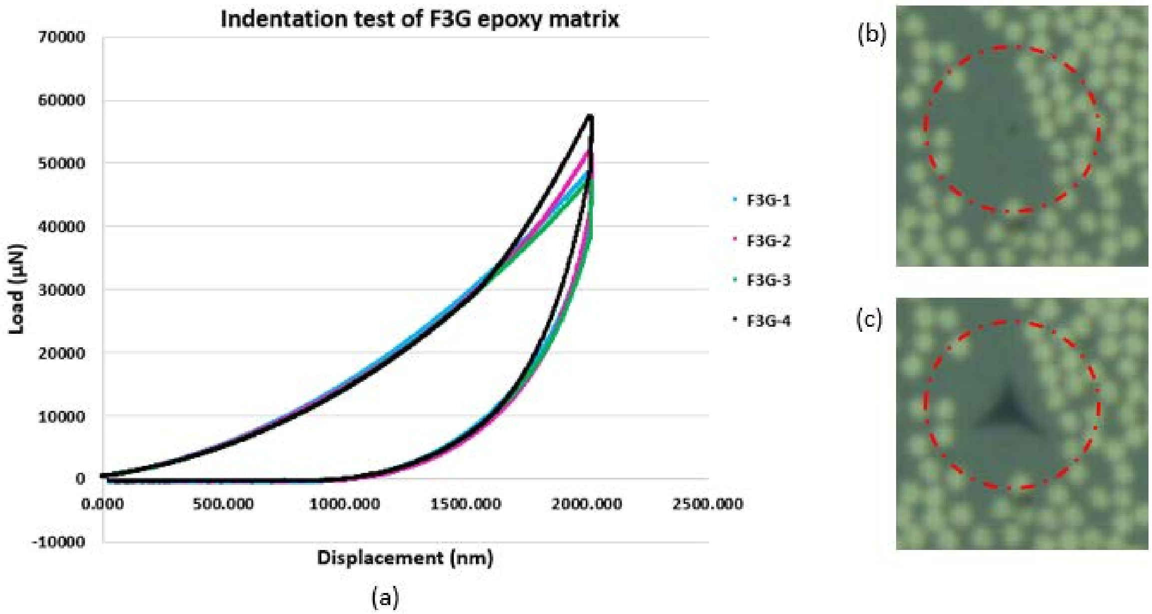

Figure 25. a) Load vs. displacement curves for indentations test in the F3G epoxy resin (250 °F curing PMT epoxy resin with 40% nanosilica), b) optical micrograph of the resin pocket before indentation, c) optical micrograph of the resin pocket after indentation

The same experiment was conducted on F3G epoxy resin. The reduced elastic modulus of the reinforced matrix was 9.87 Gpa (1.4 Msi) which would generate the elastic modulus of 8.44 Gpa (1.2 Msi).

3.3 Fiber/matrix interface characterization:

In fact, diffusion and subsequent chemical reaction between the fiber sizing and the resin during the curing procedure create a layer between fiber and matrix. This layer with finite thickness and different mechanical, chemical and physical properties than those of fiber and matrix, is known as interface [59]. The performance of CFRP composites are significantly controlled by the properties of the fiber–matrix interface, in particular, interface strength and toughness. Good interfacial bonding can help efficient load transfer from the matrix to the reinforcement, which helps to reduce stress concentrations and improve overall mechanical properties. Fracture toughness, fatigue life, compressive strength, strain to failure and impact properties are mainly sensitive to the strength of the fiber–matrix interface.

Several studies have confirmed the importance of interface properties on the overall performance of a composite material. For instance, Favre and Merienne [60] studied the interface properties of various carbon fiber composites at micro- and macro-scale. It was empirically illustrated that the interlaminar shear strength (ILSS) of the composite is proportional to the square root of interfacial shear strength (IFSS). Then, Mader et al. [61] presented a linear relation between ILSS of continuous fiber-reinforced composite and IFSS measured through single fiber pull out tests on different carbon fiber/epoxy system. Later on, Gao et al. [62] established a linear relationship between the interfacial shear strength (IFSS) obtained from macromechanical quasi-static punch shear test and the micromechanical microdroplet test on wide range of fiber sizing composite laminates, fabricated from the same constituents.

Later on, in the microbuckling model developed by Dharan and Lin [33], the thickness and mechanical properties of the interphase was integrated into the model to generate a three-phase buckling model to estimate the compressive strength of composites and compare their model predictions to experimental data from literature and the pioneer microbuckling model of Dow and Rosen [9, 63, 19]. Dow and Rosen’s model is one of the well-known theories based on fiber microbuckling where the fibers are modeled as columns held together by the shear stiffness of the matrix, following stability equations developed by Timoshenko [64]. However, composite compression strength value achieved with Rosen’s theoretical method is significantly higher than the measured strengths from experiments. While, the model developed by Dharan et al. [33] verifies that integration of interphase layer to the model can help with more accurate prediction of the compressive strength behavior of typical high-performance composites and should not be ignored.

Furthermore, Madhukar and Drzal [31] experimentally quantified the relationship between fiber-matrix adhesion with the compressive properties and failure modes of unidirectional carbon fiber reinforced polymer (CFRP) composites. They used three identical sets of composites with different fiber-to-matrix interface shear strength properties. The interfacial shear strength was modified by changing the fiber surface treatment. The results show that compressive strength of CFRP containing the high-strength IM carbon fibers is highly dependent on fiber surface treatment. In addition, regarding the failure modes, it was observed that when the fiber-matrix bonding is poor, failure occurs by delamination. While increase in the interfacial strength leads to shear failure driven by in-phase microbuckling of the fibers. The same results were observed by Ha and Nairn [32].

This brief overview shows the importance of interfaces properties on the performance of composite material, specifically in fiber direction compressive strength behavior. Despite the importance of this topic, there is not any standard test technique available to accurately characterize the interface mechanical properties. For independent measurement of the interface response to stress, several micromechanical tests have been developed. Different tests can generate results that do not correlate with the other techniques. This variation can attribute to the differences in the specimen geometries, loading conditions, and developed stress states between the test methods [65]. None of these test methods are ideal, and they have their own pros and cons which should be considered in advance, to select the adequate one for a specific purpose.

Generally, mechanical test methods to characterize and evaluate the properties of the fiber-matrix interface can be broadly divided into two groups:

1. Mechanical testing performed on single fiber specimens; such as:
    - Single fiber compression test [66]
    - Fragmentation test [67, 68, 69, 70]
    - Pull out test [71]
    - Microdroplet test [72, 73]
2. Mechanical testing performed on the actual composite coupons; such as:
    - Fiber Push-in test [74, 75]
    - Fiber Push-out test [74, 75]
    - Slice compression test [66]

One of the main challenges in the first group of testing is in the preparation of the single fiber specimen specifically for these test methods. Not only it has required additional time to prepare the samples, but also it can be expensive. On the other hand, the local environment in these samples is not representative of the mechanical conditions of actual composites. For instance, the fiber packing density, the thermal residual stresses and the polymer cross-linking density may be very different, which can make a significant change in the interface properties [76]. Therefore, to overcome these difficulties, the second group of testing techniques were proposed. They can be carried out on a specimen of the real composite. Push-in and push-out test are the most common methods among this group.

The most commonly used micromechanical tests are summarized below.

Fragmentation test:

A pre-tensioned single fiber is placed along the center of a dog-bone shaped specimen which is then filled with matrix and subsequently cured. As the specimen is loaded in tension, the fiber will progressively start to fail into shorter and shorter lengths until a saturation level is reached and the fiber can no longer break. The tensile load is transferred to the fiber through shear traction at the fiber-matrix interface. The tensile load in the fiber progressively increases up to the fiber critical stress, which eventually causes the fiber fracture. The process continues until the fiber segments are small enough that shear transferred along their length cannot break them anymore. The main requirement of this test specimen is that the strain to failure of the matrix needs to be at least three times that of the fiber to facilitate fiber fragmentation. The maximum fiber length is called the critical length and is used to calculate the IFSS, using Kelly-Tyson's model [67]. Moreover, the accurate measurement of the critical fiber length and estimation of the critical fiber stress is crucial for precise IFSS measurement and is usually obtained through linear extrapolation of the experimental data of single-fiber tests at longer gage length [68, 69]. Therefore the interfacial shear strength is calculated indirectly. The fragmentation test is adequate for composites with ductile matrices and brittle fibers [77, 70].

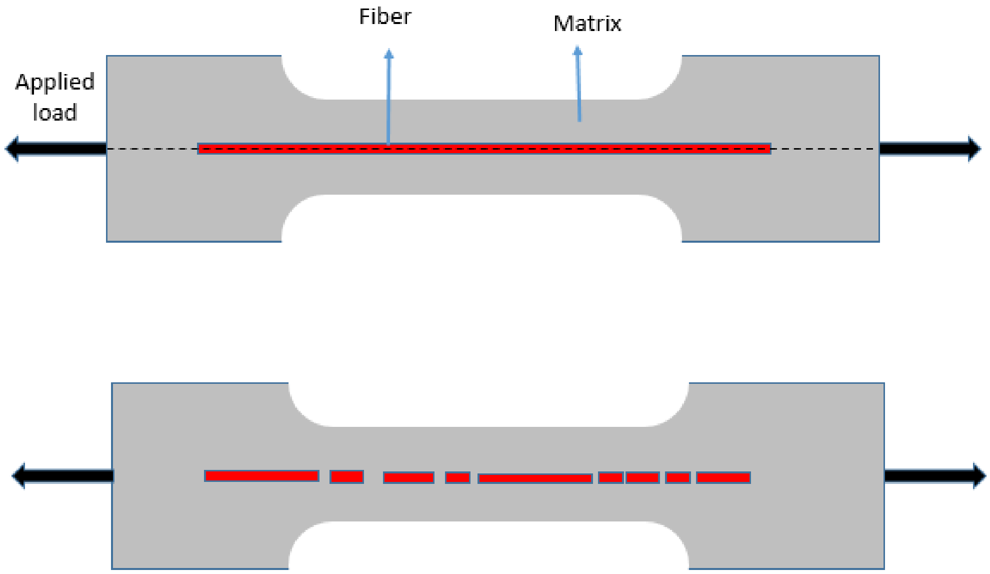

Figure 26. Schematic illustration of the fragmentation test

Micro-droplet test:

This test method was initially developed by Miller et al. [72]. The test specimen consists of a single droplet of resin matrix placed and cured on a single fiber to create a fiber-matrix interface. During the test, one of the fiber free ends of the microdroplet specimen is attached to a load cell to measure the force. The droplet is positioned under a set of blades. Usually, blades have prismatic geometry in order to make non-axisymmetric stress state in the microdroplet specimen. The blades translates downward at a controlled rate during the test to shear the matrix droplet from the fiber to shear-off the droplet such that the failure occurs along the interface. The average IFSS measured in this test set-up is geometry dependent and decreases as the droplet size (embedded length) increase.

The advantage of this test method is that it allows complete interface debonding followed by large scale sliding which enables the measurement of absorbed energy due to both debonding and frictional sliding. The disadvantage of this test include the formation of small enough droplets to ensure that the embedded fiber length is less than the critical length, to avoid fiber fracture.

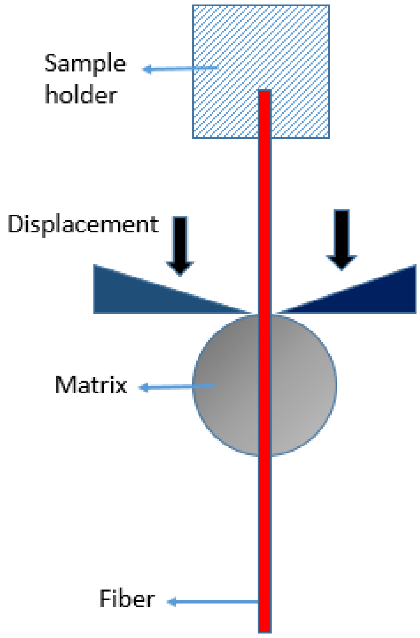

Figure 27. Schematic illustration of the microdroplet test

Fiber pull-out test:

This test is based on pulling out a partially embedded fiber from a resin specimen. A single fiber is partially embedded in a block of matrix such that the fiber's longitudinal axis is perpendicular to the free-surface of the matrix. The load is transferred from the fiber to the interface. Then, decohesion happens when the maximum shear stress of the interface is reached. During the test, the load and extension is recorded as the fiber is pulled from the matrix. The IFSS is calculated from the load data and the embedded fiber surface area. Disadvantage of this method is in controlling the embedded fiber orientation and fiber length. In addition, the debonding force depends on the embedded fiber length. The pull-out test provide good results for experiments with tough fibers embedded in a brittle matrix [71]..

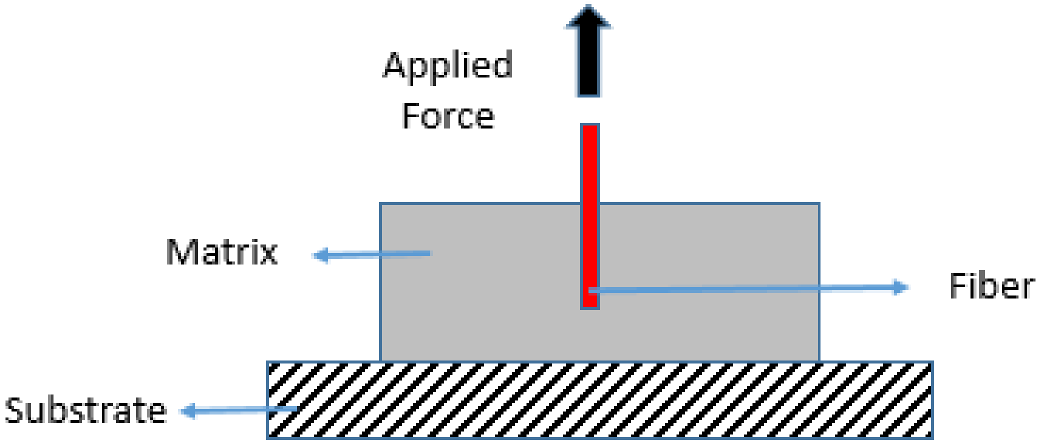

Figure 28. Schematic illustation of the pull-out test

Fiber push-in test:

In the push-in test, a single fiber is pushed in with nanoindentor on a cross-section of a bulk specimen from the unidirectional laminate until interface decohesion occurs. The main advantage of this technique is that it does not require any difficult sample preparation, but the interpretation of the results can be difficult since the length of the debonded interface below the surface is not known. Thus, the results should be analyzed in terms of a shear lag model or FE simulations of the test [56].

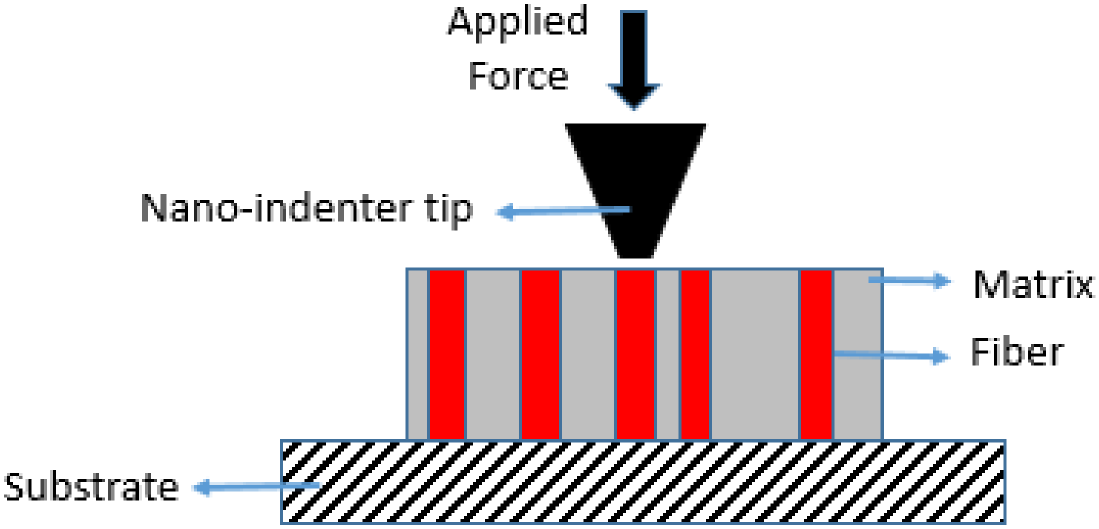

Figure 29. Schematic illustration of the push-in test

In this work, push-out test is selected to evaluate the strength of the fiber-matrix interface.

3.4 Fiber push-out test:

In general, to prepare the specimens for the push-out test, very thin slice transversal to the fibers are cut from the composite panel which are thinned by lapping and polishing process up to the desired thickness. The thickness of these samples should be between 20-100 µm. These specimens are thin enough to allow decohesion over the entire interface and the complete push out of the fiber. Next, sample is placed on the support with the groove of around 20-50 µm width.

The purpose of the groove is to provide room for fiber extraction .Then, the specimen is mounted in the nanoindenter equipped with a flat-punch tip. An indenter is used to apply force to the single fiber end. Subsequently, the indentation tests are performed until the fibers are completely pushed out of the specimen (Figure.30&31) [78, 69, 79, 74]. During the test, the load and depth of indentation are continuously recorded. Then, by measuring the maximum applied load P_{max}, where debonding occurs, fiber length (the thickness of the specimen) h, and fiber radius r, the interfacial shear strength can be calculated.

$$IFSS=\frac{Pmax}{2\pi rh} \tag{3-7}$$

One of the advantage of the fiber push-out test compared to the other methods is a relative simplicity of the testing process, in addition to the capability of making more direct measurement of the interface strength [80]. Also, since push-out specimens are required to be very thin, constant interface shear stress along the entire fiber length (specimen thickness) can be assumed.

Therefore, calculation of the IFSS can be done without FE simulations [81, 82]. However, specimen fabrication for the fiber push-out experiment has been a standing challenge [83]. As it was mentioned before, the specimen has to be thin enough to ensure complete push out of the fiber from the material. Preparing such thin Samples has been challenging as they tend to fracture during polishing, and it is very difficult to meet their constant thickness.

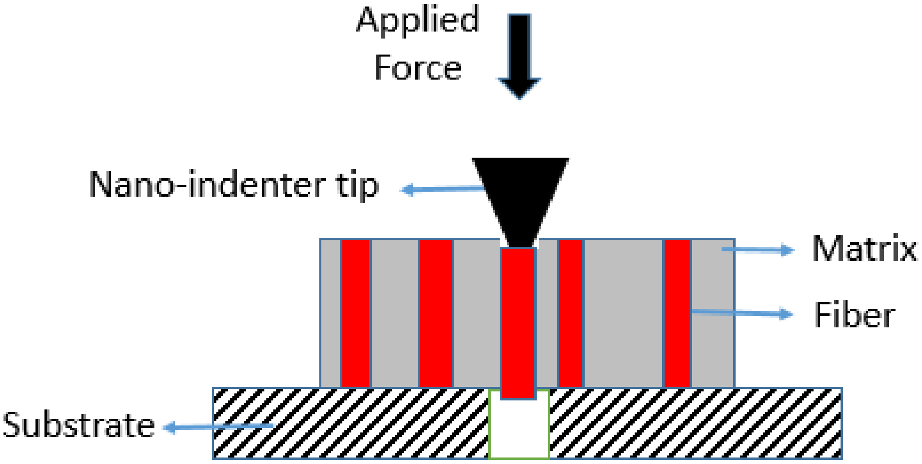

Figure 30. Schematic illustration of the push-out test

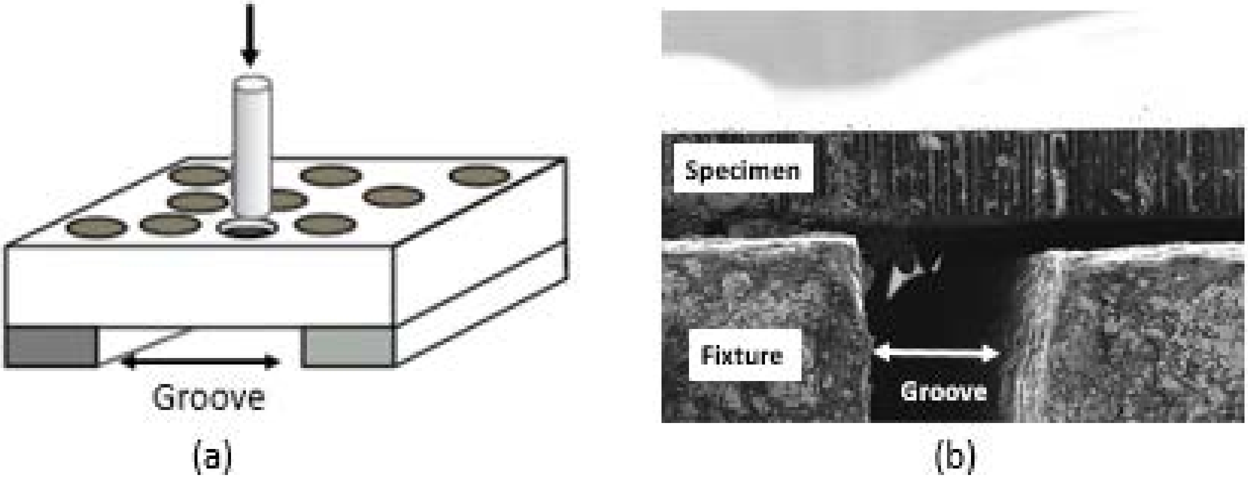

(a)

(b)

Figure 31. a) Schematic illustration of the general push-out test sample, b) SEM micrograph of a push-out sample mounted on the fixture.

Moreover, in order to avoid damaging the samples due to un-flat surface at the initial stage of polishing or breaking specimens as they get thinned, lapping and polishing process needs to be done slowly with applying minimum amount of load. Therefore, it requires significant amount of time to gradually grind the samples down to the desired thickness. Furthermore, the samples are typically not perfectly flat especially at the edges, and they are not in full contact with the fixture before the test which can creating compliance artifacts [65]. In general, specimen should be secured on the fixture perfectly flat to eliminate or reduce any compliance artifact. This procedure can be challenging since fixing the edges of the sample to the fixture cannot ensure close contact of a specimen to the substrate right above the groove. As a result, elimination of the compliance cannot be guaranteed. To address these standing challenges and improve the consistency of the samples, we have been investigating sample machining by femtosecond (fs) laser ablation to create high-quality samples for the fiber push-out tests.

3.5 New technique for specimen fabrication:

Recently, ultrafast lasers are finding application in drilling and cutting of high precision holes without thermally damaging the sample. When laser beam hits the surface of the sample, part of the beam will be absorbed by material which leads to heat generation and material removal by various mechanisms including melting, vaporizing, etc. [84]. A major challenge in material laser processing is reduction or elimination of the heat affected zone (HAZ). The extent of HAZ depends upon the laser–material interaction time. Ultra-short pulse lasers such as fs-lasers, release high pulse energy in a very short time hence most of the laser beam energy can be used for directly removing (evaporating) the target material without collateral damage to surroundings. In other words, fs-laser machining reduces the heat diffusion into the adjacent material, resulting in high-quality machining with negligible HAZ and microstructural disruption [85, 86, 87, 88, 89, 90, 91]. Also, since the material is being removed by direct vaporization away from the surface, the formation of the recast layer can be avoided as well [92].

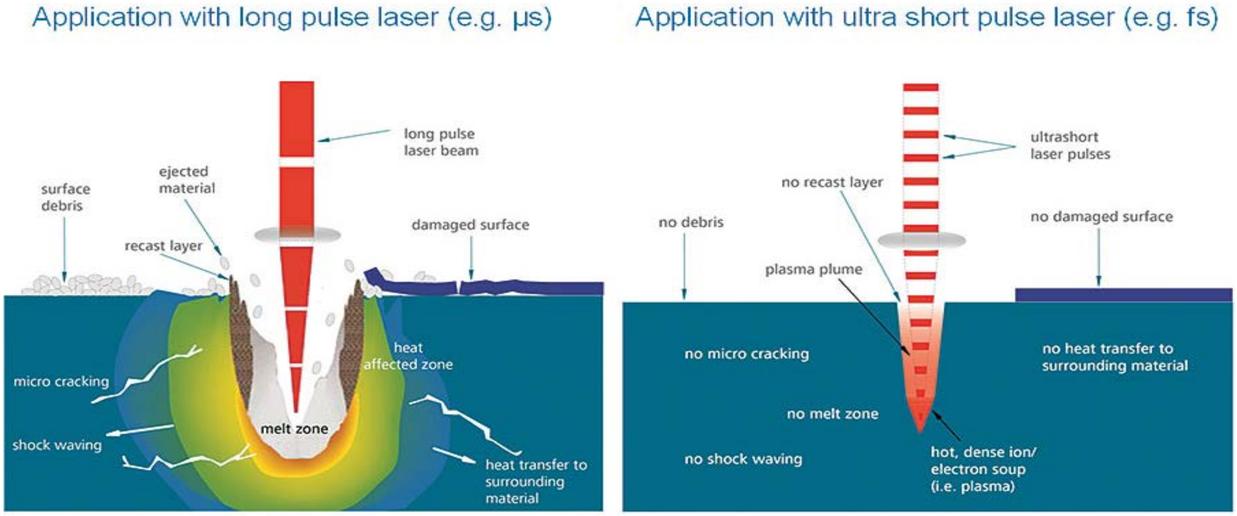

Figure 32. Comparison between microsecond and a femtosecond laser [92].

To prepare sample with laser machining technique, after polishing the top surface of the specimen, perpendicular to the fibers, fs-laser will be used to remove the material in the transverse direction close to the edge, creating a milled out section underneath the polished surface, with the intention of constructing a thin membrane. This thin membrane forms a fiber push-out specimen as shown in Fig. 33.

To experimentally verify the validity of the new proposed procedure of sample fabrication for fiber-push-out test, set of experiments were performed on general push-out samples and laser machined specimens.

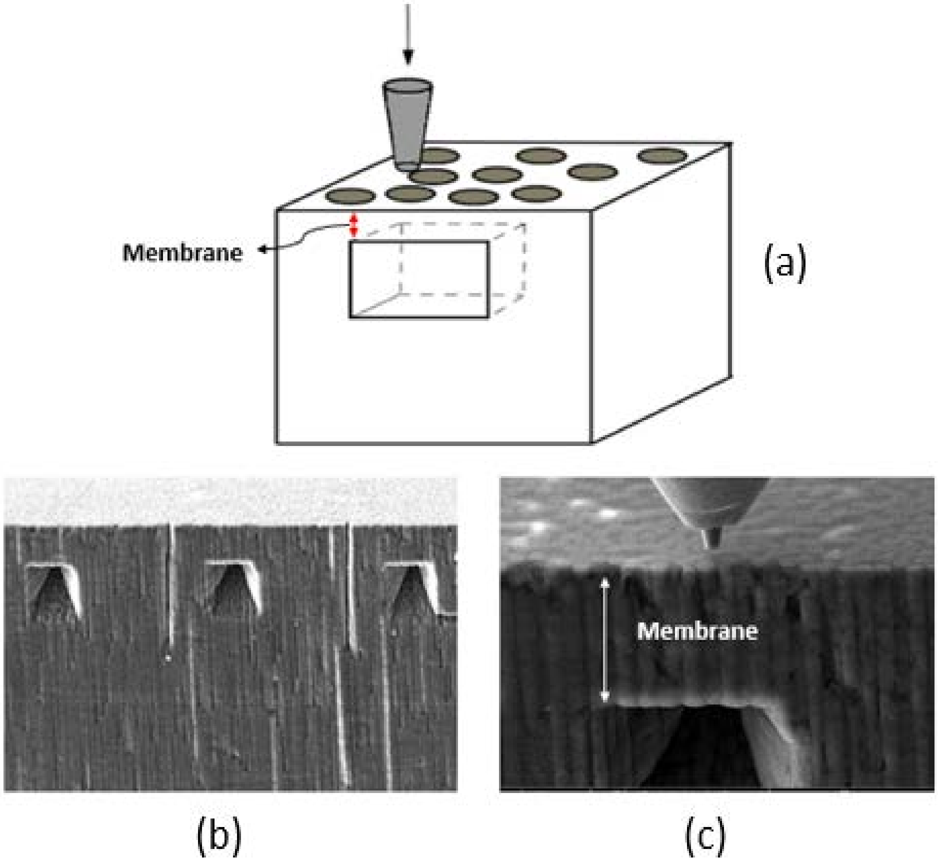

Figure 33. a) Schematic of the push-out sample prepared with laser machining technique, b& c) SEM images of the sample before the test.

3.6 Material and Sample Preparation:

The materials investigated in this study are (1) HM63/8552 HM carbon-fiber composites and (2) Intermediate modulus carbon fiber composite with the same toughened epoxy matrix.

In addition, in order to ensure consistent fiber-matrix interface shear strength assessment, fiber push-out experiments were carried out on IM CFRP specimens of two thicknesses – 30 µm and 60 µm.

For the general push-out samples (free-standing samples) small rectangular pieces with a nominal dimension of 6 x 6 x 6 mm were cut from the unidirectional composite panel. These slices were fixed on a sample mounting stub of the disk grinder with thermoplastic mounting wax (crystalbond). Then samples were thinned to 150 µm thickness by grinding them with 600 grit silicon carbide sand paper. Followed by lapping and polished with a series of decreasing grain sizes diamond papers of 15, 9, 3, and 1-micron, until the desired thickness was achieved and no scratches were seen under optical microscope. After removing the sample from grinder stub, specimen with fibers oriented in the thickness (normal) direction were mounted on a custom fixture with a groove of 50 or 100 μm width engraved on the surface of it, depending on the specimen thickness. The groove is wide enough to provide enough space for fiber extraction, while limiting specimen bending. The outer part of the samples were fixed on the fixture by silver glue or carbon/copper conductive tape to hold the samples in place and ensure close contact to the substrate (Figure.35).

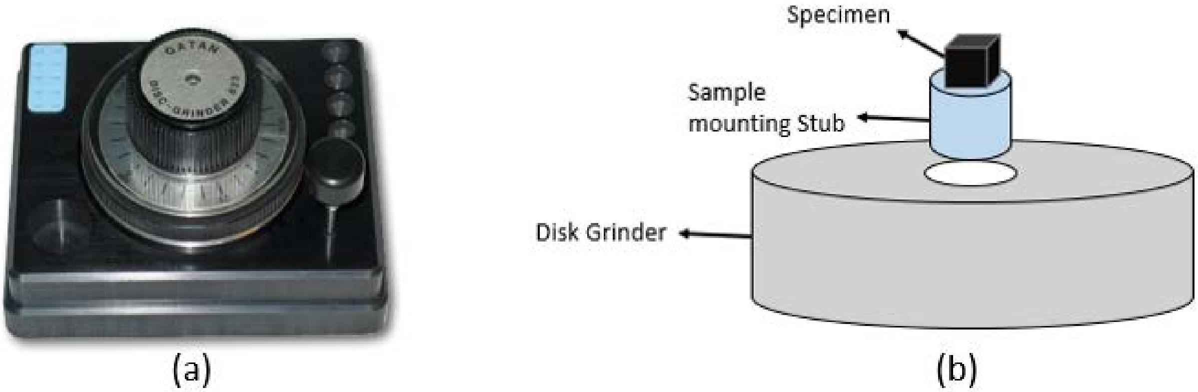

Figure 34. a) Disk grinder to prepare thin sample for push-out test, b) Schematic illustration of the sample mounting in the disk grinder

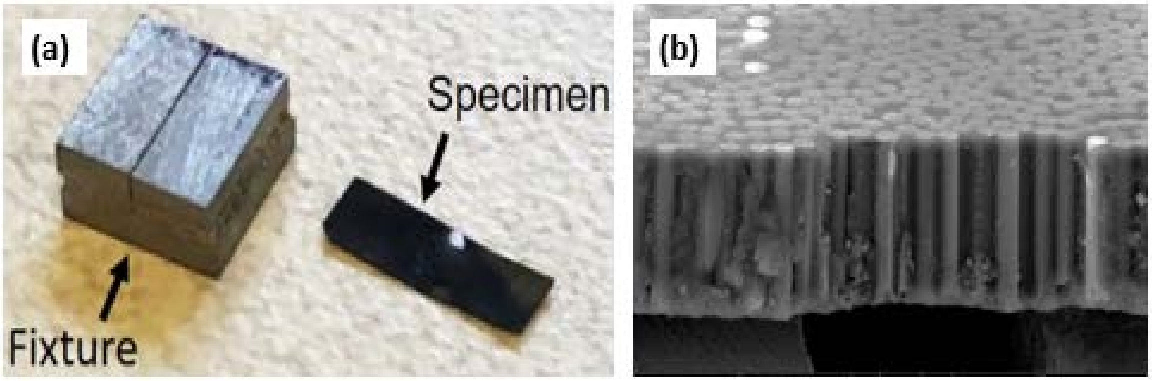

Figure 35. a) Fiber push-out specimen and fixture, b) SEM image of the sample mounted on the fixture.

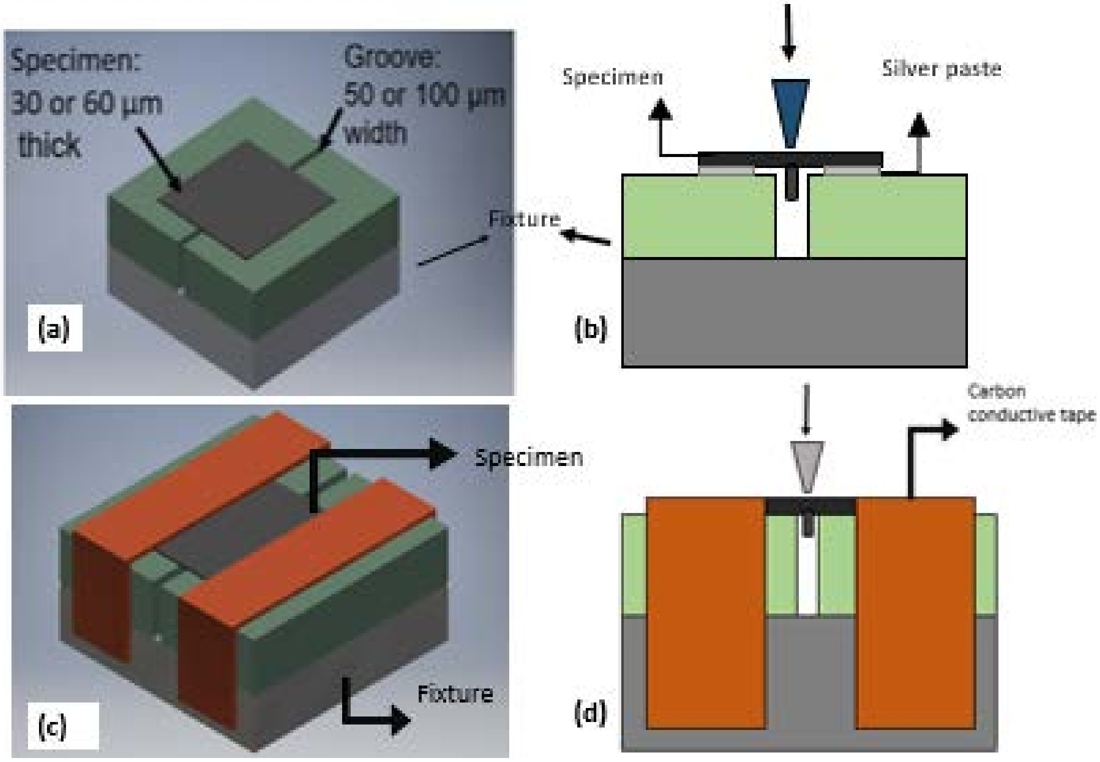

Figure 36. Schematic drawing of the general push-out specimen mounted on the fixture, a&b) specimens are fixed on the fixture with silver glue, c&d) specimens are fixed on the fixture with carbon conductive tape

On the other hand, the push-out samples for the new developed technique of laser machining (cave specimens) were obtained by cutting about 6 x 6 x 6 mm pieces from the unidirectional composite panel by a precision low speed diamond saw. Then, top surface of the sample perpendicular to the fibers was polished by following the same sequence as for the free-standing samples. Subsequently, fs-laser machining was performed using a custom laser machining apparatus to remove material in the transverse direction and create a membrane with approximately 30 or 60 µm in thickness, 50 or 100 µm in width and cutting depth of 40 µm. The thin membrane is used as a fiber push-out specimen (Fig.33).

The custom laser machining apparatus consisted of a fs-laser source, focusing optics, and computer controlled micro-positioning stages. The fs-laser generator used was a chirped pulse amplifier Ti:sapphire laser emitting at 775 nm and a 1 kHz repetition rate. The laser was directed to the focusing optics through a series of mirrors and was passed through a 1mm aperture, which transmitted ~5% of the laser intensity, to produce a well define laser spot. The laser was then focused using an infinity corrected microscope objective optimized for NIR. The resulting spot size was approximately 15 µm in diameter. Finally, 3 DOF micro-positioning stages were used to execute the desired sample geometry. The micro-positioning stages provided better than 1 µm accuracy in the horizontal plane and 1.5 µm accuracy in the vertical direction. In conjunction with the focusing optics, features as small as 10 µm could be fs-laser machined.

Using the fs-laser machining system, the caves were machined as follows. The specimen was mounted to the micro-positioning stages at a 10 degree pre-tilt. The pre-tilt was used to compensate for the taper inherent to the laser cuts such that the top of the cave was parallel with the specimen surface. During machining, the laser was operated at 20 to 30 mW continuous power. As a result, each pulse delivered 1 to 2 µJ to the sample surface; the resulting fluence was on the order of 1 J/cm^2. The laser was rastered along lines parallel to the sample edge; the lines were spaced 1 µm apart and covered an area 50 µm wide and 40 µm high. This area was located such that the resulting membrane had a final thickness of 20 to 30 µm. This process was repeated until the desired depth was achieved. After reaching the final depth, the last line closest to the edge was repeated until the taper was minimized.

All laser machining was performed using a feed rate of 0.6 mm/s.The cutting edges induced by femtosecond laser processing are very straight and smooth and there is no noticeable evidence of the thermal damage in the surroundings of membranes (Figure.33).

3.7 Single fiber push-out test:

Indentation (fiber push-out) tests on individual fibers were conducted using a FEI Versa 3D FEG dual beam SEM/FIB equipped with a Bruker PI-88 PicoIndenter micromechanical load frame. Figure 2 shows the instrumentation used in this work. SEM enable the possibility of imaging in real time during the experiment. A field emission gun (FEG) SEM uses an extremely sharp tungsten tip to produce the electron beam in the instrument. FEG SEMs are capable of producing high electron brightness and small spot sizes even at low accelerating potentials [93]. Also, environmental SEM (ESEM) technology in conjunction with low vacuum modes, allow us to work with range of samples including uncoated, non-conductive samples [94].therefore metal sputtering of nonconductive materials is not required. Besides, Bruker PI 88 PicoIndenter load frame has the sample tilt and rotation capability for the most versatile load application in addition to heating capacity up to 800°C. Also, high load transducer in this load frame would allow us to run the experiments up to 500 mN maximum force.

To perform a push-out test, sample is mounted on a SEM stub which will be loaded into the sample stage holder of the PI-88 system (Figure.38 b). The set screw that holds the SEM stub should be hand tightened to avoid breaking the piezo electrics that drive the sample stage. After a sample is mounted in the sample stage, a cone-shape diamond indenter tip with a flat tip is mounted on the transducer of the PI-88 system. The alignment of the sample and tip is checked the PI-88 system is loaded into the SEM. Afterward, the stage is tilted about 10-20º to allow both the tip and edge of the sample to be seen in the SEM view. To perform the transducer calibrations the tip is moved away from the sample to ensure that the tip will not crash into it. Afterward, a cone-shape diamond indenter tip with a flat tip is brought into contact with the fiber upper surface. Fibers placed above the groove or membrane were selected randomly to be loaded. All the tests were run under load control mode at rate of 1.67 mN/s up to never-exceed load of 200 mN, followed by unloading to the initial position. It is worth noting that the speed of the tests were slow enough to disregard any strain rate effects on the matrix, but fast enough to avoid thermal drift effect during the test. All the indentations were performed on isolated fibers, which means there is more than one fiber between pushed-out fibers to avoid any influence of previous indentation on the test results. During the test, SEM observations were conducted to investigate governing failure mode. The indentation tests were performed until the fibers are completely pushed out of the specimen.

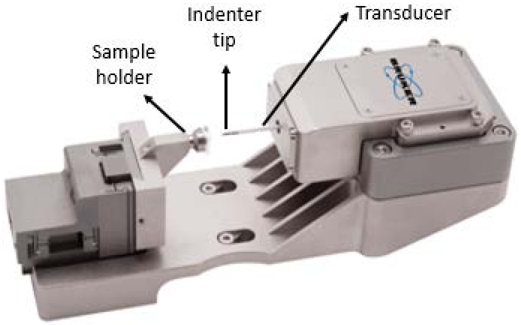

Figure 37. An image of the Bruker PI-88 picoindenter load frame.

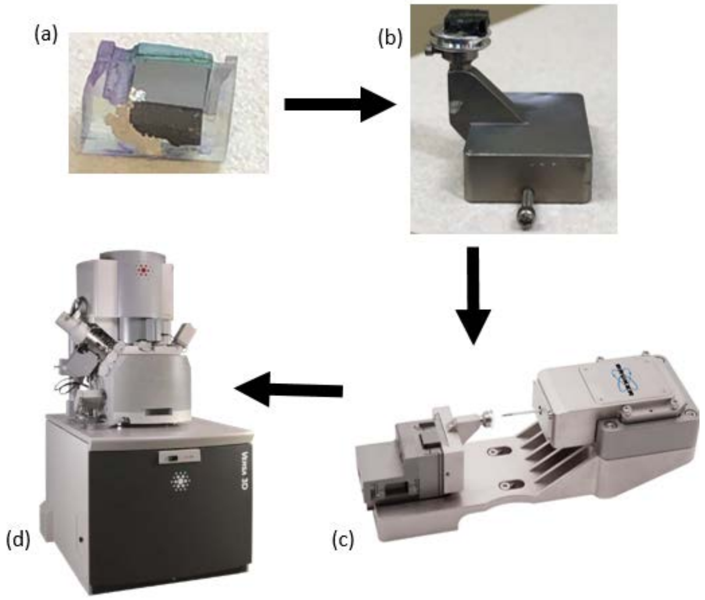

Figure 38. a) test sample, b) test sample and the sample holder of the micromechanical load frame, c) Bruker integrated PI 88 SEM PicoIndenter load frame, d) FEI Versa 3D SEM

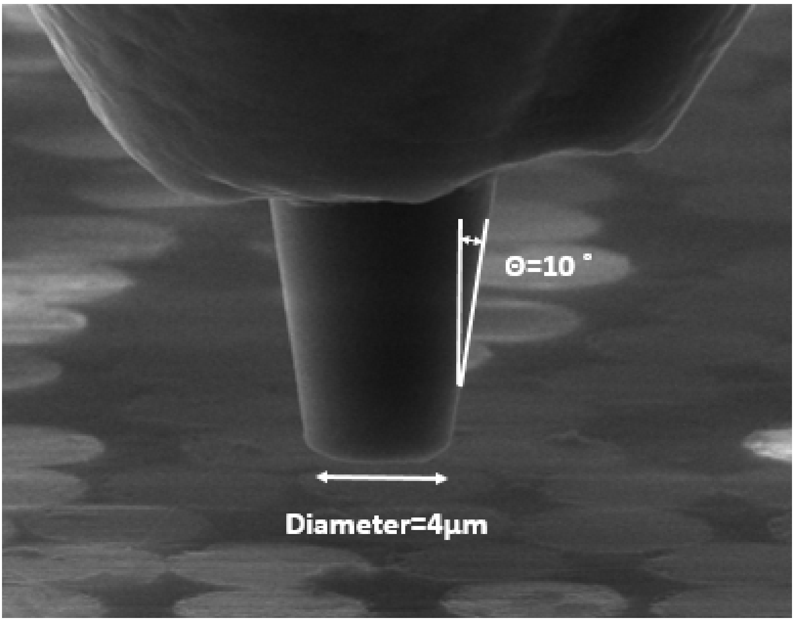

Figure 39. SEM image of the flat ended diamond tip with diameter of 4µm

3.8 Results:

A schematic of load-displacement response expectation for a single fiber push-out test is shown in Fig.40 (a). In part 1, the initial linear elastic loading zone is associated with the elastic deformation of fiber and matrix when perfectly bonded interface exist. Part 1 is followed by a non-linear region (part 2) which represents the beginning of interface failure. As interface crack grows slowly with increasing load, compliance increases until the maximum load has been reached. At this stage, crack propagation along the interface has been completed and the fiber push-out will initiate. Full de-bonding of the interface can be characterized by an abrupt load drop on the load-displacement curve (part 3).

As indicated earlier, specimens with two different thicknesses were prepared to ensure consistent fiber-matrix interface shear strength assessment and conduct a sensitivity study on the effects of sample geometry on the interface shear strength. Figure 40(b), summarizes the resulting load-displacement curves for IM CFRP composite in 30 and 60 µm thick samples.

As expected, the average maximum load for 60 µm thick samples was higher than 30 µm thick specimens. This would attribute to the fact that thicker samples with larger fiber-matrix interphase require extra load for crack propagation along the entire interface. However, when it comes to IFSS measurement , Fig. 41 verifies that the average measured IFSS value has been in agreement between the thick and thin samples – 15.9 Ksi (110±6 Mpa) and 13.9 Ksi (96±11 Mpa) for 30 µm and 60 µm thick specimens respectively.

This result confirms that IFSS is an intrinsic property of the material as the size (thickness) of the sample doesn’t have a significant effect. Nevertheless, experimental investigations indicate that by increasing the membrane thickness, other failure modes such as fiber fracture start to interfere with the interface de-cohesion.

Figure 41 shows examples of unintended failure modes in a 40 µm thick membrane. However, push-out experiments on samples with membrane thickness below 30 µm generate successful interface fracture results across different materials. On the other hand, thickness below 20 µm results in excessive bending of the membrane in the current test configuration, creating additional challenges in the fiber-matrix interface shear strength assessment due to a non-uniform stress distribution along the interface.

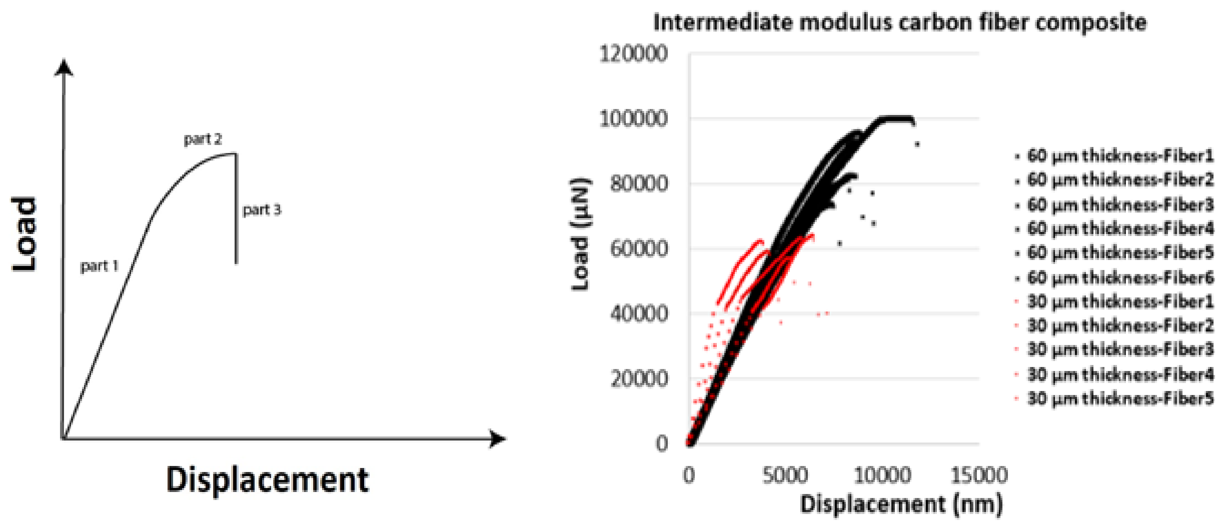

(a) (b)

Figure 40. a) Schematic of load-displacement response expectation for a single fiber push-out test, b) Experimentally measured load-displacement curve from push-out tests on IM modulus carbon fiber composite

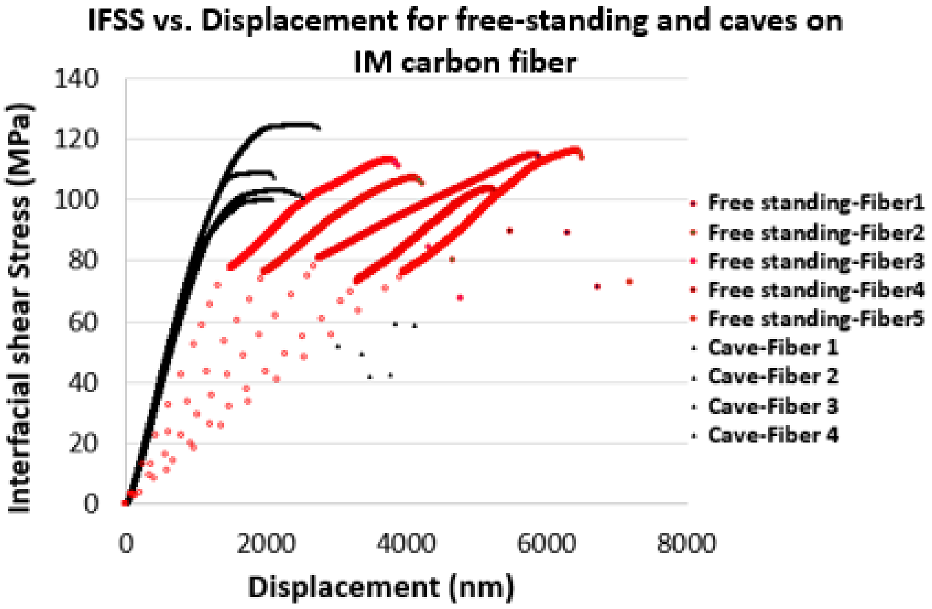

Figure 41. Fiber-matrix interface shear stress vs. indentation depth (displacement) obtained from fiber push-out tests on IM carbon fiber composite

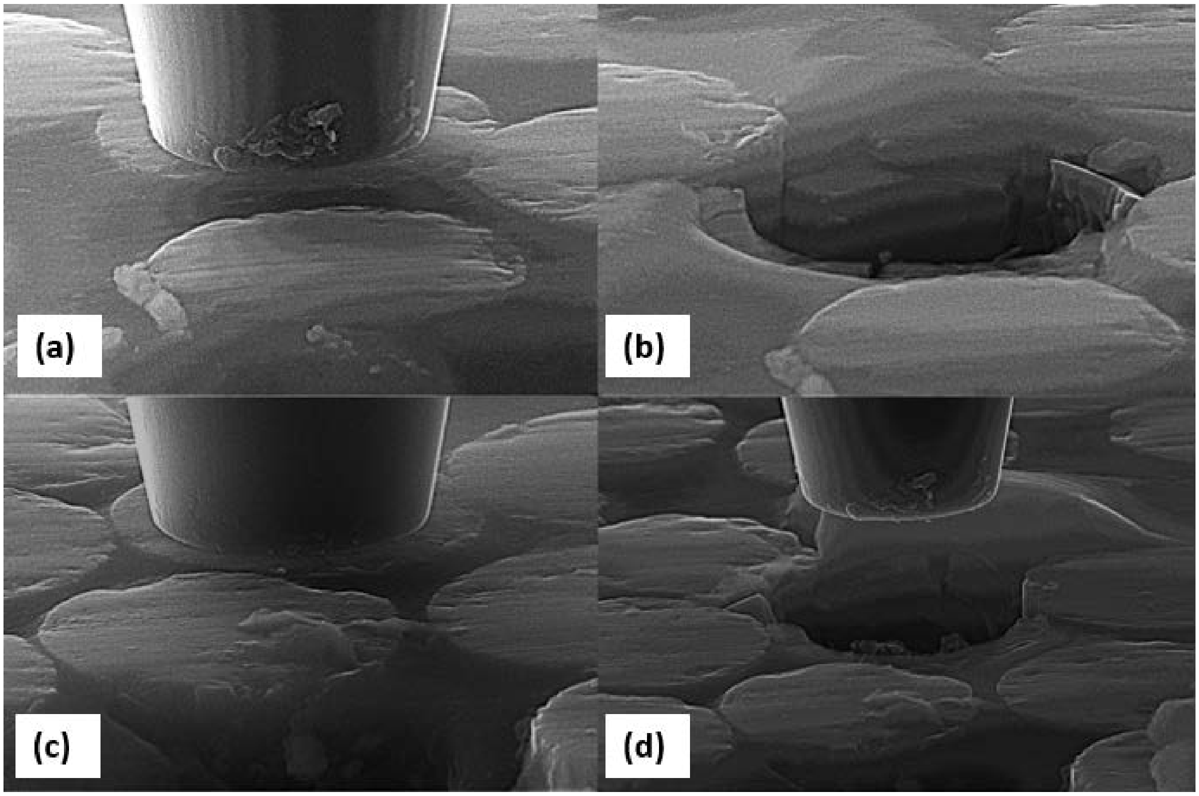

Figure 42. SEM images of carbon fiber push-out in approximately 40 µm thick membrane, a& c) 5 µm diameter carbon fibers before test, b) test data showing signs of fiber fracture, d) test data showing matrix damage.

Furthermore, a study to compare fiber-matrix interface shear strength in cave and free-standing samples has been performed in both materials. According to the preliminary experimental results in Fig. 41, average IFSS of the IM carbon fiber composite was estimated as 15.9 Ksi (110 MPa) for free-standing samples while cave specimens had average IFSS of 15.8 Ksi (109 MPa). On the other hand, HM carbon fiber composites demonstrate IFSS of 14.2 Ksi (98 MPa) and 15.5 Ksi (107 MPa) in free-standing and cave samples respectively.

Thus, IFSS value measured by cave and free-standing specimens are in the good agreement. It is also worth noting that large scatter in the IFSS results of free-standing sample in IM CFRP composite in Fig.41 was due to the compliance variations of the specimen at the beginning of the test. The compliance variations were caused by a thick layer of the silver glue that was applied around the edges underneath the specimen to keep it in place during the SEM vacuum process (Fig.36 a & b). Therefore, sample was not touching the substrate and it was sitting on the glue .When the probe came into contact with the fiber surface, it was pushing the specimen down until it reached the fixture. Such compliance concern was significantly reduced in HM composites (Fig.43), by fixing the edge of the sample on the fixture with carbon conductive tape instead of glue. Although taping the sample reduced the compliance, but they were not still in full contact with the fixture before the test to completely eliminate the compliance artifacts. However, the compliance artifact in cave samples are noticeably minimized. Because boundary conditions, drastically reduces the rigid body motion of the sample.

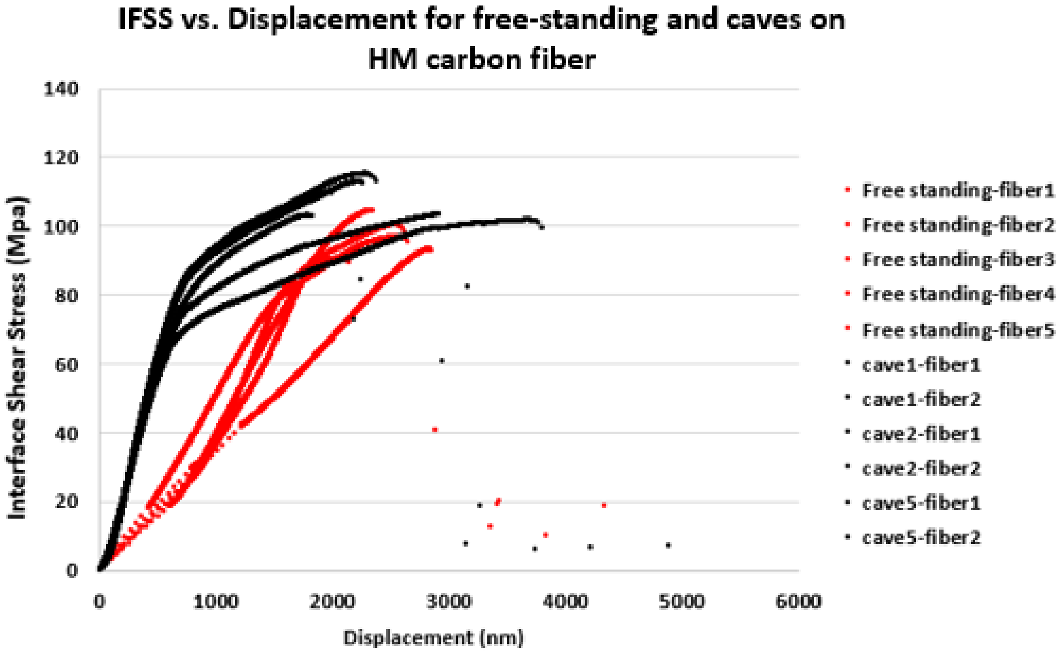

Figure 43. *Fiber-matrix interface shear stress vs. indentation depth (displacement) obtained from fiber push-out tests on HM carbon fiber composite*

Figure 44 & 45 shows typical SEM images after tests providing evidence of the fiber-matrix interface failure.

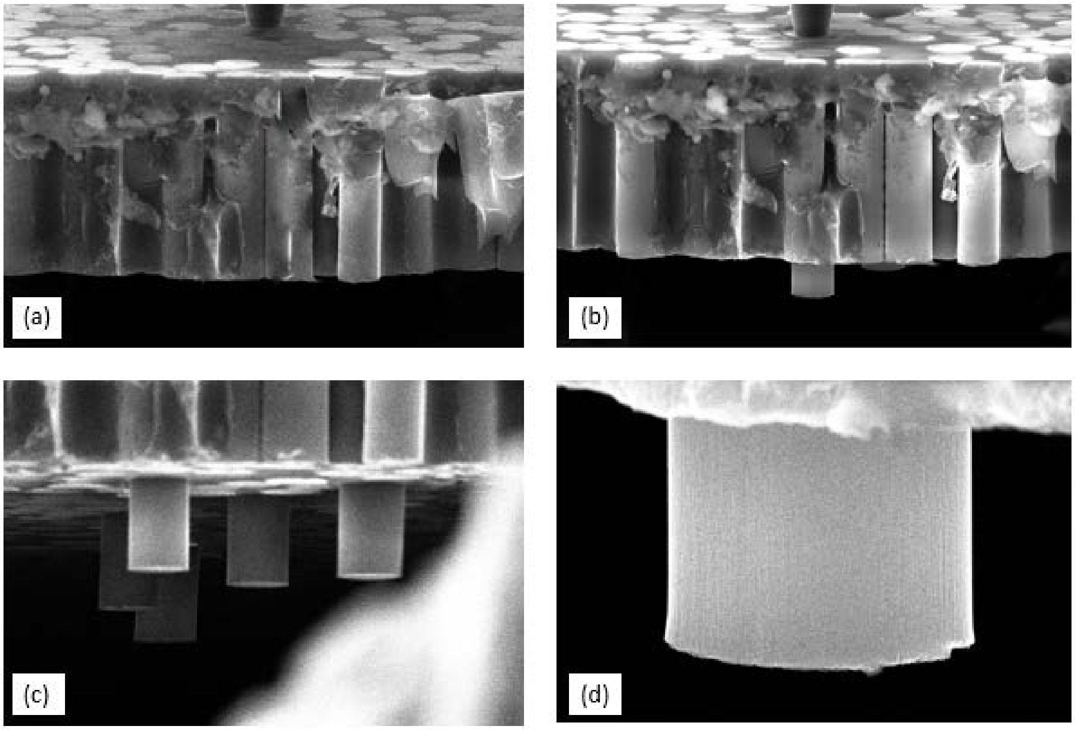

Figure 44. Typical post-test SEM images showing pushed out fibers in general push-out sample (Free-standing sample)

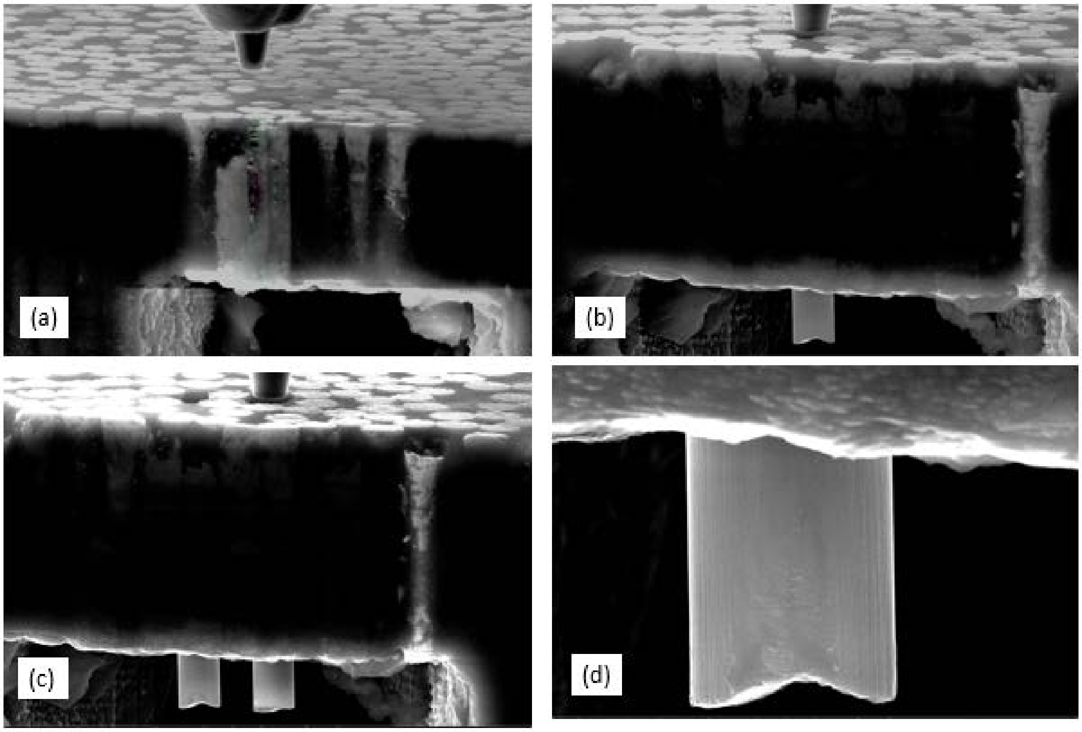

Figure 45. Typical post-test SEM images showing pushed out fibers in laser machined specimen (cave sample)

3.9 Concluding remarks:

In order to measure fiber-matrix interface shear strength input material property for the micro-buckling model, in-situ SEM based fiber push-out experiment was selected to be performed.

Due to the challenging process of specimen preparation for the general fiber push-out test, new technique for the sample fabrication was proposed. In the new method, femtosecond laser machining is used to create a thin membrane in the unidirectional CFRP composite coupon with the aim of avoiding or limiting the damage to the material. Push-out experiments were successfully accomplished for selected HM and IM CFRP's. The results verify that laser machined samples (cave samples) have very smooth cutting edges and there is not any noticeable evidence of the typical thermal damage such as molten material or burning sign around the processed section. Cave specimens are more stable than free standing samples during the test, which would help with extraction of a more consistence and accurate interface properties.

Moreover, Sample fabrication with laser processing in fast and because of the boundary condition of the membranes, rigid body motion of the specimen is minimized which can lead to elimination of the compliance artifacts. Average interface shear strength (IFSS) values measured by laser machined samples (cave specimens) and general pushout samples (free-standing samples) are in the good agreement. Results of this work support the idea of using femtosecond laser machining technique to produce samples for push-out test instead of traditional lapping/polishing process.

CHAPTER 4

Understanding Compressive Strength Improvement of new material system

In this chapter we look into fiber-matrix interface strength as a potential mechanism driving the compression strength improvement of the new material system. In-situ scanning electron microscopy (SEM) based experiments will be conducted to measure fiber-matrix interface shear strength of the HM and IM carbon fiber ingredients of the new high-performing hybrid material system developed in chapter 2.

4.1 Introduction:

As it was described in Chapter 2, significant improvement in the fiber-direction compressive strength of HM carbon-fiber composites can be achieved by hybridizing IM and HM carbon fibers in HM CFRP toughened with nano-silica. In particular, a new HM material solution achieving fiber-direction compressive strength of IM legacy composites but with more than 30% higher axial modulus has been developed [1]. Figure 1 compares axial modulus and fiber-direction compressive strength of the new hybrid HM CFRP with various HM and IM carbon fiber-reinforced epoxy-matrix tape composites.

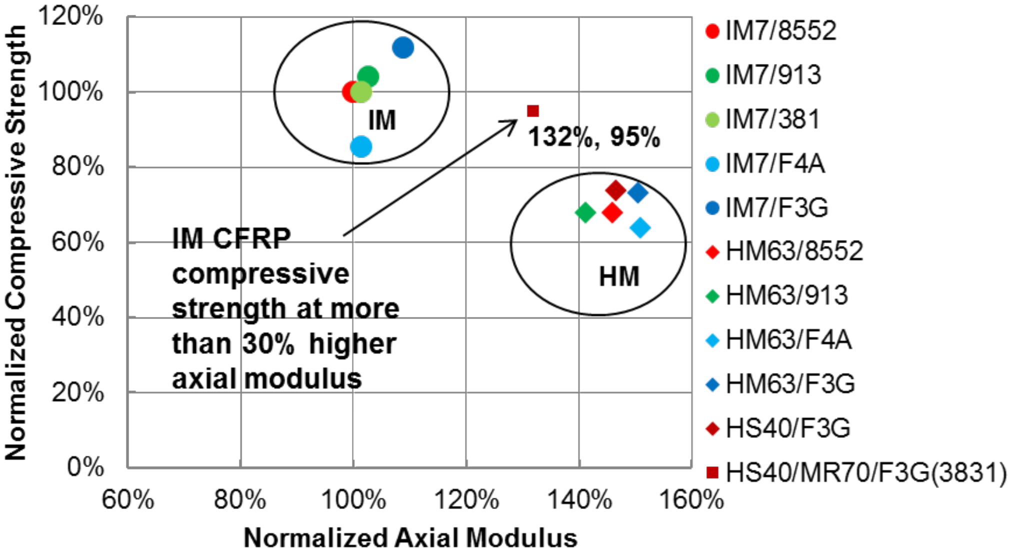

Figure 46. Axial modulus and fiber-direction compressive strength of HM and IM carbon fiber-reinforced epoxy-matrix tape composites [1].

The material performance in Figure 46 has been normalized to Hexcel IM7/8552 – a benchmark 350° F curing prepreg tape composite material system for aircraft structures. It is worth noting that all HM carbon fibers, as well as IM carbon fibers considered in the recent material development research are Polyacrylonitrile-based or PAN-based. Accordingly, fiber-direction compressive strength of PAN-based continuous carbon fiber-reinforced polymeric tape composites is presumably governed by microstructural stability, unlike that of pitch-based HM carbon fibers exhibiting longitudinal splitting failure mode [16].

Perhaps the first question to answer is what major failure mechanism may be responsible for the fiber-direction compression strength reduction of the HM CFRPs compared to their IM counterparts. Fiber-matrix interface strength has been among strong candidates. Microbucking analyses [33, 95, 18, 31] indicate strong sensitivity of the fiber-direction compressive strength to fiber-matrix interface strength. Also, interlaminar shear strength (ILSS) results generated from macro-scale shear tests reported in Ref. [95] show almost 20% ILS reduction for HM63/8552 (HM

CFRP) compared to IM7/8552 (IM CFRP). This indicates that HM fiber-matrix interface may be weaker than IM fibers. And if the weak fiber-matrix interface is responsible for low fiber-direction compressive strength of HM CFRP's one can look into improving the interface strength, which might be challenging. However, if off-the-shelf IM fiber-matrix interface is stronger in shear, and such fibers have higher shear modulus compared to HM fibers, a viable solution could be integrating off-the-shelf IM carbon fibers into a HM carbon-fiber composite to offload the HM fibers thus improving shear micro-buckling driven fiber-direction compressive strength of the HM composite system. HM carbon fibers do have approximately 10% to 15% lower shear modulus compared to IM carbon fibers, according to Refs. [95, 96].

This work looks into fiber-matrix interface strength as a potential mechanism driving the compression strength improvement of the new material system. In-situ scanning electron microscopy (SEM) based experiments will be used to measure fiber-matrix interface shear strength of the HM and IM carbon fiber ingredients of the new high-performing hybrid material system developed in chapter 1 [1]. A micromechanical load frame integrated with SEM will be utilized to capture fiber-matrix interface strength behavior.

4.2 In-situ SEM Experiments to Measure Fiber-Matrix Interface Shear Strength

To this date, there are no standard test methods available to characterize fiber-matrix interface mechanical behavior. However, a number of different experimental techniques, including fragmentation test [77, 70, 69], fiber pull-out test [71], fiber push-in test [74, 75] and fiber push-out test [97] have been developed. Among such methods, fiber push-out has been the most widely used in the in-situ characterization of interfaces in composites [83]. However, as it was explained in detail in chapter 3, specimen fabrication for the fiber push-out experiment has been a standing challenge [83].Because, specimen has to be thin enough (20-100μm) in order to allow decohesion over the entire fiber-matrix interface and ensure completely pushing out the fibers [83, 78, 56, 79, 69].These thin samples are obtained by lapping and polishing process, and they tend to fracture during polishing. Also, it is very difficult to meet their constant thickness. Furthermore, the samples are typically not perfectly flat especially at the edges, and they are not in full contact with the fixture before the test, as shown in Figs. 47, 48, creating compliance artifacts [65].

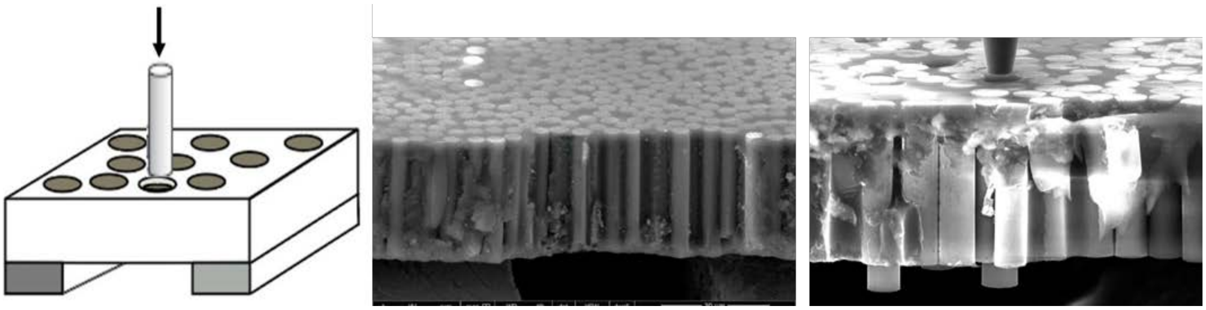

Figure 47. Left to right, schematic of a carbon fiber push-out sample and SEM images of the sample before and after the test. Fiber diameter approximately 5 μm.

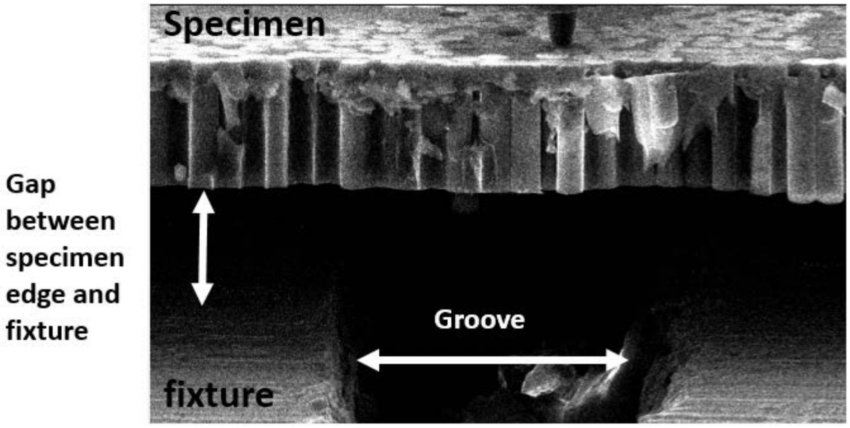

Figure 48. SEM image of a fiber push-out specimen prepared via a polishing process. A gap between the specimen edge and the fixture is evident despite taping down/adhesively bonding the specimen to the fixture.

To address these standing challenges and improve the consistency of the samples, we have employed femtosecond (fs) laser machining to create high-quality samples for the fiber push-out tests.

After polishing the top surface of the specimen, perpendicular to the fibers, fs-laser has been used to remove the material, creating a milled out section underneath the polished surface, with the intention of constructing a thin membrane with 20-30 μm thickness, 50 μm width and cutting depth of 40 μm. This thin membrane forms a fiber push-out specimen as shown in Fig. 49.

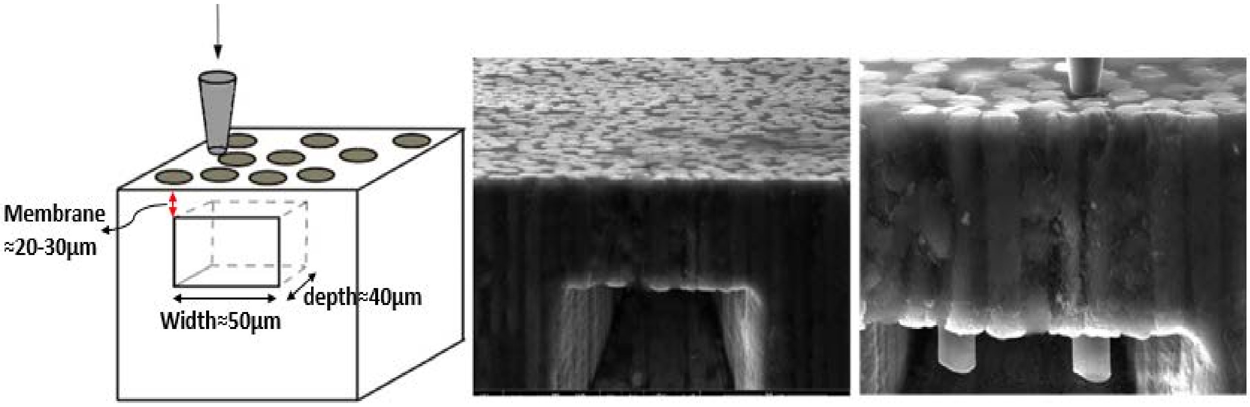

Figure 49. Left to right, schematic of a fs-laser machined specimen, and SEM images of the specimen before and after test.

4.3 Sample Preparation:

The carbon fiber push-out samples were obtained by cutting about 6 x 6 x 6 mm pieces from unidirectional CFRP panels by a precision low speed diamond saw. The cutting has been followed by polishing the top surface of the samples perpendicular to the fibers with diamond papers of 15, 9, 3, and 1-μm grain size. Subsequently, fs-laser machining was performed using a custom laser machining apparatus.

The apparatus consisted of a fs-laser source, focusing optics, and computer controlled micro-positioning stages. The fs-laser generator used was a chirped pulse amplifier Ti: sapphire laser emitting at 775 nm and a 1 kHz repetition rate. The laser was directed to the focusing optics through a series of mirrors and was passed through a 1mm aperture, which transmitted ~5% of the laser intensity, to produce a well define laser spot. The laser was then focused using an infinity corrected microscope objective optimized for near infrared spectrum. The resulting spot size was approximately 15 µm in diameter. Finally, 3 DOF micro-positioning stages were used to execute the desired sample geometry. The micro-positioning stages provided better than 1 µm accuracy in the horizontal plane and 1.5 µm accuracy in the vertical direction. In conjunction with the focusing optics, features as small as 10 µm could be machined with this laser.

Using the fs-laser machining system, the samples were machined as follows. The specimen was mounted to the micro-positioning stages at a 10 degree pre-tilt. The pre-tilt was used to compensate for the taper inherent to the laser cuts such that the bottom of the membrane was parallel with the specimen surface. During machining, the laser was operated at 20 to 30 mW continuous power. As a result, each pulse delivered 1 to 2 µJ to the sample surface; the resulting fluence was on the order of 1 J/cm^2. The laser was rastered along lines parallel to the sample edge; the lines were spaced 1 µm apart and covered an area 50 µm wide and 40 µm high. This area was located such that the resulting membrane had a final thickness of 20 to 30 µm. This process was repeated until the desired depth was achieved. After reaching the final depth, the last line closest to the edge was repeated until the taper was minimized. All laser machining was performed using a feed rate of 0.6 mm/s. As can be seen in Fig.5, the cutting edges induced by femtosecond laser processing are very straight and smooth and there is no noticeable evidence of the thermal damage in the surroundings of membranes. The target membrane thickness was 20-30 µm. Based on test evidence in chapter 3, thicker membranes may entail multiple failure modes competing with the fiber-matrix interface shear decohesion, e.g. fiber fracture and matrix damage. On the other hand, thickness below 20 µm results in excessive bending of the membrane in the current test configuration, creating additional challenges in the fiber-matrix interface shear strength assessment.

4.4 Carbon Fiber Push-out Test:

Indentation (fiber push-out) tests on individual fibers were performed using a FEI Versa 3D SEM equipped with a Bruker PI-88 PicoIndenter micromechanical load frame. In situ SEM enables the possibility of imaging in real time during the experiment. A sample was mounted on a PI-88 sample stage holder. Then, the load frame was placed inside the SEM and a cone-shape diamond indenter tip with a flat tip was brought into contact with the fiber upper surface. Fibers imaged on top of the membrane were selected at random to be pushed-out. All the tests were run under load control mode at rate of 1.67 mN/s up to never-exceed load of 200 mN, followed by unloading to the initial position. It is worth noting that the speed of the tests was slow enough to disregard any appreciable strain rate effects on the matrix, but fast enough to avoid thermal drift during the test. A spacing of more than one fiber between the pushed-out fibers has been maintained to avoid the interferences. Real-time SEM imaging has been conducted during the experiments. If the indenter tip was determined to be not centered on the fiber during the experiment, resulting in load eccentricity, the data was rejected.

It is worth noting that failure mode is affected by the tip diameter. Figure 50 shows that a 1 µm diameter tip entails fiber fracture and a 5 µm diameter tip naturally creates damage around a 5 µm diameter carbon fiber. A 4 µm diameter tip has been used in this work and it provided the most consistent test data. In fact, all fiber push-out test data presented in this work exhibited the same fiber-matrix shear decohesion failure mode based on SEM imaging.

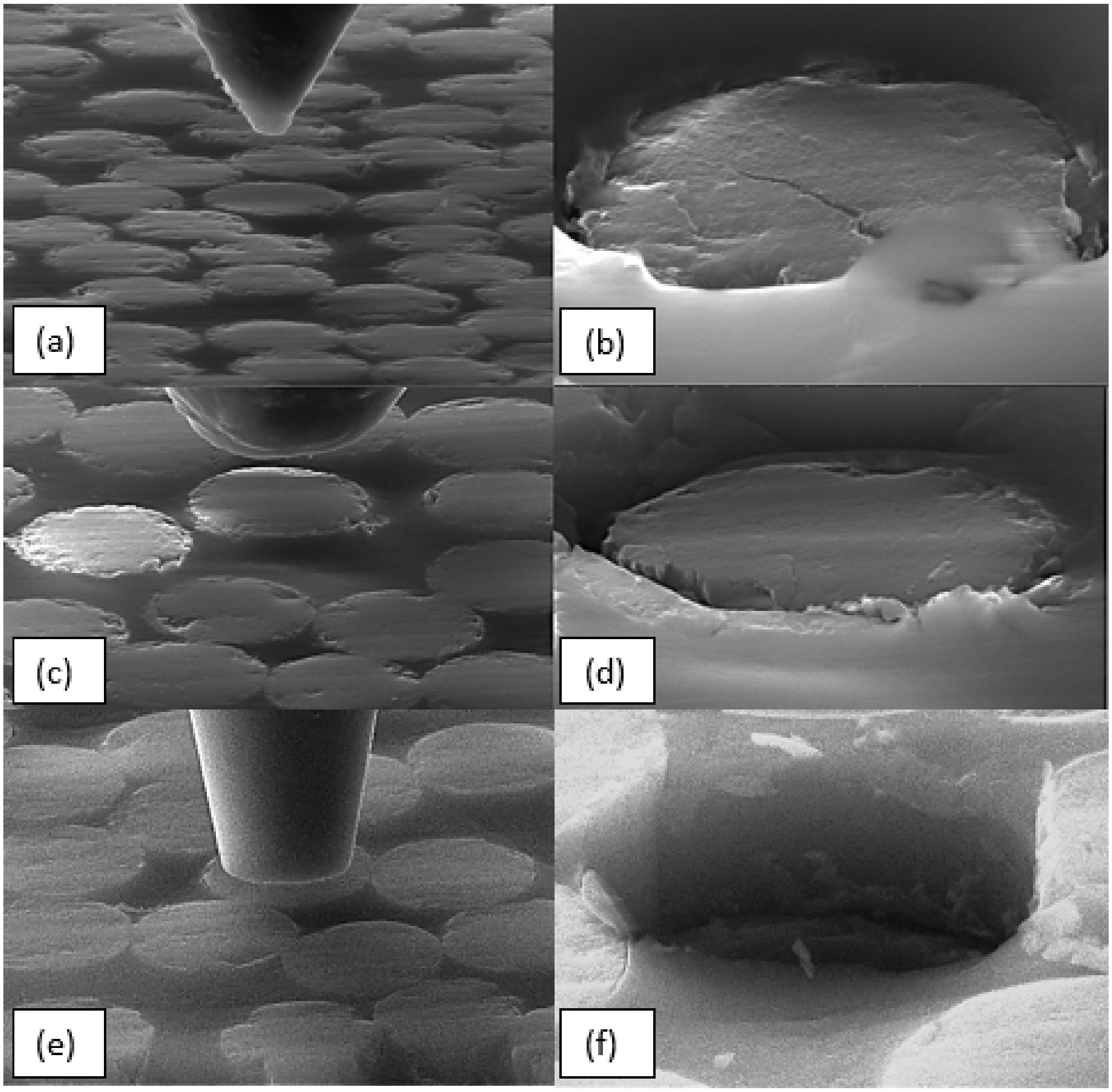

Figure 50. Fiber push-out experiments using indenters of different sizes. a& b) flat ended diamond tip with a 1µm diameter, c& d) a diamond tip with a 5µm diameter, (e& f) fiber push-out test with a 4 µm diameter probe.

The indentation tests were performed until the fibers completely lost the load carrying capacity and they were pushed out of the specimen. During the test, the load and depth of indentation (displacement) were continuously recorded. Consequently, by measuring the maximum applied load P_{max}, fiber length (the thickness of the membrane) h, and fiber radius r, the (average) interface shear strength (IFSS) has been calculated as

$$IFSS = \frac{P_{max}}{2\pi r h} \tag{4-1}$$

4.5 Materials:

The materials considered in this work are (1) the new hybrid HM CFRP (HS40 MR70/F3G) and (2) the corresponding HM CFRP (HS40/F3G). Figure 51 shows optical micrographs of the polished membrane surfaces, perpendicular to the fibers, for both materials. The micrographs are obtained using a Keyence VHX-950F white light optics microscope at a 1,000x magnification. Remarkably, the light reflection/absorption difference results in dissimilar colors of the HM and IM fibers as evident in the micrographs. This observation has been extremely useful for distinguishing the HM and IM fibers as they are otherwise identical in diameter and the surface morphology; and other means of differentiating the fibers including computed tomography did not work as the fibers had similar densities. Also, SEM imaging could not distinguish the HM and IM carbon fibers. Based on comparing the optical micrographs of the hybrid CFRP and the HM CFRP, generated using the same light conditions, the darker color in the hybrid CFRP represents the HM fibers. Fiber push-out test results presented in the next section verify this assumption.

The color difference in optical micrographs allowed us to distinguish the different types of carbon fibers in the fiber push-out test specimens. The optical microscopy was used to identify the different fiber types in the membranes and map them for the in-situ SEM testing. Figure 52 shows that specific fibers could be strategically selected for the push-out experiments.

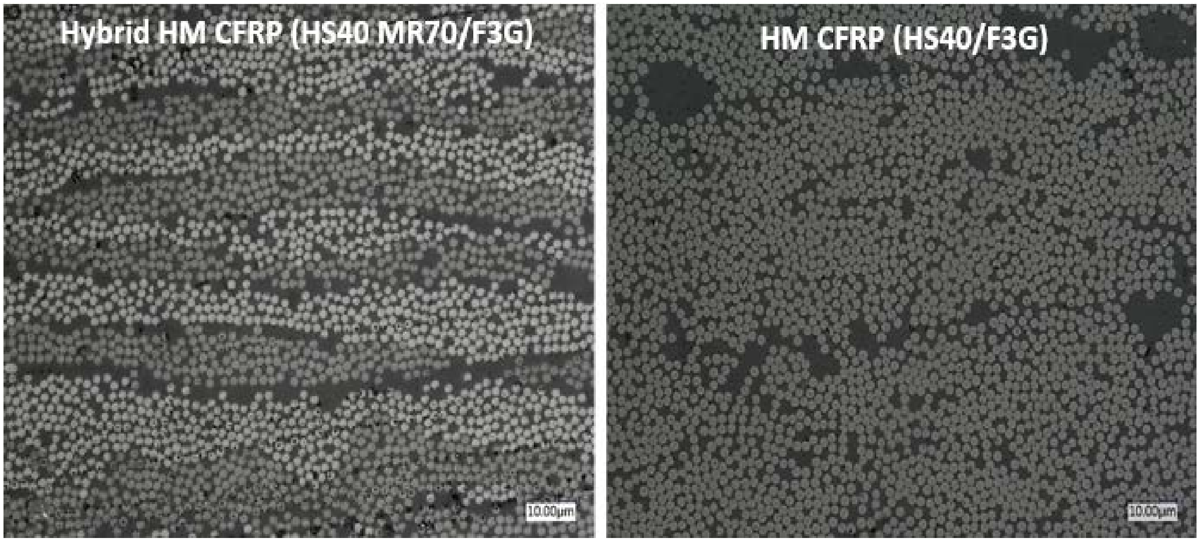

Figure 51. Optical microscope observation of CFRP showing the carbon fibers uniformly distributed in the resin matrix

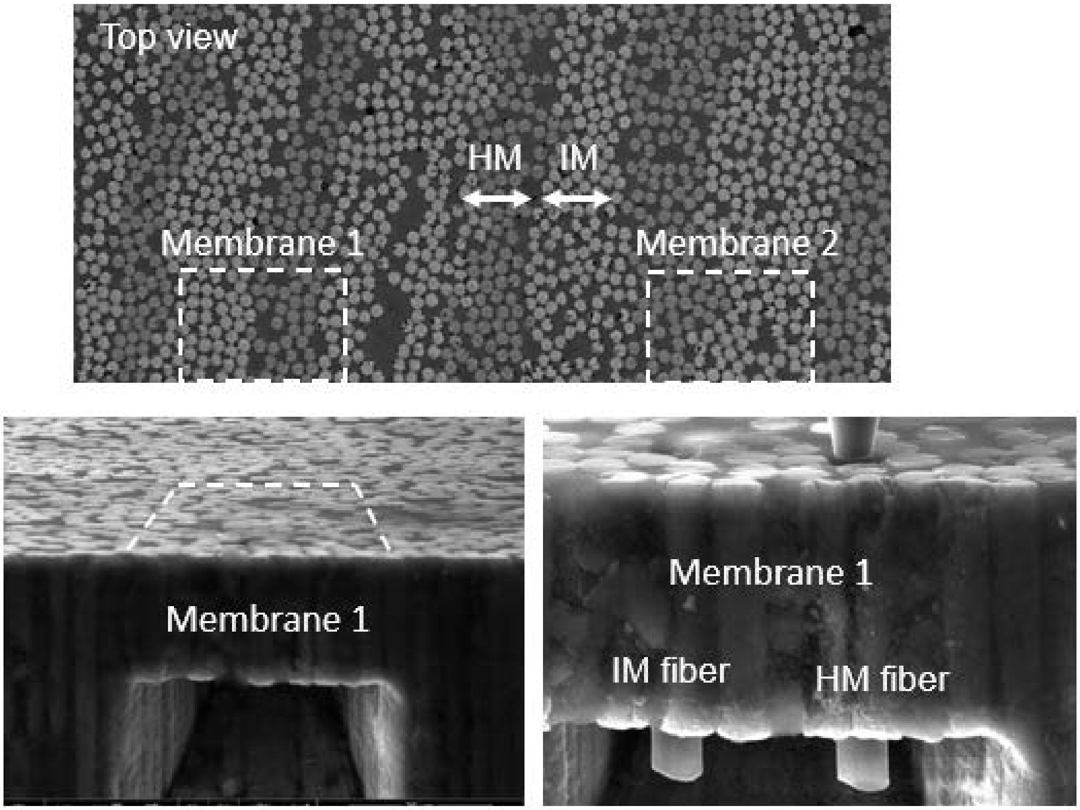

Figure 52. Optical microscopy has been used to identify different fiber types and map them for in-situ SEM testing.

4.6 Results and Verification:

This section lists the fiber push-out test results for the new hybrid HM CFRP (HS40 MR70/F3G) and for the corresponding HM CFRP (HS40/F3G). All the tests exhibited fiber-matrix shear interface failure mode based on SEM imaging. Figure 53 shows typical SEM images after tests providing evidence of the fiber-matrix interface failure.

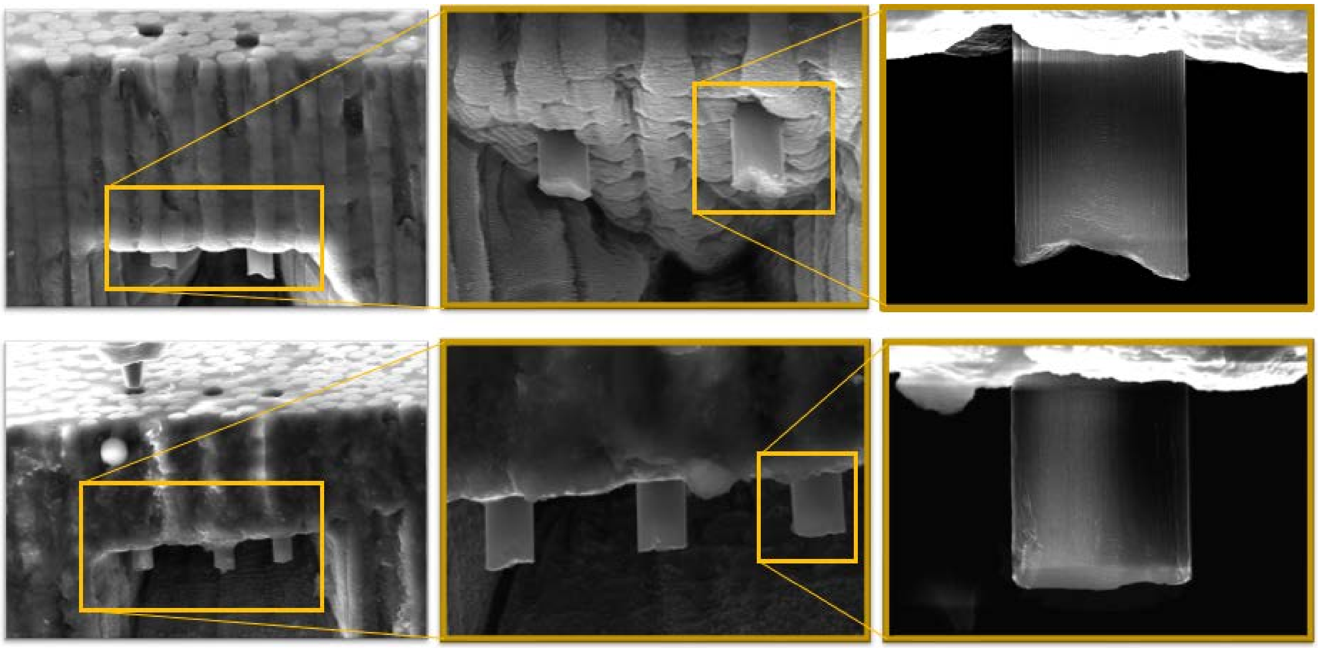

Figure 53. Typical post-test SEM images showing pushed out fibers.

To verify the assumption that darker fibers in the optical micrographs are indeed the HM carbon fibers, such fibers, mapped in the hybrid CFRP membranes, as well as randomly selected fibers in the HM CFRP on membranes were pushed out. Figure 54 shows interface shear stress – displacement (indentation depth) test data. A 15.8 Ksi (109 Mpa) average fiber-matrix IFSS value and a 10% coefficient of variation (COV) were obtained in the hybrid CFRP panel while the HM CFRP panel without the integrated IM carbon fibers provided a very similar 15.9 Ksi (110 Mpa) average IFSS value and a 9% COV. Such test results also demonstrate a consistent HM fiber-matrix interface shear strength across different material configurations including the hew hybrid HM CFRP as well as another CFRP with HM fibers only.

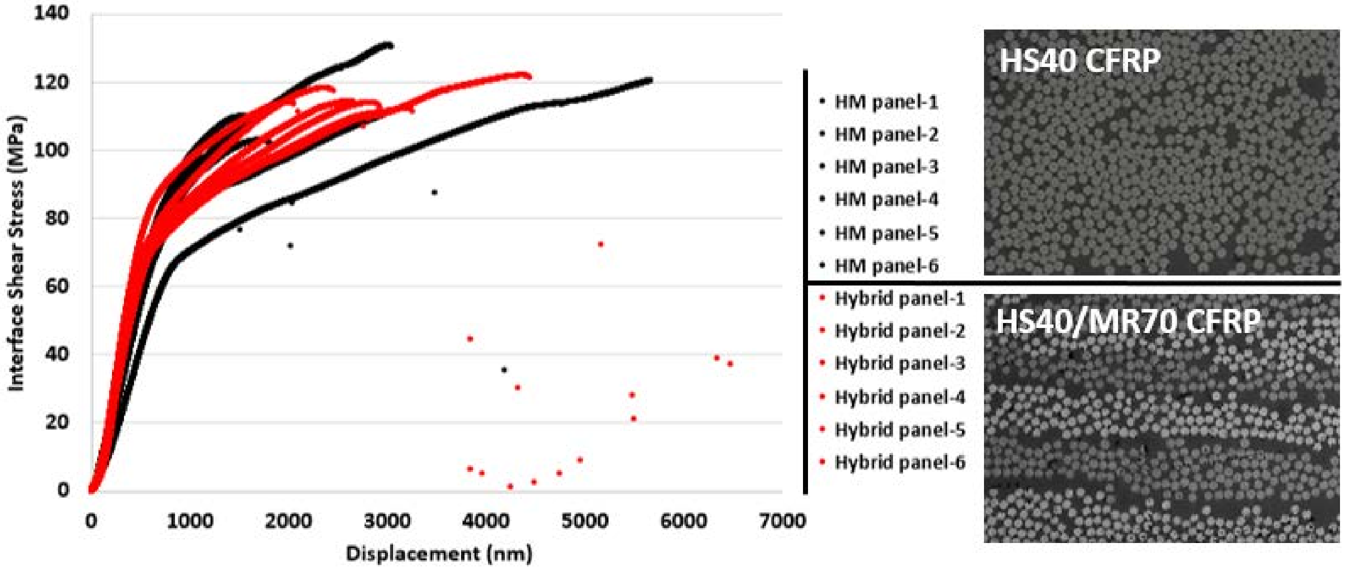

Figure 54. Fiber-matrix interface shear stress vs. indentation depth (displacement) obtained from fiber push-out tests on HM carbon fibers in hybrid and HM CFRPs.

Figure 55 shows interface shear stress – displacement results for the different fiber types in the new hybrid HM CFRP material system. The IM (MR70) carbon fibers exhibited a 22.3 Ksi (154 MPa) average IFSS value and a 7% COV while the HM (HS40) fibers had a 15.8 Ksi (109 MPa) average IFSS value – a 30% reduction indicating much weaker HM fiber-matrix interface compared to the IM carbon fibers.

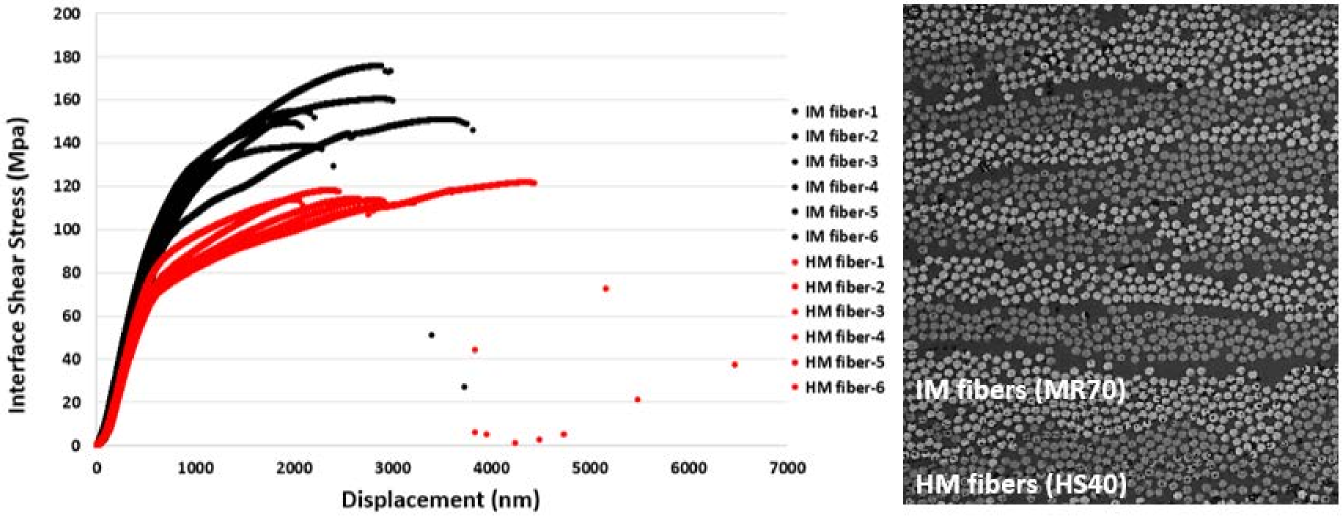

Figure 55. Fiber-matrix interface shear stress vs. indentation depth (displacement) obtained from fiber push-out tests on IM and HM carbon fiber in hybrid CFRP.

The fiber-matrix interface shear strength reduction has been verified on the HM CFRP without the integrated IM fibers (Fig. 55). It is worth noting that such a strong IFSS reduction corresponds to a much lower fiber-direction compressive strength of the HM CFRP. Indeed, the new hybrid HM CFRP has a 204 ksi (1.41 GPa) fiber-direction compressive strength [1, 95] while the HM CFRP without the integrated IM fibers exhibits a 22% lower 158 ksi (1.09 GPa) fiber-direction compressive strength [95].

Furthermore, in an ideal configuration of the push-out experiment, the probe should applies force parallel to the axis of the fiber. However, if the application of the load is not perfectly parallel to the fiber direction, the complex stress state at interface can generate both normal and shear stress. However, the push-out test can only quantifies the interface shear stress properties. So, Ogihara et al. [98] conducted several experiments with different fiber angles with respect to the loading direction to make various stress state of normal and shear at the interface. Subsequently, they found that value of the interfacial normal strength (IFNS) is 2/3 of the IFSS value.

As a conclusion, the experimentally characterized values of the mechanical properties of the matrix and fiber-matrix interfaces are summarized in the following Table.

Table 4.interface shear and normal strength values for HM and IM carbon fibers in the new developed hybrid material developed at AMSL

Carbon fiber in hybrid CFRP	**Interfacial shear strength (IFSS)**	**Interfacial normal strength (IFNS)**
IM carbon fiber (MR70)	≈ 204 ksi (1.41 GPa)	≈136 ksi (0.94 GPa)
HM carbon fiber (HS40)	≈158 ksi (1.09 GPa)	≈105 ksi (0.73 GPa)

4.7 Microstructural modeling:

This section discusses the development of the computational micromechanics model for the compressive strength estimation of the unidirectional (UD) fiber reinforced composite ply. The computational micromechanics framework enables conducting the parametric investigation for the composites with various material systems in reliable and efficient fashion [99, 100]. We investigate the behavior of the composite numerically via Finite Element Analysis (FEA) in the commercial software package ABAQUS.

A statistically representative volume elements (RVE) of the UD composite ply is shown to be computationally expensive for parametric studies of micromechanical parameters under compressive loading [100]. On the other hand, a simplified unit cell with a single circular fiber embedded in the resin material containing the same fiber volume faction as the statistically representative RVE is suitable for the parametric analysis. We developed a simplified three-dimensional (3D) unit cell using the custom procedure implemented in a python script. The model has a sinusoidal shape to introduce the initial misalignment angle. The misalignment angle controls compressive failure by initiating fiber kinking, as shown in [101, 1]. We begin the model generation by creating a 2D mesh with quadrilateral elements of the unit cell initial cross-section. The initial cross-section is extruded along the fiber's direction to form a 3D unit cell. To introduce the initial misalignment, each cross-section is scaled according to a half-length of the sinusoidal wave. The length of the unit cell is set to 500 μm, as suggested in [102]. In addition, each cross-section is oriented in a way that its normal coincides with the local fiber path to avoid excessive element distortion and shear locking. The resulting model contains fully integrated brick (C3D8) linear elements. A typical 3D model, as illustrated in Figure 56, contains approximately 300,000 DOF's.

The unit cell is subjected to periodic boundary conditions in all three directions using Micromechanics Plugin for ABAQUS/CAE [103]. The plugin forces the homologous nodes on the opposite faces of the unit cell to deform in a compatible way by imposing the constraint equations [104, 105, 106]. The unit cell is subjected to the compressive load in the fiber's direction by prescribing the displacement to a corresponding master node. It is worth noting that master nodes link sets of the corresponding nodes are located on the opposite faces on the unit cell. The resulting system of FE equations is solved by the Newton-Rapson method available in the commercial software package ABAQUS. The results of the FE simulations are processed via a custom python script to extract volume averaged stress and strain components, as outlined in [107].

In this work, we model carbon fibers as linear elastic and transversely isotropic material. Local material orientations are prescribed for the fiber following a sinusoidal path via a custom python script. Epoxy resin is idealized as linear elastic material with the possibility to undergo plastic deformations and accumulate damage under tensile loading, as modeled in Ref. [108] . In particular, the extended

Drucker-Prager model available in ABAQUS standard material library [109] is used for the constitutive model of the 8552 epoxy resin considered in this work. The fiber-matrix interface is represented by surface-based cohesive interactions similar to [108].

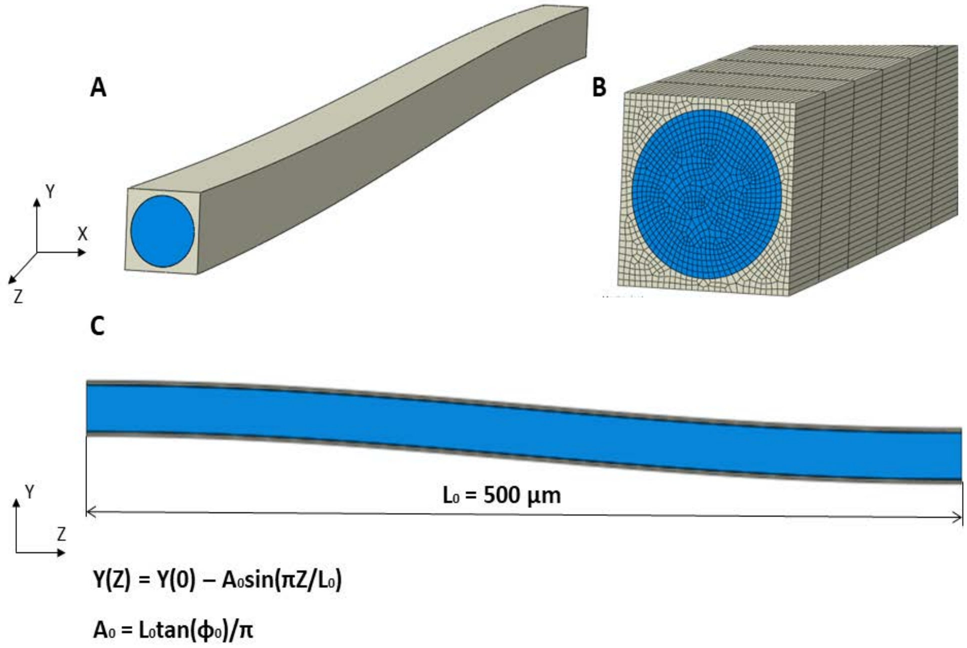

Figure 56. *a) Geometry of a 3D unit cell with a single circular fiber of 60 % volume fraction embedded in the epoxy resin; b) zoomed-in view of a unit cell mesh; c) side view of the unit cell cross-section illustrating the initial misalignment angle of* $\varphi_0 = 2°$

Interface properties were recognized as one of the essential micromechanical parameters significantly influencing the compressive strength of the composite [100, 1]. Therefore, we focus our attention on the investigation of the fiber-matrix interface strength on the response of the UD composite ply. The parametric study is carried out for the IM7/8552 legacy composite system due to its widespread applicability and availability of the material properties. Fiber and matrix elastic properties are extracted from the literature [110]. Non-linear matrix properties used in the extended Drucker-Prager model for 8552 epoxy matrix are taken from Ref. [108] and include internal friction angle β, tensile strength σ_{myt}, compressive strength σ_{myc} and fracture energy ζ_m. Indentation experiments are performed in this work to extract interface shear strength for the IM7/8552 tape material system. The properties are listed in Table 4.

Table 5. Material properties for the IM7/8552 legacy material system used in our simulations

IM7 carbon fibers properties								
Young's moduli			Poisson's ratio			Shear Moduli		
E_{11}(Msi)	E_{22}(Msi)	E_{33}(Msi)	ν_{12}	ν_{13}	ν_{23}	G_{12}(Msi)	G_{13}(Msi)	G_{23}(Msi)
40.0	2.18	2.18	0.2	0.2	0.07	2.18	2.18	1.02

8552 epoxy resin properties					
Young's modulus	Poisson's ratio	Internal friction angle	Tensile strength	Compressive strength	Fracture energy
E_m (Msi)	ν_m	β (deg)	σ_{myt} (ksi)	σ_{myc} (ksi)	ζ_m (lbf/ft)
0.677	0.39	29	17.5	25.5	0.571

IM7/8552 interface properties					
Interface strength properties			Critical energy release rates		
σ_N (ksi)	τ_T (ksi)	τ_S (ksi)	ζ_{IC} (lbf/ft)	ζ_{IIC} (lbf/ft)	ζ_{IIIC} (lbf/ft)
9.28	13.9	13.9	0.0114	0.0342	0.0342

Figure.57 illustrates the Cauchy stress vs. logarithmic strain curves of the unit cell with (1) the perfect fiber-matrix interface and (2) the interface modeled by surfaced-based cohesive behavior. It is apparent that the compressive strength of the model with the cohesive interface is greatly reduced. The compressive strength value which accounts for the measured fiber-matrix interface strength is 241 ksi (1.66 GPa) for the unit cell with the cohesive interface, while the estimated value for the model with a perfect interface is 319 ksi (2.2 GPa). The introduction of the cohesive interactions leads to early interface damage initiation due to low interface strength. Once damage starts, it propagates rapidly in the longitudinal and transverse directions. As damage reaches its critical value, the unit cell becomes unstable, and the load capacity rapidly starts to degrade.

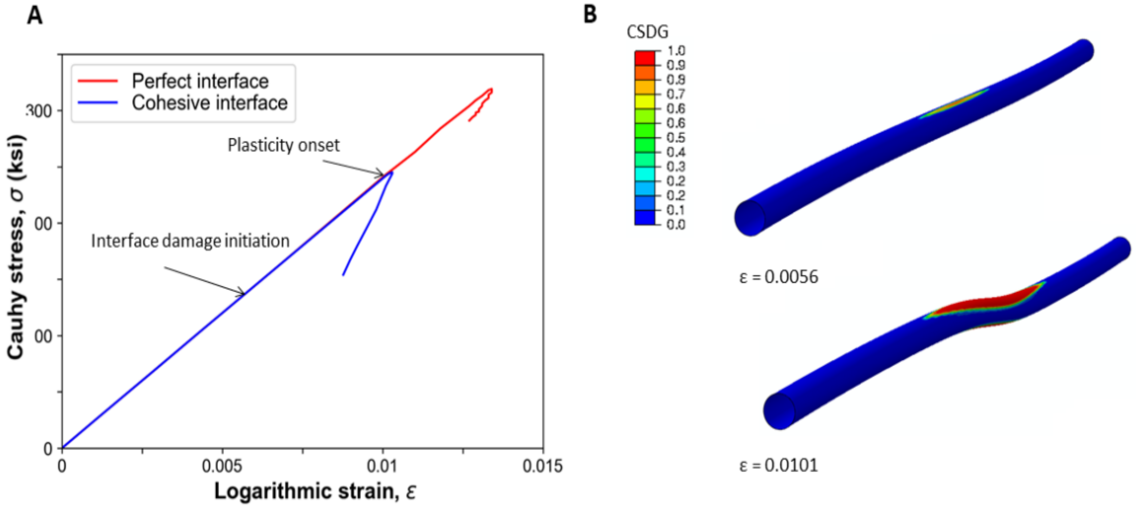

Figure 57. a) Strain-stress curves predicting the compressive strength by a unit cell with perfect fiber/matrix interface and the interface modeled by cohesive surface interactions; b) interface progressive damage evolution.

The influence of the fiber-matrix interface strength is illustrated in Fig. 58. The sensitivity study is performed by altering fiber-matrix interface shear strength σ_S while keeping the fiber and matrix material properties constant. As can be seen, the reduction of the fiber-matrix interface shear strength, resulted in the drastic drop of the compressive strength by 22%. Alternatively, as a matter of fact, in carbon fiber-reinforced resin matrix composite, the failures are normally dominated by the ILSS. Thus, to some extent, the interface strength can be evaluated indirectly from the short-beam shear test. We are extensively using customized short-beam shear (SBS) testing for effective characterization of interlaminar shear (ILS) strength/fatigue behavior of composite systems [111]. And SBS results in the 1-3 principal material plane demonstrate a 16 ksi (110 MPa) ILS strength for IM7/8552 compared to almost

20% lower 13 ksi (90 MPa) ILS strength for HM63/8552. This 22% drop agrees with the 20% reduction of ILS value extracted from SBS tests and it indicates that HM fiber-matrix interface is potentially far weaker than with IM fibers. Due to insufficient material characterization for HM63 carbon fibers, longitudinal Young's modulus of the fiber (64 Msi) [112] is the only material input property changed in the model in addition to the fiber-matrix interface shear strength. As 3D material properties of HM63 fibers become available similar to IM7, other properties can be changed. Nevertheless, the micromechanical model confirmed significant effects of the weaker HM fiber-matrix interface compared to IM fibers on the fiber-direction compressive strength.

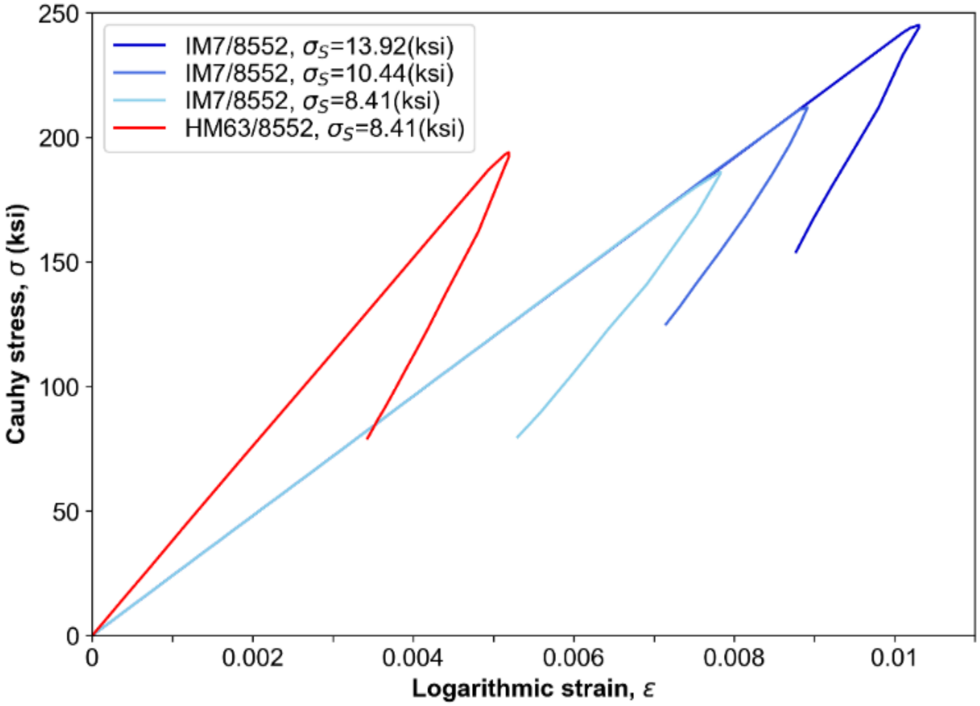

Figure 58. Influence of the fiber-matrix interface shear strength σ_S on the response of the UD composite ply

4.8 Concluding remarks:

This work has contributed to improving our understanding of fiber-direction compressive strength Improvement of HM CFRPs with Varying Modulus Fibers. Weaker HM fiber-matrix interface than with IM fibers has been corresponding to significantly lower fiber-direction compressive strength of the HM CFRP compared to their hybrid HM/IM composite material system.

The results of the in-situ scanning electron microscopy (SEM) based experiments show a strong decrease in the average values of the fiber-matrix interface shear strength for the HM carbon fibers compared to the IM carbon fibers in the new material system. The fiber-matrix interface shear strength reduction has been verified on the HM CFRP without the integrated IM fibers. And such a strong reduction corresponds to a much lower fiber-direction compressive strength of the HM CFRP. The results support the idea of integrating off-the-shelf IM carbon fibers with stronger fiber-matrix interface and higher shear modulus into a HM CFRP to improve fiber-direction compressive strength of the HM composite material system. As off-the-shelf IM fiber-matrix interface is stronger in shear, and such fibers have higher shear modulus compared to HM fibers (which has been confirmed), integrating the appropriate off-the-shelf IM carbon fibers into a HM carbon-fiber composite may offload the HM fibers thus improving shear-driven fiber-direction compressive strength of the HM composite system.

CHAPTER 5

Fiber Microbuckling

Kink-band formation has been widely assumed to drive fiber-direction compressive strength of IM tape CFRPs [12-19]. On the other hand, fiber-direction failure in HM CFRPs has received much less attention.

Many previous experimental investigations focused on kink-band formation in IM CFRPs have used notched unidirectional (UD) laminates with relatively large width to thickness ratio [20-22]. In this work we used a notched UD four-point-bend (FPB) specimen developed by Laffan et al. [113]. However, a large 0.25 in. thickness of the original FPB specimen entails large energies of damage progression which results in two-piece fracture of the specimens before a stable damage progression can be observed. HM CFRPs exhibit brittle fiber-direction compressive strength behavior with much lower strain to failure compared to IM CFRPs, which makes observing the failure mode in HM CFRPs even more challenging. Accordingly, we reduced the FPB specimen width to approximately 0.02 in., which allowed for a stable failure progression in the HM and IM CFRPs considered in this work.

The material systems that were studied for the kink-band formation at the micromechanical level include (1) IM7/8552 IM carbon-fiber composite (2) HM63/8552 HM carbon-fiber composites and (3) HS40 MR70/F3G hybrid HM CFRP with various HM and IM carbon fiber-reinforced epoxy-matrix tape composites.

To manufacture UD composite panels 2-3 layers of prepreg were laid up manually to achieve final panel thickness of 0.01-0.02 in.. Then materials were cured according to the instructions from the respective suppliers. The FPB specimens with nominal dimensions of 6 in. length, 0.5 in. width were machined from the panel using a wet saw with the fibers aligned in the longitudinal direction of the specimen. Eventually, a notch with radius of 0.0004 in and depth of 0.25 in. was made with grinder using decreasing wheel tip sizes. All the specimens were checked by non-destructive computed tomography (CT) inspection after manufacturing, to confirm that no major defects were presents.

Figures 3 and 4 show a representative thin notched FPB specimen and the test configuration. The specimen is bonded to Plexiglas antibuckling guides on both sides, except in the gage section. The guides have step joints (hinges) in the gage section to avoid load sharing by the guides. Additional Plexiglas antibuckling supports were clamped to the specimen for stability. The bolts in these supports are hand-tight to minimize any clamping effect on the specimen compressive strength behavior.

FPB specimens were tested using a Shimadzu AGS-X Series electromechanical load frame with a 2 Kip load cell. Each specimen was loaded under displacement control at a rate of 0.01 in/min. load and crosshead displacement were continuously recorded during the test. One 16-megapixel stereo camera system was used to monitor a highly magnified image of the notch tip. The magnified images were used to determine the failure progression. A μ-CT inspection clearly demonstrates fiber-direction compression failure due to microbuckling. CT volume slices of IM, HM and HM/IM hybrid (New Material) CFRPs in Fig.5 show out-of-plane kink bands across the thickness of the specimens.

Observing the kink-band formation across the different fiber types confirms that fiber-direction compressive strength is indeed governed by microstructural stability, which can be used as a basis for developing a rigorous modeling strategy and meeting the material input data requirements.

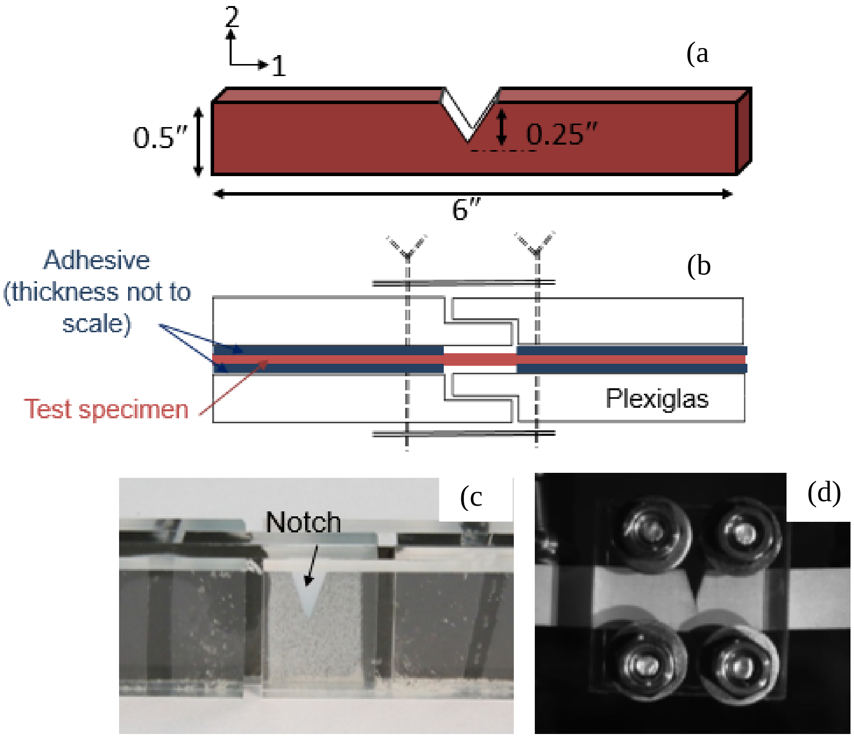

Figure 59 a) Schematic illustration of the FPB specimen with dimensions, b) schematic illustration of the specimen and Plexiglas assembly, c) specimen bonded to Plexiglas antibuckling guides, d) specimen and Plexiglas antibuckling supports

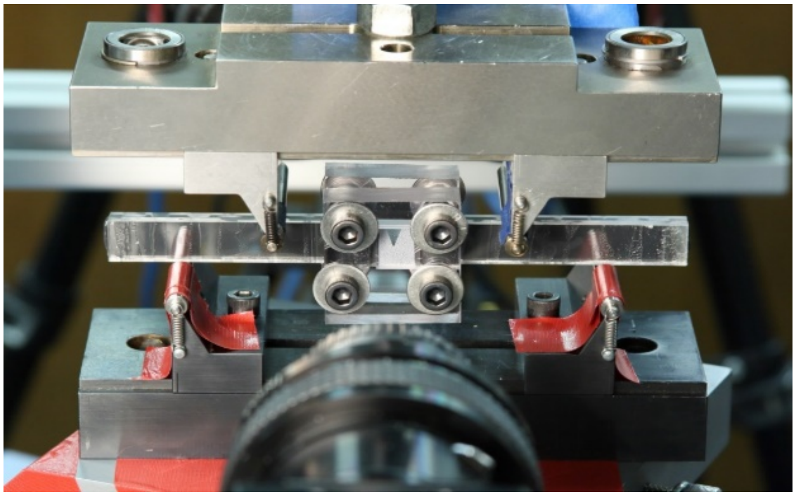

Figure 60 Four point bend notched test configuration

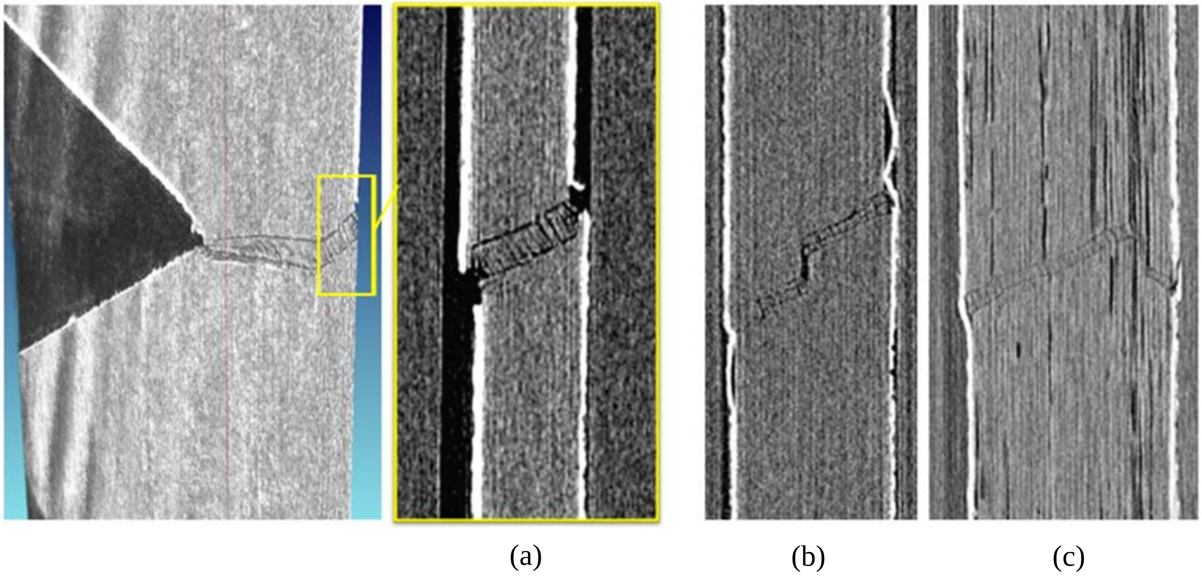

Fig. 61 A CT volume slice showing out-of-plane kink-band, a) Kink band formation in a 0.015 in. thick IM CFRP FPB specimen, b) Kink band in a 0.019 in. thick HM CFRP FPB specimen, c) Kink band in a 0.028 in. thick hybrid HM/IM CFRP (New Material) FPB specimen. Manufacturing defects (gaps) due to poor prepreg quality are evident in the hybrid material

CHAPTER 6

Conclusion and Future work

In the absence of accurate models to predict fiber-direction compressive strength of HM carbon-fiber polymeric composites, and driven by a substantial need from industry for developing a continuous HM CFRPs approaching fiber-direction compressive strength of IM carbon legacy composites at 30% (or greater) higher Young’s modulus, this work presented an experimental approach of reinforcing material surrounding HM fibers to improve microstructural stability governing fiber-direction compressive strength behavior. Observation of the compressive strength behavior across different fiber and resin combinations showed a remarkable trend that fiber-direction compressive strength increases with increasing the shear modulus to axial modulus ratio of composite material systems which inspired the idea to hybridize carbon fibers with varying moduli. The results demonstrate that the new hybrid HM carbon composite with comingled IM and HM fibers in addition to the nano-sized structural reinforced matrix, achieved fiber-direction compressive strength of IM composites but with more than 30% higher axial modulus.

On the other hand, enabling effective design of the new high-performing composite materials requires accurate physics-based models to capture fiber-direction compressive strength behavior of HM CFRPs. However providing accurate input properties for the model is one of the most challenging parts of the microstructural model development. In fact, composite materials represent very complex systems, including many components, e.g., carbon fiber, polymer matrix, fiber sizing, matrix toughening nanoparticles, etc. To develop an accurate model for these multicomponent materials, micromechanical performance of each constituent and the complex interaction between them should be understood and characterized. Among all these components, fiber-matrix interface strength, ignored by the current micromechanical buckling models, is one of the critical input parameters that can significantly affect the fiber-direction compressive strength behavior of the composite. Therefore, we looked into fiber-matrix interface as a potential mechanism driving the compression strength improvement of the new material system. To characterize the properties of the fiber-matrix interface, it was decided that performing the experiments and observing the failure phenomenon at a scale small enough for the important features and events to be captured would be the most rigorous way to generate accurate properties.

As a result, an innovative micromechanical characterization technique with in-situ scanning electron microscopy (SEM) based experiments by means of fiber push-out was introduced to measure interface shear strength- new laser machining technique for specimen fabrication for the push-out test was developed. Sample fabrication with laser processing is fast and because of the boundary condition of the specimen created with this technique, rigid body motion of the sample is minimized which can lead to elimination of the compliance artifacts. The results of this work support the idea of using femtosecond laser machining technique to produce samples for push-out test instead of traditional processing methods (lapping and polishing process).

Furthermore, the experiments show approximately 30% decrease in the average values of the fiber-matrix interface shear strength for the HM carbon fibers compared to the IM carbon fibers in the new material system. The fiber-matrix interface shear strength reduction has been verified on the HM CFRP without the integrated IM fibers. And such a strong reduction corresponds to a 22% lower fiber-direction compressive strength of the HM CFRP. The results support the idea of integrating off-the-shelf IM carbon fibers into a HM CFRP to improve fiber-direction compressive strength of the HM composite material system. As off-the-shelf IM fiber-matrix interface is stronger in shear, and such fibers have higher shear modulus compared to HM fibers (which has been confirmed), integrating the appropriate off-the-shelf IM carbon fibers into a HM carbon-fiber composite may offload the HM fibers thus improving shear-driven fiber-direction compressive strength of the HM composite system. The methodology developed in this work provides the initial step as well as the foundation for further material development

Despite the major impact of the fiber-matrix interface shear strength on the fiber-direction compressive strength of the composite material, there are other potential mechanisms, such as matrix inelasticity, which should also be investigated. Also, the interface modeling may require more accurate characterization of the local fracture properties which we can address in future work. For instance, instead of push-out test, we can perform some push-in experiments to presumably extract some information regarding interface fracture properties.

And most importantly, we must ensure that we fully understand the fiber-direction compressive failure modes in the composite materials with varying modulus carbon fibers. As we currently assume fiber microbuckling (fiber kinking), we must observe the kink-band formation for the practical material range including HM, IM, and hybrid carbon fiber-reinforced composites. Then we can focus on developing fiber-direction compressive strength models that reflect the physics phenomenon, and effectively use such models in sensitivity analysis to identify the critical material characteristics to be measured. It is worth noting that fiber-direction failure in HM CFRPs is not well-documented in literature, which raises the question whether the fiber-direction compressive strength of PAN-based continuous HM CFRPs and HM/IM hybrids is indeed governed by microstructural stability (fiber kinking), as it is most commonly accepted and observed in IM CFRPs. We were able to observe the kink-band formation in HM CFRPs for the first time. Observing the kink-band formation across the different fiber types confirms that fiber-direction compressive strength is indeed governed by microstructural stability, which can be used as a basis for developing a rigorous modeling strategy and meeting the material input data requirements.

References

[1] A. Makeev , S. Ghaffari and G. Seon, "Improving compressive strength of high modulus carbon-fiber reinforced polymeric composites through fiber hybridization," *International Journal of Engineering Science,* vol. 142, pp. 145-157, 2019.

[2] Toray, "M55J High Modulus Carbon Fiber, M55J Rev. 1: Updated April 13, 2018.," 26 February 2019. [Online]. Available: https://www.toraycma.com/file_viewer.php?id=5096.

[3] F. Naya, C. Gonzalez, C. S. Lopes, S. Van der Venn and F. Pons, "Computational micromechanics of the transverse and shear behavior of unidirectional fiber reinforced polymers including environmental effects," *Composites Part A: Applied Science and Manufacturing,* vol. 92, pp. 146-157, 2017.

[4] J. H. Ahn and A. M. Waas, "A micromechanics-based finite element model for compressive failure of notched uniply composite laminates under remote biaxial loads," *Journal of Engineering Materials and Technology - Transactions of the ASME,* vol. 121, no. 3, p. 1999, 360–366.

[5] B. Budiansky and N. A. Fleck, "Compressive failure of fibre composites," *Journal of the Mechanics and Physics of Solids,* vol. 41, no. 1, pp. 183-211, 1993.

[6] N.A. Fleck, D. Liu and J. Y. Shu, "Microbuckle initiation from a hole and from the free edge of a fibre composite," *International Journal of Solids and Structures* , vol. 37, pp. 2757-2775, 2000.

[7] C. R. Schultheisz and A. M. Waas, "Compressive failure of composites, part I: testing and micromechanical theories," *Progress Aerospace Science,* vol. 32, 1996.

[8] N. Fleck, "Compressive failure of fiber composites," *Advances in applied mechanics* , vol. 33, pp. 43-117, 1997.

[9] N. F. Dow and B. W. Rosen, "Evaluations of filament-reinforced composites for aerospace structural application," NASA CR-207, 1965.

[10] N. A. Fleck, L. Deng and B. Budiansky, , "Prediction of kink width in compressed fiber composites," *Journal of Applied Mechanics,* vol. 62, p. 329–336, 1995.

[11] C. Soutis and N. A. Fleck, "Static Compression Failure of Carbon Fibre T800/924C Composite Plate with a Single Hole," *Journal of Composite Materials,* vol. 24, no. 5, p. 536–558, 1990.

[12] P. M. Jelf and N. . A. Fleck, "Compression Failure Mechanisms in Unidirectional Composites," *Journal of Composite Material,* vol. 26, no. 18, p. 2706–2726, 1992.

[13] B. Budiansky, "Mechanics of materials and material characterization:Micromechanics," *Computers & Structures,* vol. 16, no. 1-4, pp. 3-12, 1983.

[14] A. S. ARGON, "Fracture of Composites," *Treatise on Materials Science & Technology,* vol. 1, pp. 79-114, 1972.

[15] G. M. Martinez, M. R. Piggott, D. R. Bainbridge and B. Harris, "The compression strength of composites with kinked, misaligned and poorly adhering fibres," *Journal of Materials Science,* vol. 16, no. 10, p. 2831–2836, 1981.

[16] A. M. Waas and C. R. Schultheisz, "Compressive failure of composites, part II: Experimental studies," *Progress in Aerospace Sciences*, vol. 32, no. 1, pp. 43-78, 1996.

[17] R. . A. Chaudhuri, "Prediction of the Compressive Strength of Thick-Section Advanced Composite Laminates," *Journal of Composite Materials*, vol. 25, no. 10, p. 1244–1276, 1991.

[18] N. F. Dow and I. J. Gruntfest, "Determination of Most-Needed,Potentially Possible Improvements in Materials for Ballistic and Space Vehicles," T. I. S. R60SD389, General Electric Company AirForce Contract AF 04 (6471-269, 1960.

[19] B. W. Rosen, "in Fiber Composite Materials," in *Mechanics of Composite Strengthening*, 1965, pp. 37-75.

[20] M. J. Shuart, "Short-wavelength buckling and shear failures for compression-loaded," NASA Technical Memorandum 87640, Hampton,Virginia, 1985.

[21] R. Gutkin and S. T. Pinho, "Review on failure of laminated composites: Experimental perspective and modelling," Department of Aeronautics,South Kensington Campus,Imperial College London, London,UK, 2010.

[22] T. Hayashi, "On the Shear instability of Structures Caused by Compressive Load," in *AIAA Paper No. 65-770*, 1965.

[23] H. Schuerch, " Prediction of Compressive Strength in Uniaxial Boron Fiber - Metal Matrix Composite Materials," *AIAA Journal*, vol. 4, no. 1, pp. 102-106, 1966.

[24] W. Chung and R. B. Testa, "The Elastic stability of Fibers in a Composite Plate," *Journal of Composite Materials*, vol. 3, no. 1, pp. 58-80, 1969.

[25] J. B. Lager and R. R. June, "Compressive Strength of Boron- Epoxy Composites," *Journal. of Composite Materials*, vol. 3, no. 1, pp. 48-56, 1969.

[26] K. H. Lo and E. S.-M. Chim, "Compressive Strength of Unidirectional Composites," *Journal of Reinforced Plastics and Composites*, vol. 11, no. 8, 1992.

[27] I. . M. Daniel , H.-M. Hsiao and S.-C. Wooh , "Failure mechanisms in thick composites under compressive loading," *Composites Part B*, vol. 27, no. 6, pp. 543-552 , 1996.

[28] F. Naya, M. Herráez, C. S. Lopes, C. González, S. Van der Veen and F. Pons, "Computational micromechanics of fiber kinking in unidirectional FRP under different environmental conditions," *Composites Science and Technology*, vol. 144, pp. 26-35, 2017.

[29] Q. Sun, H. Guo, G. Zhou, Z. Meng, Z. Chen, H. Kang, S. Keten and X. Su, "Experimental and computational analysis of failure mechanisms in unidirectional carbon fiber reinforced polymer laminates under longitudinal compression loading,," *Composite Structures*, vol. 203, pp. 335-348, 2018.

[30] S. Kyriakides, R. Arseculeratne, E. Perry and K. Liechti, "On the compressive failure of fiber reinforced composites," *International Journal of Solids and Structures*, vol. 32, no. 6-7, pp. 689-738, 1995.

[31] M. S. Madhukar and L. . T. Drzal, "Fiber-Matrix Adhesion and Its Effect on Composite Mechanical Properties. III. Longitudinal (0°) Compressive Properties of Graphite/Epoxy Composites," *Journal of Composite Materials*, vol. 26, no. 3, p. 310–333, 1992.

[32] J.-B. Ha and J. A. Nairn, "Compression failure mechanisms of single-ply, unidirectional, carbon-fiber composites," *SAMPE Quarterly*, vol. 23, pp. 29-36, 1992.

[33] C. K. H. Dharan and L. Chun-Liang, "Longitudinal Compressive Strength of Continuous Fiber Composites," *Journal of COMPOSITE MATERIALS*, vol. 41, no. 11, 2007.

[34] S. Kumar and T. E. Helminiak, "Compressive strength of high performance fibers," *MRS online Proceedings library archive 134*, 1988.

[35] A. Makeev, C. Bakis, E. Strauch, M. Chris, P. Holemans, G. Miller, D. Nguyen, D. Spencer and N. Patz, "Advanced Composite Materials Technology for Rotorcraft through the Use of Nanoadditives. Journal of the A," *Journal of the American Helicopter Society*, vol. 60, no. 3, pp. 1-10, 2015.

[36] S. Hackett, J. Nelson, A. Hine, P. Sedgwick, R. Lowe, D. Goetz and W. Schultz, "Improved Carbon Fiber Composite Compression Strength and Shear Stiffness through Matrix Modification with Nanosilica," in *American Society for Composites 25th Technical Conference*, 2010 'a'.

[37] S. Hackett, J. Nelson, A. Hine, P. Sedgwick, R. Lowe, D. Goetz and W. Schultz, "The Effect of Nanosilica Concentration on the Enhancement of Epoxy Matrix Resins for Prepreg Composites," SAMPE, 2010 'b'.

[38] A. Kinloch and R. Young, Fracture Behaviour of Polymers, Elsevier Applied Science Publishers Ltd., 1983.

[39] Hexcel Corporation, "“HexTow® IM7 Carbon Fiber”, Product Data Sheet," 2018. [Online]. Available: https://www.hexcel.com/user_area/content_media/raw/IM7_HexTow_DataSheet.pdf. [Accessed 26 February 2019].

[40] Hexcel Corporation, "“HexTow® HM63 Carbon Fiber”, Product Data Sheet," 2016 'c'. [Online]. Available: https://www.hexcel.com/user_area/content_media/raw/HM63_Aerospace_HexTow_DataSheet.pdf. [Accessed 26 February 2019].

[41] RockWest Composites, "PYROFIL™ HS40 12K Typical Fiber Properties," 2008. [Online]. Available: https://www.rockwestcomposites.com/downloads/HS40-12K_(07-2008).pdf.

[42] Cytec, "“CYCOM 381 Epoxy Prepreg, Technical Data Sheet”," 2012. [Online].

[43] Hexcel Corporation, "“HexPly® 913 257°F (125°C) Curing Epoxy Matrix”, Product Data Sheet," 2016 'b'. [Online]. Available: https://www.hexcel.com/user_area/content_media/raw/HexPly_913_us_DataSheet.pdf. [Accessed 26 February 2019].

[44] Hexcel Corporation, "“HexPly® 8552 Mid-Toughened, High Strength, Damage-Resistant, Structural Epoxy Matrix”, Product Data Sheet," 2016 'a'. [Online]. Available: https://www.hexcel.com/user_area/content_media/raw/HexPly_8552_us_DataSheet.pdf. [Accessed 26 February 2019].

[45] SACMA SRM 1R-94, "“Test Method for Compressive Properties of Orientated Fiber-Resin Composites”Suppliers of Advanced Composite Materials Association," Arlington, VA, 1994.

[46] Hexcel Corporation, "“HexTow® IM8 Carbon Fiber”, Product Data Sheet," 2016 'd'. [Online]. Available: https://www.hexcel.com/user_area/content_media/raw/IM8_HexTow_DataSheet.pdf. [Accessed 26 February 2019].

[47] A. Makeev, C. Ignatius, Y. He and B. Shonkwiler, "A Test Method for Assessment of Shear Properties for Thick Composites," *Journal of Composite Materials*, pp. 3091-3105, 2009.

[48] A. Makeev , Y. He , P. Carpentier and B. Shonkwiler, "A Method for Measurement of Multiple Constitutive Properties for Composite Materials.," *Composites: Part A,* p. 2199–2210, 2012.

[49] A. Makeev, G. Seon, J. Cline and B. Shonkwiler, "In Quest of Methods for Measuring 3D Mechanical Properties of Composites," *Composites Science and Technology,* pp. 105-112, 2014.

[50] A. Makeev, G. Seon, Y. Nikishkov, D. Nguyen, P. Mathews and M. Robeson, "Analysis Methods Improving Confidence in Material Qualification for Laminated Composites," *Journal of the American Helicopter Society,* 2019.

[51] K. W. McElhaney, J. J. Vlassak and W. D. Nix, "Determination of indenter tip geometry and indentation contact area for depth-sensing indentation experiments," *Journal of Materials Research,* vol. 13, no. 5, pp. 1300-1306, 1998.

[52] W. C. Oliver and G. M. Pharr, "An improved technique for determining hardness and elastic-modulus using load and displacement sensing indentation experiments," *Journal f Materials Research,* vol. 7, no. 6, p. 1564–1583, 1992.

[53] A. P. Ternovskii, V. P. Alekhin, M. K. Shorshorov, M. M. Khrushchov and V. N. Skvortsov, "Micromechanical Testing of Materials by Depression," *Zavodskaya Laboratoriya,* vol. 39, no. 10, pp. 1242-1247, 1974.

[54] I. N. Sneddon, "The relation between load and penetration in the axisymmetric boussinesq problem for a punch of arbitrary profile," *International Journal of Engineering Science,* vol. 3, no. 1, pp. 47-57, 1965.

[55] W. C. Oliver and G. M. Pharr , "Measurement of hardness and elastic modulus by instrumented indentation: Advances in understanding and refinements to methodology," *Journal of Materials Research,* vol. 19, no. 1, pp. 3-20, 2004.

[56] L. P. Canal, C. Gonzalez, J. Segurado and J. Llorca, "Intraply fracture of fiber-reinforced composites:Microscopic mechanisms and modeling," *Composites Science and Technology,* vol. 72, no. 11, pp. 1223-1232, 2012.

[57] Bruker, "Nanomechanical Test Instrument," [Online]. Available: https://www.bruker.com/products/surface-and-dimensional-analysis/nanomechanical-test-instruments/standalone-nanomechanical-test-instruments/ti-950-triboindenter/overview.html. [Accessed 13 November 2019].

[58] Bruker, "Nanomechanical Testing Probes," [Online]. Available: https://www.bruker.com/products/surface-and-dimensional-analysis/nanomechanical-test-instruments/nanomechanical-upgrade-options/test-probes.html. [Accessed 13 November 2010].

[59] J. Kim and Y. Mai , Engineered interfaces in fiber reinforced composites, First Edit. Elseview Science Ltd, 1998.

[60] J. -P. Favre and M. -C. Merienne, "Characterization of fibre/resin bonding in composites using a pull-out test," *International Journal of Adhesion and Adhesives,* vol. 1, no. 6, pp. 311-316, 1981.

[61] E. Mäder, K. Grundke, H. -J. Jacobasch and G. Wachinger, "Surface, interphase and composite property relations in fibre-reinforced polymers," *Composites,* vol. 25, no. 7, pp. 739-744, 1994.

[62] X. Gao, J. W. Gillespie, R. E. Jensen, W. Li, B. Z. (. Haque and S. H. McKnight, "Effect of fiber surface texture on the mechanical properties of glass fiber reinforced epoxy composite," *Composites Part A,* vol. 74, pp. 10-17, 2015.

[63] B. W. Rosen, ""Mechanics of Composite Strengthening," in Fiber Composite Materials," *American Society for Metals,* pp. 37-75, 1965.

[64] S. P. Timoshenko and J. M. Gere, Theory of the elastic stability, McGraw-Hill, 1961.

[65] P. J. Herrera-Franco and L. T. Drzal, "Comparison of methods for the measurement of fibre/matrix adhesion in composites," *Composites,* vol. 23, no. 1, pp. 2-27, 1992.

[66] D. Adams, "Composite World," 1 January 2011. [Online]. Available: https://www.compositesworld.com/articles/fiber-matrix-interfacial-bond-test-methods. [Accessed June 2018].

[67] A. Kelly and W. Tyson, "Tensile properties of fibre-reinforced metals: Copper/tungsten and copper/molybdenum," *Journal of the Mechanics and Physics of Solids,* vol. 13, no. 6, pp. 329-338, 1965.

[68] X.-F. Zhou, J. Nairn and H. Wagner, "Fiber–matrix adhesion from the single-fiber composite test: nucleation of interfacial debonding," *Composites Part A: Applied Science and Manufacturing,* vol. 30, no. 12, pp. 1387-1400, 1999.

[69] X. Zhou, H. Wagner and S. Nutt, "Interfacial Properties of polymer composites measured by push-out fragmentation test," *Composites:Part A,* pp. 1543-1551, 2001.

[70] R. Young, C. Thongpin, J. Stanford and P. Lovell, "Fragmentation analysis of glass fibres in model composites through the use of Raman spectroscopy," *Composites Part A: Applied Science and Manufacturing,* vol. 32, no. 2, pp. 253-269, 2001.

[71] S. Zhandarov and E. Mäder, "Characterization of fiber/matrix interface strength: applicability of different tests, approaches and parameters," *Composites Science and Technology,* vol. 65, no. 1, pp. 149-160, 2005.

[72] B. Miller, P. Muri and L. Rebenfeld, "A Microbond Method for Determination of the Shear Strength of a Fiber/Resin Interface," *Composites Science and Technology,* vol. 28, no. 1, pp. 17-32, 1987.

[73] H. Wang, H. Wang, W. Li, D. Ren and Y. Yu, "An improved microbond test method for determination of the interfacial shear strength between carbon fibers and epoxy resin," *Polymer Testing,* vol. 32, no. 8, pp. 1460-1465, 2013.

[74] D. B. Marshall, "An Indentation Method for Measuring Matrix-Fiber Frictional Stresses in Ceramic Composites," *The American Ceramic Society,* vol. 67, no. 12, pp. 259-C-260, 1984.

[75] D. B. Marshall and W. C. Oliver, "Measurement of Interfacial Mechanical Properties in Fiber-Reinforced Ceramic Composites," *American Ceramic Society,* vol. 70, no. 8, pp. 542-548, 1987.

[76] M. Kharrat, A. Chateauminois, L. Carpentier and P. Kapsa, "On the interfacial behaviour of a glass/epoxy composite during a micro-indentation test:assessment of interfacial shear strength using reduced indentation curves," *Composites part A,* pp. 39-46, 1997.

[77] J. A. Nairn and Y. C. Liu, "STRESS TRANSFER INTO A FRAGMENTED,ANISOTROPIC FIBER THROUGH AN IMPERFECT INTERFACE," *International Journal of Solids Structures,* vol. 34, no. 10, pp. 1255-1281, 1996.

[78] F. Naya, J. Molina-Aldareguia, C. Lopes, C. Gonzalez and J. LLorca, "Interface Characterization in Fiber-Reinforced Polymer-Matrix Composites," *The minerals,Metals & Materials Society,* 2016.

[79] R. J. Kerans and T. A. Parthasarathy, "Theoretical Analysis of the Fiber Pullout and Pushout Tests," *Jornal Of the American Ceramic Society,* 1991.

[80] A. Godara, L. Gorbatikh, G. Kalinka, A. Warrier, O. Rochez, L. Mezzo, L. Luizi, A. van Vuure, S. Lomov and I. Verpoest, "Interfacial shear strength of a glass fiber/epoxy bonding in composites modified with carbon nanotubes," *Composites Science and Technology,* pp. 1346-1352, 2010.

[81] M. Tanoglu, S. H. McKnight, G. R. Palmese and J. W. Gillespi, "A new technique to characterize the fiber/matrix interphase properties under high strain rates," *Composites Part A: Applied Science and Manufacturing,* vol. 31, no. 10, pp. 1127-1138, 2000.

[82] M. Tanoglu, S. H. McKnight, G. R. Palmese and J. W. Gillespi, "The effects of glass-fiber sizings on the strength and energy absorption of the fiber/matrix interphase under high loading rates," *Composites Science and Technology,* vol. 61, no. 2, pp. 205-220, 2001.

[83] J. Sha, J. Dai, J. Li, Z. Wei, J.-M. Hausherr and W. Krenkel, "Measurement and analysis of fiber-matrix interface strength of carbon fiber-reinforced phenolic resin matrix composites," *Journal of Composite Materials,* vol. 48, no. 11, pp. 1303-1311, 2014.

[84] A. Salama, L. Li, P. Mativenga and A. Sabli, "High-power picosecond laser drilling/machining of carbon fibre-reinforced polymer (CFRP) composites," *Applied physics A,* vol. 73, no. 122, 2016.

[85] A. . N. Samant and N. B. Dahotre, "Laser machining of structural ceramics—A review," *Journal of the European Ceramic Society,* vol. 29, p. 969–993, 2009.

[86] C. Loumena, M. Nguyen, J. Lopez and R. Kling, "Potentials for lasers in CFRP production," *International Congress on Applications of Lasers & Electro-Optics,* no. 1, pp. 1026-1034, 2012.

[87] H. Niino, Y. Harada, K. Anzai, M. Matsushita, K. Furukawa, M. Nishino, A. Fujisaki and T. Miyato, "Laser Cutting of Carbon Fiber Reinforced Plastics (CFRP and CFRTP) by IR Fiber Laser Irradiation," *JLMN-Journal of Laser Micro/Nanoengineering,* vol. 11, no. 1, pp. 104-110, 2016.

[88] R. S. Patel and J. M. Bovatsek, "LASER MACHINING OF CFRP," in *21st International Conference on Composite Materials*, Xi'an, 2017.

[89] M. H. El-Hofy and H. El-Hofy, "Laser beam machining of carbon fiber reinforced composites: a review," *The International Journal of Advanced Manufacturing Technology,* vol. 101, p. 2965–2975, 2019.

[90] R. Suriano, A. Kuznetsov, S. . M. Eaton, R. Kiyan, G. Cerullo, R. Osellame, B. N. Chichkov, M. Levi and S. Turri, "Femtosecond laser ablation of polymeric substrates for the fabrication of microfluidic channels," *Applied Surface Science,* vol. 257, no. 14, pp. 6243-6250, 2011.

[91] R. Weber, T. Graf, P. Berger, V. Onuseit, M. Wiedenmann, C. Freitag and A. Feuer, "Heat accumulation during pulsed laser materials processing," *Optics Express,* vol. 22, no. 9, pp. 11312-11324, 2014.

[92] G. Shannon and S. Hypsh, "Femtosecond Laser Processing in the Medical Device Industry," 14 January 2015. [Online]. Available: https://www.productionmachining.com/articles/femtosecond-laser-processing-in-the-medical-device-industry. [Accessed June 2018].

[93] D. J. Stokes, Principles and Practice, John Wiley & Sons Ltd, 2008.

[94] F. V. 3. datasheet, "product data," FEI .

[95] S. Ghaffari, A. Makeev, D. Kuksenko and G. Seon, "Understanding High-Modulus CFRP Compressive Strength Improvement," in *ASC 34th Technical Conference,* Atlanta, 2019.

[96] D. D. Chung, Carbon Fiber Composites, Elsevier, 2012.

[97] N. Chandra and H. Ghonem, "Interfacial mechanics of push-out tests: theory and experiments," *Composites: Part A,* vol. 32, pp. 575-584, 2001.

[98] S. Ogihara and J. Koyanagib, "Investigation of combined stress state failure criterion for glass fiber/epoxy interface by the cruciform specimen method," *Composites Science and Technology,* vol. 70, no. 1, pp. 143-150, 2010.

[99] D. Kuksenko, H. J. Böhm and B. Drach, "Effect of micromechanical parameters of composites with wavy fibers on their effective response under large deformations," *Advances in Engineering Software,* vol. 21, pp. 206-222, 2018.

[100] F. Naya, M. Herráez, C. S. Lopes, C. González, S. Van der Veen and F. Pons, "Computational micromechanics of fiber kinking in unidirectional FRP under different environmental conditions," *Composites Science and Technology* , vol. 144, pp. 26-35, 2017.

[101] S. Pinho, C. Dávila, P. Camanho, L. Iannucci and P. Robinson, Failure Models and Criteria for FRP Under In-Plane or Three-Dimensional Stress States Including Shear Non-Linearity, 2005.

[102] R. Gutkin, S. Pinho, P. Robinson and P. Curtis, "Micro-mechanical modelling of shear-driven fibre compressive failure and of fibre kinking for failure envelope generation in CFRP laminates," *Composites Science and Technology,* vol. 70, pp. 1214-1222, 2010.

[103] R. McLendon, "Micromechanics Plugin For Abaqus/CAE," 2016.

[104] J. Segurado and J. Llorca, "A numerical approximation to the elastic properties of sphere-reinforced composites," *Journal of the Mechanics and Physics of Solids,* vol. 50, pp. 2107-2121, 2002.

[105] H. J. Böhm, "A short introduction to basic aspects of continuum micromechanics," Vienna, 2018.

[106] D. Kuksenko and B. Drach, "Effective conductivity of materials with continuous curved fibers," *International Journal of Engineering Science,* vol. 118, pp. 20-81, 2017.

[107] B. Drach, D. Kuksenko and I. Sevostianov, "Effect of a curved fiber on the overall material stiffness," *International Journal of Solids and Structures,* Vols. 100-101, pp. 211-222, 2016.

[108] F. Naya, C. Gonzalez, C. Lopes, S. Van der Veen and F. Pons, "Computational micromechanics of the transverse and shear behaviour of unidirectional fiber reinforced polymers including environmental effects," *Composites:Part A,* pp. 146-157, 2017.

[109] "Dassault Systèmes, Abaqus 6.14 Online Documentation," 2014.

[110] A. Arteiro, G. Catalanotti, A. R. Melro, P. Linde and . P. Camanho, "Micro-mechanical analysis of the in situ effect in polymer composite laminates," *Composite Structures,* vol. 116, pp. 827-840, 2014.

[111] A. Makeev, C. E. Bakis, E. Strauch, M. Chris, P. Holemans, G. Miller, D. Nguy and N. Patz, "Advanced composite materials technology for rotorcraft through the use of nanoadditives," *Journal of the American Helicopter Society,* 2015.

[112] "Hexcel Corporation, HexTow® HM63 carbon fiber, product data sheet.," 2019. [Online]. Available: www.hexcel.com/user_area/content_media/raw/HM63_Aerospace_HexTow_DataSheet.pdf. [Accessed 27 June 2019].

[113] M. J. Laffan, S. T. Pinho , P. Robinson , . L. Iannucci and A. J. McMillan, "Measurement of the fracture toughness associated with the longitudinal fibre compressive failure mode of laminated composites," *Composites: Part A,* vol. 43, no. 11, pp. 1930-1938, 2012.

\